ELSEVIER

Journal of Neuroscience Methods 157 (2006) 364–373

JOURNAL OF NEUROSCIENCE METHODS

www.elsevier.com/locate/jneumeth

Building spike representation in tetrodes

Dorian Aur*, Mandar S. Jog

Department of Clinical Neurological Sciences, Movement Disorders Program, London, Ont., Canada

Received 2 March 2006; received in revised form 12 April 2006; accepted 1 May 2006

Abstract

This paper presents a new technique for analyzing the recorded information from tetrodes in freely behaving rats, based on independent component analysis (ICA). The ion-specific pumps and channels allow fast transfer of charges such as Na^+, K^+, Cl^- and eventually Ca^{2+} during each action potential (AP). These groups of charges under an electrical field have distinct spatial trajectories. Therefore, the generated signals within a tetrode are considered to be composed mainly by statistically independent signal sources that can be obtained by performing ICA. In order to compute the position of independent sources during AP generation, the triangulation method uses an iterative Newton-Raphson algorithm. The representation of the independent signal sources in three-dimensional tetrode space is then obtained. Since the charge movements are extensively spread on the neuron's surface, the representation in tetrode space reveals electrical spatial patterns of activation during each AP. The analysis of several spikes coming from the same neuron reveals small changes from spike to spike in the 3D shape. Since information within spikes is highly transferred by ionic fluxes these electrical patterns of activation reflect neuronal computation occurring during each AP.

Keywords: Tetrode; Independent component analysis; Newton-Raphson; Spatial coding; Neuronal computation

1. Introduction

The study of neuronal structure and the relationship to its computational mechanisms and function is one of the greatest challenges in neuroscience. In neurophysiology, recordings in vitro have explored the detailed electrical properties of single neurons while in vivo extracellular recordings have attempted to combine this with behavior. However, single-electrode recording methods have substantial difficulty in separating recordings from multiple neurons. The problem occurs because the electrode tip is surrounded by many neurons and the electrode detects the electrical events generated by all the neurons and dendrites in the area. Multichannel electrodes such as tetrodes can effectively address this issue of signal source resolution. Innovative methods in recording hardware and software with tetrodes (Buzsáki, 2004; Hulata et al., 2002; Jog et al., 1999, 2002; Takahashi et al., 2003; Wilson and McNaughton, 1993) or multi-channel electrode arrays (Bierer and Anderson, 1999; Oweiss and Anderson, 2002) have been introduced in an attempt to improve signal source separation.

Tetrode recordings provide a four-dimensional view of every incoming signal. These signals arise successively from many neurons that surround the tetrode tips. Numerous methods have been developed to manually or automatically classify (cluster) these signal sources into putative individual neurons. These methods use the significant difference in amplitudes or power of the action potentials across the four channels of the tetrode, termed "stereo effect" (Gray et al., 1995; Jog et al., 2002; Rebrik et al., 1999) in order to accomplish signal separation.

The role of the dendritic tree was minimized by early work of Ramón y Cajal that assumed that AP travels only along axons. For example, the role of fast prepotentials was still unclear until the simultaneous application of optical techniques and direct dendritic measurements (Kasuga et al., 2003; Oesch et al., 2005). Activity-dependent attenuations in extracellular spike amplitude appear during behavior and are dependent on back-propagation of the action potentials into the dendritic arbor (Quirk et al., 2001). The active back-propagation of somatic action potentials into dendrites is highly regulated and mediated by voltage-gated Na^+ and/or Ca^{2+} channels (Häusser et al., 2000; Kerr and Plenz, 2002). Dendrites and soma are equipped with several voltage-gated ion channels that greatly enrich the observed charge flow. Several studies have pointed out that gated ion channels interact with plastic changes in the synaptic strength to influence behavior (Nolan et al., 2004).

* Corresponding author. Tel.: +1 519 685 8300.
E-mail address: daur2@uwo.ca (D. Aur).

0165-0270/$ – see front matter © 2006 Elsevier B.V. All rights reserved.
doi:10.1016/j.jneumeth.2006.05.003

Variation in spike directivity can be estimated by using charge movement model (CMM) and computing singular value decomposition of the estimated 3D trajectory data (Aur et al., 2005). Using this method we have been able to show that spike directivity is correlated with behavior. Additionally, by performing simulation of Hodgkin-Huxley model we proved that information transfer takes place within ionic fluxes in each spike (Aur et al., 2006). Our analysis revealed the fact that mutual information (MI) between input signal and sodium flux is about two times that between input signal and output spikes during each spike within a millisecond-level time domain.

Since electrical "communication is computation" (Cover and Thomas, 1991) we expect to find in each spike a strong connection between information, computation and physical appearance of electrical patterns. Therefore, these patterns generated by spatial distribution of charges seen previously in the form of activity-dependent attenuations (Quirk et al., 2001) or back-propagation phenomena (Häusser et al., 2000; Kerr and Plenz, 2002) reflect the physics of neuronal computation expressed by ionic flow.

Since CMM gives only a linear approximation of charge flow in order to understand the physics of computation it is important to implement a method able to reveal details of electrical patterns.

This paper extends CMM further by presenting a novel method in which independent component analysis is used to determine details in electrical spatial pattern of activation during each AP.

The use of ICA algorithms is not accidental, specifically ICA techniques are well known for their ability in demixing noisy signal sources (Amari et al., 1997; Bell and Sejnowski, 1995; Hyvärinen et al., 2001; Lee et al., 2000).

Spatial and temporal patterns measured in extracellular space reveal "much about the location and timing of currents in the cell" (Holt and Koch, 1999). Therefore, this information regarding electrical flow can be extracted from extracellular measurements using computational techniques. This paper presents a new method that is able to show spatial patterns of charge flow from each spike. The charge movement model allows the description of the trajectory and main directivity of a spike. By using the ICA method this paper advances the CMM method substantially to reveal complex patterns during each action potential.

A brief overview of the ionic mechanisms of transmission within an action potential is also provided. This is followed by a methods section on data collection and analysis techniques that have been developed. A results section demonstrates the outcome from the methods discussed in the paper. The importance of this method in addressing neuronal spatial pattern of activation in an in vivo recording paradigm is then provided. However, this important method is of general use in the study of electrical patterns of neuronal activation in vivo and in vitro.

2. Ionic mechanisms

Each signal source or action potential (AP) in the neuron can be thought of as being generated by charge flow that includes sodium, potassium, chloride and calcium. The significant increase in the ionic conductance during the action potential is generated by an abrupt change in the permeability characteristics of the membrane that for short term becomes more permeable to Na^+ ions than to K^+ ions. The generation of an action potential is then the result of an increase in the ionic conductance of the membrane and the activation of voltage sensitive ionic channels.

The propagation of excitation along the dendrites and the axon of a neuron can be described by a partial differential equation (Scott, 2002; Toth and Crunelli, 1999):

$$C_{\mathrm{m}}\frac{\partial V(r,t)}{\partial t} = \alpha(r)\frac{\partial^2 V(r,t)}{\partial r^2} + \beta(r)\frac{\partial V(r,t)}{\partial r} - I_{\mathrm{ionic}} + I_{\mathrm{in}}(r,t) \quad (1)$$

where C_{m} is the membrane capacitance, and $I_{\mathrm{in}}(r,t)$ represents the injected current density along the neuron's membrane. The coefficients α and β depend on the dendrite's shape and account for eccentricity in the dendrite cross-section (Toth and Crunelli, 1999). I_{ionic} is the sum of all ionic current densities including I_{leak} in the following equation:

$$I_{\mathrm{ionic}} = I_{\mathrm{Na}} + I_{\mathrm{K}} + I_{\mathrm{leak}} \quad (2)$$

where the currents I_{Na}, I_{K} are determined by the ionic flux of Na^+ and K^+, respectively. After membrane depolarization, Na^+ permeability increases even more therefore an avalanche of Na^+ is produced and consequently Na^+ ions invade the cell. However, the process is transient and is accompanied by an increase in the already high K^+ permeability and by Na^+ current inactivation. Immediately following an action potential there is a time interval during which no stimulus can generate a second action potential and this time interval is called the refractory period.

Groups of several ionic charges are therefore responsible for this AP mechanism. A detailed analysis of individual action potentials recorded from a neuron on the basis of charge movement model could provide valuable insights regarding electrical flow of information within each neuron, and across chains or circuits of neurons. This can also be achieved in vitro using slice recordings and high-resolution techniques using an ultra small array of electrodes to observe the electrical activity of neurons controlling the synaptic input of individual neurons (Spencer et al., 2004). In vivo techniques such as two-photon microscopy (Helmchen et al., 1999), surface imaging and directional analysis in tetrode recordings (Takahashi et al., 2003) have tried to capture electrical flow during action potential. However, such systems cannot determine any impact of behavior on the electrical flow in the neurons. An analysis of electrical flow in an in vivo system that utilizes behaving animals would therefore be extremely useful in order to understand pattern changes within APs during behavior.

This paper proposes a novel approach to obtain a representation for electrical flow of charges during each AP, based upon an independent component analysis technique. Having separated the multiple signal sources into putative individual neurons using established spike sorting techniques (Jog et al., 2002), our method advances the understanding of the properties

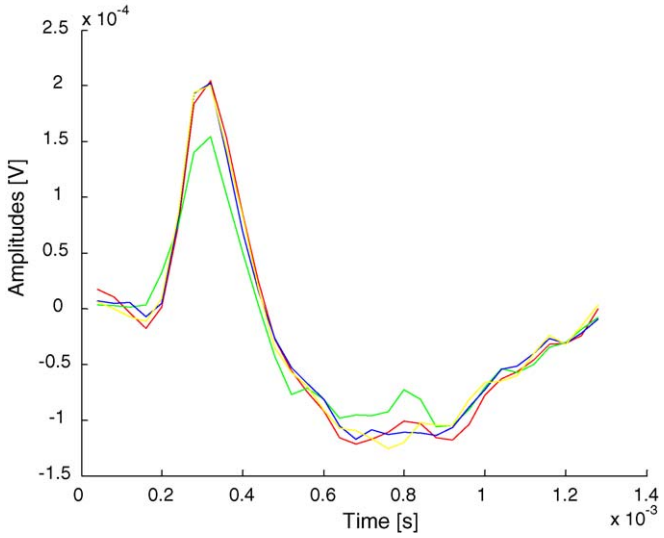

Fig. 1. An example of waveforms measured by the four channels of a tetrode. Visible attenuation called "stereo effect" is present by the difference in amplitudes seen across channels.

of individual action potentials assigned to one putative neuron. The method uses the four-dimensional views (Fig. 1) of every action potential generated by tetrode recordings and provides details regarding electrical pattern of activation within each spike.

3. Data collection materials and methods

3.1. Implantable electrophysiology hardware

The headstage, carrying the tetrodes, is an autoclavable and reusable lightweight device (ca. 7 g for rat), MRI compatible, particularly useful for neurophysiological recordings made in the awake, behaving rodent. The headstage body holds 12 identical microdrives, each microdrive holding a single tetrode (Jog et al., 2002). The tetrode, which is made of four twisted microwires, is an extracellular recording microelectrode with four closely spaced recording tips. Tetrodes are independently moved (lowered or raised) many times over the course of an experiment (Jog et al., 1999, 2002). However, in a given experiment, the location of the tetrodes is kept constant.

3.2. Surgery

The animals were maintained on feeding restriction not less than 80% of baseline weight. The animals were anesthetized, a burr hole was drilled for the purposes of tetrode penetration (for Striatum: AP 9.2 mm, DV 5.9 mm, L 3.5 mm) and dura was removed. The headstage drive was lowered such that the cannula holding the tetrodes just touched the surface of the brain (Jog et al., 1999, 2002). Upon the rat awakening postoperatively, the tetrodes were lowered out of the cannula. Tetrodes were advanced partially on each day so as to allow the brain to settle. The brain targets were reached by day 3 or 4 operatively. Recordings commenced after this was achieved.

3.3. Experimental setup

During experiments, the tetrodes were connected, through high impedance fixed gain (100×) preamplifiers to the multichannel interface (Neuralynx© 48) of an acquisition computer. The input signal, taken from the headstage preamplifier (1–2 mV) was amplified up to 10 V, bandpass filtered (0.3–9 kHz), sampled at 25 kHz per channel and converted to digital samples (12 bits/sample). Twelve tetrodes (48 channels) were used for neural activity recording. The cross-section of the bottom tip which is not insulated is 10 μm and these tips were gold plated to have impedance between 0.2 and 0.8 MΩ. Data were analyzed offline on a PC computer (Pentium 4, 2.8 GHz, 512 MB RAM) with Matlab-MathWorks, Inc. All the routines were custom developed or are freely available on the world-wide-web.

4. Computational methods

4.1. Beyond line approximation—three charge model

The approach performed in (Aur et al., 2005) gives the best linear approximation of charge flow in a selected spike. This linear approximation is obtained by considering the largest singular vector and the corresponding "right" singular vector that represents direction cosines of the best linear approximation. The energy contents of the matrix $P \in \Re^{nx3}$ that contains trajectory coordinates $(x(k),y(k),z(k))$ is equal to the sum of the squared singular values. About 20% of the spike energy in real spikes does not obey this directivity and is included in two additional directivities represented within SVD. In this view the spike is completely represented by a *three charge model* (TCM) with their three directivities. This representation of the spike in tetrode space gives more insight of spatial phenomenon than a linear approximation of charge flow. An example that shows spike trajectory and three directivities is represented in Fig. 2 for a selected spike (Fig. 1).

However the number of charges within each AP is far greater than three and even TCM is a rough approximation of spatial charge flow. Any group of ionic charges $q_1, q_2, \ldots, q_N$ in movement that have close enough adjacent trajectories could be considered equivalent to a single charge $Q = \sum_{i=1}^{N} q_i$ in movement. Reciprocally the movement of a single ionic charge can be decomposed in the movement of a group of several charges that have adjacent trajectories as a direct consequence of the superposition principle effect (Griffiths, 1999).

4.2. Why independent component analysis

To reveal the link between spatial trajectory of charges and statistical independence of generated signals within an electrode, a simple theoretical experiment is proposed.

Consider three charges q_1, q_2, q_3 in a weak electric field $\vec{E} = 0.28\,\mathrm{V/m}$. The force acting on each charge is $\vec{F}_i = q_i\vec{E}$ $(i = 1, 3)$ that can be written $\vec{F}_i = m_i\vec{a}_i$ where m_i is the mass of charge and $\vec{a}_i$ is the acceleration. Given the initial spatial position, $\vec{r}_0^1, \vec{r}_0^2, \vec{r}_0^3$ and initial velocities $\vec{v}_0^1, \vec{v}_0^2, \vec{v}_0^3$ between 1 and

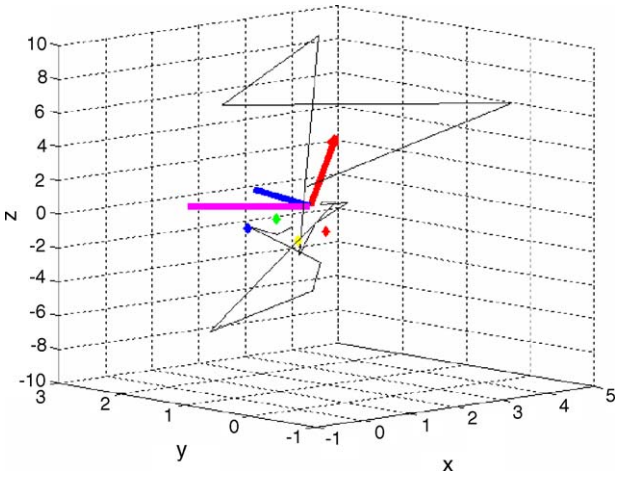

Fig. 2. Three charge model representation of spike. The spike trajectory is in black and the computed directivities of the corresponding three charges (red, blue and magenta arrows) represent the three right singular vectors. Each division is approximately 20 μm (for interpretation of the references to color in this figure legend, the reader is referred to the web version of the article).

5 m/s, the equations of motion can be integrated numerically:

$$\vec{v}^i = \vec{v}_0^i + \frac{q_i \vec{E}}{m} \mathrm{d}t \tag{3}$$

$$\vec{r}^i = \vec{r}_0^i + \vec{v}\,\mathrm{d}t \tag{4}$$

and the trajectories can be plotted (Fig. 3A and B).

For a realistic simulation Gaussian noise is added to the computed output $\vec{r}$. Due to different initial velocities and electrical field, charge trajectories describe a parabola in 2D space and after 3 ms their position is highly different. The current $s_1(t)$ generated in a tip of tetrode by drop of potential in a length Δl of the conductor by charge q_1 is (Aur et al., 2005):

$$\frac{1}{4\pi\varepsilon}\frac{q_1}{r_1^a(t)} - \frac{1}{4\pi\varepsilon}\frac{q_1}{r_1^b(t)} = \frac{s_1(t)\Delta l}{\sigma A} \tag{5}$$

where ε is medium permittivity, A the area, σ the conductivity of the conductor and $r_1^a(t)$, $r_1^b(t)$ are distances from charge to electrode ends. For charge q_2:

$$\frac{1}{4\pi\varepsilon}\frac{q_2}{r_2^a(t)} - \frac{1}{4\pi\varepsilon}\frac{q_2}{r_2^b(t)} = \frac{s_2(t)\Delta l}{\sigma A} \tag{6}$$

and charge q_3:

$$\frac{1}{4\pi\varepsilon}\frac{q_3}{r_3^a(t)} - \frac{1}{4\pi\varepsilon}\frac{q_3}{r_3^b(t)} = \frac{s_3(t)\Delta l}{\sigma A} \tag{7}$$

similar equations can be written. Here, $s_1(t)$, $s_2(t)$ and $s_3(t)$ represent the currents corresponding to the three charges q_1, q_2 and q_3 that describe the trajectories magenta, blue and red in Fig. 3A.

The total drop of potential in a length Δl of the conductor can be seen as a linear mixture of these currents:

$$V(t) = a_1 s_1(t) + a_2 s_2(t) + a_3 s_3(t) \tag{8}$$

where a_1, a_2, a_3 are constants.

However, the medium is complex and this might result in anisotropic signal propagation. To surmount this issue, for each discrete measurement k ($k \in N$) the measured potential $V(k)$ can be written to depend on currents generated at moment k, and their previous history at $k-1$, $k-2$, ...:

$$V(k) = a_1 s_1(k) + a_2 s_2(k) + a_3 s_3(k) + a_4 s_1(k-1) + a_5 s_2(k-1) + a_6 s_3(k-1) + \cdots \tag{9}$$

Statistical analysis performed over generated currents $s_1(t)$, $s_2(t)$ and $s_3(t)$ is able to reveal the fact that the statistical independence of these signals is increased if their spatial trajectories are farther apart. Since almost each ICA algorithm is designed to maximize information, this statement can be verified by computing mutual information (MI) values between generated currents during the movement of each of the three charges. The details regarding MI estimation are given in (Aur et al., 2006).

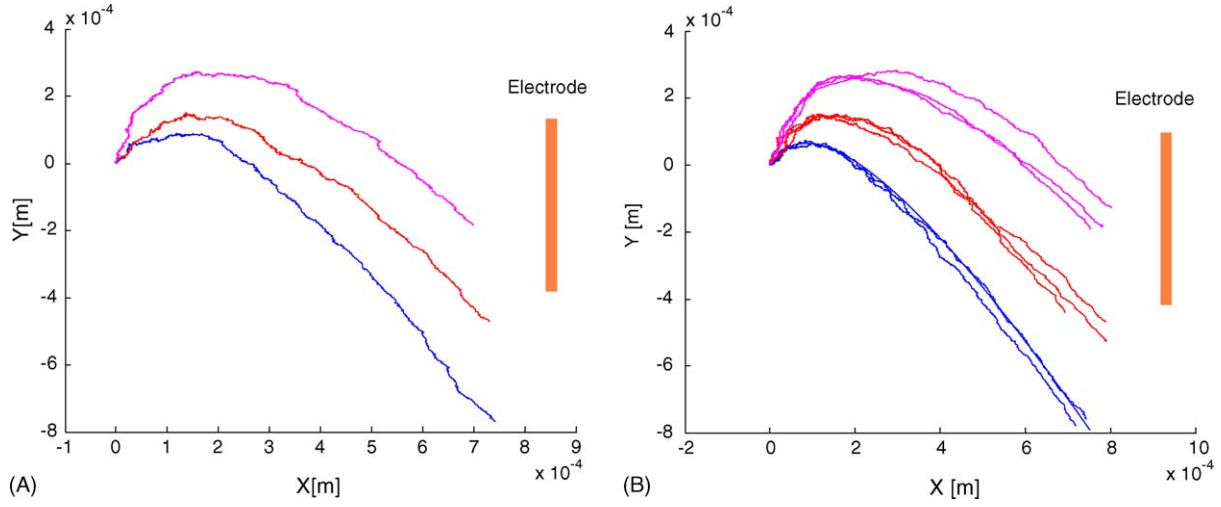

Fig. 3. Simulation of charge trajectories in a weak field $\vec{E} = 0.28$ V/m that generates a current in an electrode length of $\Delta l = 0.6$ μm. (A) Simulation for three charges with initial velocities between 1 and 5 m/s. The three charges q_1, q_2, q_3 and their corresponding trajectories represented in magenta, blue and red color. (B) Simulation for nine different charges with initial velocities between 1 and 5 m/s. An increase in initial velocity within each colored clustered trajectories (magenta, red and blue) is less than 10% (for interpretation of the references to color in this figure legend, the reader is referred to the web version of the article).

For example, the average mutual information I_{13} between $s_1(t)$ and $s_3(t)$ is about two-fold higher than the average mutual information I_{12} between signal $s_1(t)$ and signal $s_2(t)$. If trajectories are close enough (Fig. 3B) average mutual information between signals within each colored clustered trajectories varies less than 5%. Both results were obtained under condition that the signal noise ratio is SNR < 20 dB where "the signal" was considered to be the value $\Delta r = \vec{v}\,\mathrm{d}t$.

A relative comparison of mutual information values reveals the fact that signals $s_1(t)$ and $s_3(t)$ are less statistically dependent and this type of independence is closely related to spatial separation between trajectories of charges. During every AP each charge or more accurately several group of charges that move independently in space (Fig. 3) could be treated as satisfying a certain degree of statistical independence. Therefore, an ICA algorithm would perform a transformation of the recorded signals to obtain its components as independent as possible. In this example we considered an unfavorable case when charges velocities and electric field have low values. One may find these values in active dendrites, during action potential propagation (Saraga et al., 2003). If velocities and differences between velocities are higher, then the trajectories are far apart and MI analysis reveals higher differences between generated signals.

Since the cable equation (Eq. (1)) is a non-linear electrostatic diffusion phenomenon (Scott, 2002), the neuron during each spike can be described by several signal sources (charges in movement) distributed in space. The description from Eqs. (5)–(7) that can be generalized for N charges in movement reveals spatial ionic flow. This electrical phenomenon can be directly linked with the drop in potential that occurs in the electrode as described in Eq. (8).

We had some doubts initially regarding ICA performance. Therefore, before using ICA in this experiment, we performed several tests in case of several mixed speech sources with background noise, using fewer microphones than sources of signal. The ICA outcome can easily be interpreted in this case. Before the test, none could figure out what speakers were talking about. After performing ICA, each channel that was "statistically independent" proved to be a speaker.

In this application, instead of speakers there are charges or group of charges that have statistically distinct "voices" if their trajectories are far apart. Instead of microphones, recordings are made by tetrode tips where charges generate potential differences during their movements.

Therefore the main role of ICA in tetrode experiment is to obtain the signals generated by charges or group of charges in movement during AP. Charges that have far apart trajectories will generate "statistical independent" signals in electrode.

4.3. Spike representation—N charge model

The charge movement model is considered to be the basis of using independent component analysis for the recorded action potential. Measurements of inter-tip distances from tetrodes show that the average spacing between tips is approximately 20 μm with a measurement error of approximately 3 μm for each tip. (Jog et al., 2002). We assumed this inter-tip distance of 20 μm in computations. Since the computations are performed for spikes within the same frame of reference, a relative change in electrical patterns between spikes can be perceived and therefore the relative position tetrode-neuron is not required. This type of analysis was performed and explained in detail in our previous paper (Aur et al., 2005).

Several phases of data processing are required to obtain a 3D image of the neuronal spike. The first phase involves standard signal filtering and positively triggered data capture during acquisition. Since this phase is a standard electrophysiological technique, it will not be discussed further. The second phase, known as spike sorting, uses template matching and K-means clustering analysis in order to find the prototype spikes $P_K, k \in N$ (discussed in detail in Jog et al., 2002). As the closest neurons to tetrode tips generate the strongest signal, the third phase consists in sorting the prototypes P_K in decreasing order of their amplitude. The next phase performs computations for localization of the estimated independent signal sources in the "tetrode space" (Aur et al., 2005) for the prototypes P_K that defines the neuron closest to tetrode tips.

Once the data has been separated into putative individual neurons or clusters, each spike from the neuron is analyzed in detail. Each spike within every cluster has four waveforms associated with it, one from every channel of the tetrode labeled (t_1,t_2,t_3,t_4) (Fig. 1). Eq. (10) can be then rewritten for each spike data:

$$x = Ms + v \tag{10}$$

where $x \in \mathbf{R}^m$ is data obtained from tetrode tip, $M \in \mathbf{R}^{m\times n}$ mixing matrix, $s \in \mathbf{R}^n$ signal matrix and $v \in \mathbf{R}^m$ noise signal vector. The two most commonly used techniques that can provide an internal model of the data include principal components analysis (PCA) and independent component analysis (ICA). If the noise signal vector is null, ideally we would like to find a transformation:

$$x = As \tag{11}$$

where $AA^{\mathrm{T}} = I$ that estimates the source signal s from the corresponding linear combination matrix. A weaker form of independence is "uncorrelatedness" for which PCA is a statistical method that determines the optimal linear transformation. In the PCA case, the rows of the matrix A are the eigenvectors of the covariance matrix $\sum_{xx}$ of the data matrix. In our case, columns of A, a_j ($j = 1, 2, \ldots, n$) could be a basis set for a subspace $\mathbf{\Omega} \subset \mathbf{R}^{m\times n}$ and its dimension Dim($\mathbf{\Omega}$), is equal to r, the number of vectors in the basis set. If noise is assumed to be purely random, the directions where the data variation is maximal could be used for an internal model. Then, the coordinate y in the new basis is given by

$$y = (Z^{\mathrm{T}}Z)^{-1}Z^{\mathrm{T}}x \tag{12}$$

Here, Z is the estimate of M from Eq. (11) and if M is a square matrix the inverse could be computed directly. In the general case when M is a nonsquare matrix the Moore-Penrose generalized inverse of Z is a unique matrix which satisfies the Penrose conditions (Tian, 2004). It is interesting to note that PCA represents a special case of ICA under the constraints that matrix A

is restricted to rotations, $A^{-1} = A^{T}$ and the signal has a Gaussian distribution. However, it is known that PCA does not always produce the best result in the sense of recovering sources from the mixed signals and that higher-order methods are necessary to find more meaningful transformations. In this sense ICA, as a higher-order generalization of principal components analysis, separates statistically independent components in the inputs. Since independence implies uncorrelatedness, many ICA methods constrain the estimation procedure so that it always gives uncorrelated estimates of the independent components.

Developing ICA involves three distinct phases: the preprocessing of the data, the computation of a non-gaussianity measure and optimization of an objective function (Sanchez, 2002). The preprocessing phase commonly utilizes data centering and data whitening. Measures of non-gaussianity are kurtosis, differential entropy, negentropy and mutual information. Using measures of non-gaussianity the ICA algorithms are able to separate statistically independent components in the inputs: a higher-order generalization of PCA (Amari et al., 1997; Bell and Sejnowski, 1995; Lee et al., 2000). The aim of ICA is to find the estimate of signal sources s and the corresponding linear combination matrix A. Similar to the PCA case, an independent component basis set could be computed.

The identifiability of the model from Eq. (12) can be assured if the number of observed linear mixtures is at least as large as the number of independent components. However, it was proved by Cardoso (1991) that even in the case where $m < n$, the mixing matrix is identifiable. Writing y for the estimate of s, and Z for the estimate of M from Eq. (11) is equivalent to

$$y = Z^{-1}x - Z^{-1}v \tag{13}$$

In the general case the noise effect can be reduced by a soft threshold.

To obtain independent component estimation we used extensively the FastICA algorithm (Hyvärinen et al., 2001). Almost each ICA algorithm designed to maximize information is able to provide a 3D image representation of spikes in tetrode space. We have extensively tested several ICA algorithms; however a detailed analysis of ICA algorithms is beyond our purpose in this paper and will be discussed further elsewhere.

Since the collected data are recorded at low frequency (25 KHz) for each spike less than 32 points can be represented in 3D tetrode space. The best way to increase the number of represented points is to use a higher frequency for recording the data. If the sampling frequency is 10 times higher there will be about 320 values recorded for each spike and therefore a better resolution for each 3D spike image. However, since many recordings are performed at this low frequency, in order to have a better resolution of the physical phenomenon, a cubic spline interpolation may be performed in advance. Interpolation has two major effects on recorded data x. First, it acts like a filter. Then, by increasing the number of points in the data, interpolation sensibly improves the resolution. However, as presented below this increasing in the number of points in noisy data has to be kept at reasonable values to maintain the error of interpolation under a certain limit.

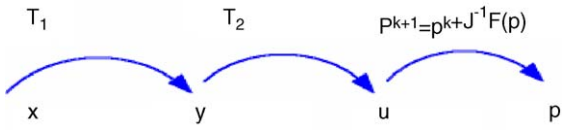

Fig. 4. Flow chart for spike representation algorithm.

Since the charge flow during AP is generated along dendrites and neuron's axon one can establish the position of several charge sources in the three-dimensional space using the following algorithm:

(a) Determine the transformation $Z_0 = \arg\min_z ||y_i - (Z_i^{T}Z_i)^{-1}Z_i^{T}x_i||$, $i = 1, 2, 3, 4$;
(b) Construct $T_1 = (Z_0^{T}Z_0)^{-1}Z_0^{T}$
(c) Calculate $y_i = T_1 x_i$ $i = 1, 2, 3, 4$ for every channel
(d) Construct the transformation T_2, as the law of cosines $u_i = T_2(y_i)$ (Aur et al., 2005; Griffiths, 1999).
(e) Construct the non-linear function F that relates u_i to geometrical tips position as presented below (Jog et al., 2002).
(f) Compute the position p_k of electrical sources in the "tetrode space".

Practically speaking, one may extend the triangulation principle of determining the spike position for independent components obtained after ICA algorithm is performed (Fig. 4). In this case using the values of u_i from each of the four tips, independent signal source positions can be found at the intersections of four spheres (Jog et al., 2002). The non-linear system can be written in the form:

$$\frac{u_{i0}}{u_{i1}} = \frac{(x-x_1)^2 + (y-y_1)^2 + (z-z_1)^2}{x^2 + y^2 + z^2} \tag{14}$$

$$\frac{u_{i0}}{u_{i2}} = \frac{(x-x_2)^2 + (y-y_2)^2 + (z-z_2)^2}{x^2 + y^2 + z^2} \tag{15}$$

$$\frac{u_{i0}}{u_{i3}} = \frac{(x-x_3)^2 + (y-y_3)^2 + (z-z_3)^2}{x^2 + y^2 + z^2} \tag{16}$$

where $x_j, y_j, z_j, j = 1, 2, 3, 4$ are the coordinates of the four channel tips. For each channel $u_i = T_2(y_i)$, $i = 1, 2, \ldots, 4$ one may write the Eqs. (15)–(17) as a non-linear system $f_j(x,y,z) = 0$, $j = 1, 2, 3$ where $F = (f_1, f_2, f_3)$. The iterative Newton-Raphson scheme is used to find a solution for the non-linear system:

$$p_{k+1} = p_k - J^{-1}F(p_k), \quad k \in N \tag{17}$$

where the Jacobian J of function F is

$$J = \begin{pmatrix} \frac{\partial f_1}{\partial x} & \frac{\partial f_1}{\partial y} & \frac{\partial f_1}{\partial z} \\ \frac{\partial f_2}{\partial x} & \frac{\partial f_2}{\partial y} & \frac{\partial f_2}{\partial z} \\ \frac{\partial f_3}{\partial x} & \frac{\partial f_3}{\partial y} & \frac{\partial f_3}{\partial z} \end{pmatrix} \tag{18}$$

and p_k are the positions of independent sources projections in the tetrode space. Clearly, the position of independent sources

is determined when there is a solution p_{k+1} for the non-linear system (Brenan et al., 1989). Each spike is more or less a superposition of several sources of signal. Since generated signals in electrode correspond to charge movements the APs from distant neurons are highly attenuated as results from the analysis of Eq. (5) and therefore are filtered out by ICA and Newton-Raphson algorithms.

5. Results

We analyzed recordings from more than 20 tetrodes. Spike sorting produced an average of five clusters per tetrode. Each tetrode provided one or two neurons that had large enough amplitudes that could be used for this analysis. These neurons corresponded to those that were closest to the tetrode and had the best signal profiles. After a cubic spline interpolation, the four-dimensional data for each spike was used to estimate the corresponding independent components. The final result was to find the positions of several groups of charges in the tetrode space during each spike that reveals electrical patterns of activation during each AP.

Our algorithm was tested for an artificially generated spike. The method to obtain artificial spikes is to move a single or group of charges in the proximity of tetrode tips. Such an experiment can be easily performed by using computer simulations and has been presented in detail (Aur et al., 2005). Dependence of mean absolute percentage error for cubic spline interpolation (De Boor, 1978) over the noise level is displayed in Fig. 5. If the number of points is increased less than five times, the mean absolute percentage error is maintained under 3% for a signal noise ratio greater than 25 dB (SNR > 25 dB).

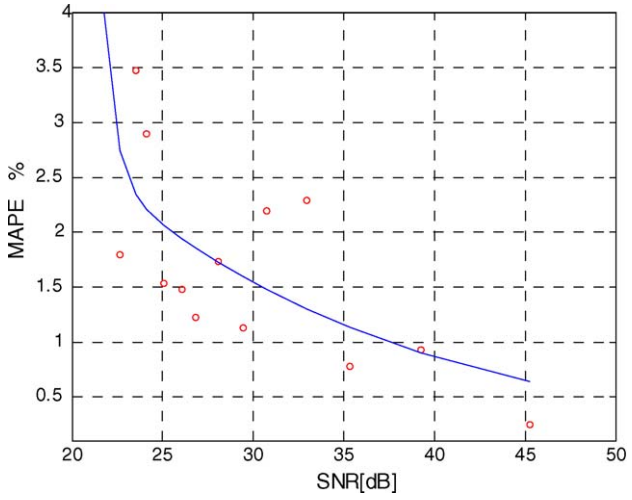

Fig. 5. The dependence of percentage error over SNR for a cubic spline interpolation. The number of points was increased by four in a charge movement model simulation. Mean absolute percentage error is computed MAPE = $1/N\sum_{i=1,N}|y_i - y_i^{\mathrm{intr}}/y_i| \times 100$ where y_i are data obtained from simulation and y_i^{intr} are data obtained from spline interpolation. Red circles are the computed MAPE values obtained from several simulations with decreasing SNR while the blue curve represents the optimal non-linear approximation (for interpretation of the references to color in this figure legend, the reader is referred to the web version of the article).

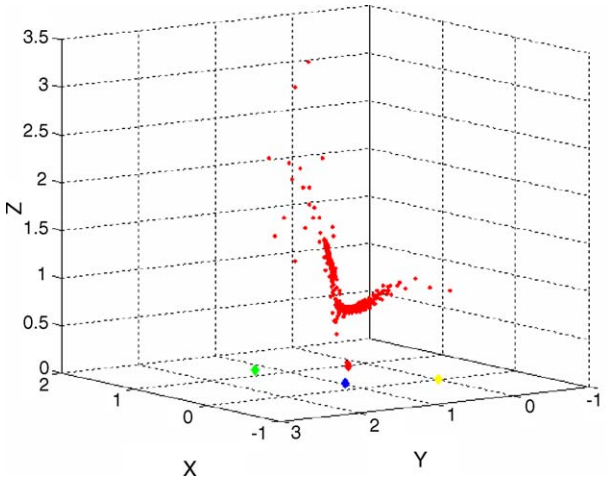

Fig. 6. Red dots correspond to a computed trajectory from a single charge movement from an artificial generated spike. Noise was added to simulate real recorded signals from measurements. Computed trajectory from spike is bent while simulated charge movement was linear (for interpretation of the references to color in this figure legend, the reader is referred to the web version of the article).

The representation of the estimated independent components for a single charge in movement is shown in Fig. 6. Gaussian noise was added to simulate recorded signals from real tetrode measurements. Even though the movement of the simulated charge is linear the computed charge trajectory in "tetrode space" is bent. Next, the trajectory "image" is obtained from ICA components by the described computational process. The non-linearity introduced by the computational equations has this "mirror effect" on the representation in the tetrode space. Since this "charge in motion" describes, in real space, a linear trajectory, it could very well define an electric cable or any other conducting device where charges are moving. In the case of tetrode data, such a trajectory computation as demonstrated by our methods can be viewed as representing an actual cable level image of the spiking neuron. This image however will appear transformed, specifically bent as we have shown.

Imagine seeing the real environment in a parabolic mirror. Objects appear deformed and sometimes would be hard to figure out as to what they do represent. Therefore, an attempt to reconstruct "the real physical space" would be more useful to visualize the results in the same way we are used to.

A bent representation of the estimated independent components from a real recorded action potential is shown in Fig. 7, while another view for the same AP is shown in Fig. 8. In these plots the tips of the tetrode are represented by colored diamonds starting with red for the first channel, green, blue and yellow for the second, third and fourth channel of tetrode, respectively. Each dot represents an estimated independent component which can be visualized potentially as group of electrical charges in movement.

The spatial shapes for several successive AP from the same neuron are slightly different. Differences in the amplitude and width of AP are highly visible even in single-electrode recordings but coherent explanations about the causes of this phenomenon have not been advanced. Now, viewed by tetrodes as

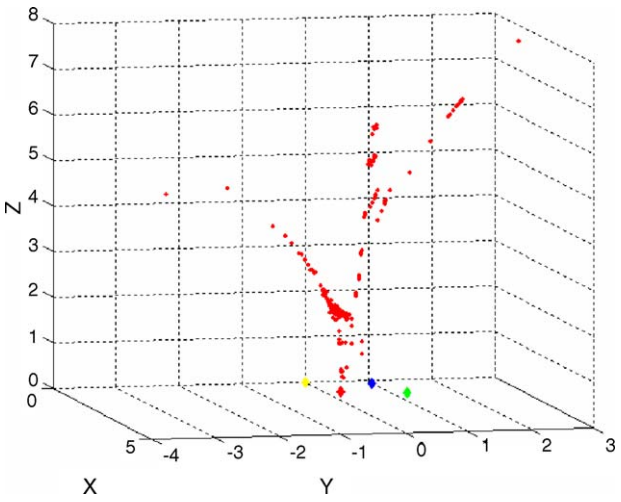

Fig. 7. Bent representation in tetrode space of electrical pattern of activation based on ionic flux. Each division on the axes is approximately 20 μM.

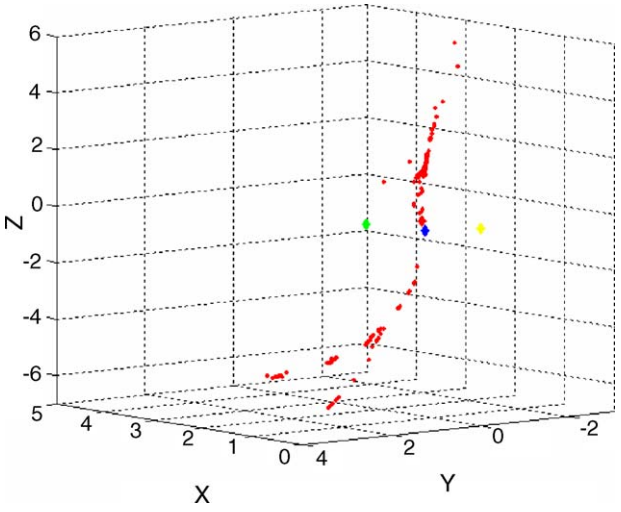

Fig. 8. 3D-view of electrical pattern of activation during an action potential. This representation tries to "de-bend" the directivity. Each division on the axes is approximately 20 μm.

a flux of charges, spikes are clearly not the same. More important in this story is that 3D spike representation may show an activation mechanism that controls electrical flow in each spike responsible for neuronal computation. This phenomenon of electrical flow control in spikes may be well associated to synaptic modulation and learning phenomena.

6. Discussion

Neurons function to transduce information via electrochemical mechanisms during behavioral tasks, acting as units performing several transformations on incoming signals. Since many results cannot be extrapolated from an in vitro scenario to the world of behaving animals, a method that can examine the detailed properties of neuronal activity in vivo would therefore be extremely valuable. Application of the methods suggested in this paper to extracellular recordings sheds a light on electrical processes within neurons during each spike, in vivo. Intracellular recordings in behaving animals could also provide similar information (Fee, 2000). However, this technique is extremely difficult to apply, uses only one electrode and therefore can be very limited in perceiving spatiality of electrical phenomenon.

The method proposed in this paper uses established, tetrode-based multichannel extracellular recordings in order to provide electrical spatial patterns of activation during each spike in freely behaving animals. This data analysis technique can be used by any system that can capture a neuronal spike signal simultaneously in four views, i.e., in a system where the four tips of the recording device are close together. The 3D image representation of the spike is possible because virtually each phase in our algorithm filters the recorded data. Starting from real hardware filtering in the preprocessing phase, ICA and finally the projection in the tetrode space by Newton-Raphson algorithm could all be considered filtering stages.

Besides 3D spike representation, the value of this technique is that it creates a potentially useful method to study the phenomena of learning and information flow in a neuronal network. For example, different dendritic activation patterns observed during each spike shows a spatial coding phenomenon that reflects in fact the physics of neuronal computation expressed within ionic flow.

From a mathematical perspective, computation is processing of information based on a finite set of operations or rules. Computation is mathematically defined by inputs, set of rules and outputs. In a simple computation, such is an arithmetic operation $a+b=c$, the inputs consist in values 'a' and 'b', the rule is '$+$' and the output is 'c'. However, to obtain the output value 'c' in a computer each quantity 'a', 'b' and 'c' need to have a physical correspondence. (e.g. current, voltage, etc.). We know that electron fluxes are responsible for fluctuations in voltage or currents. Therefore, the physical essence of classical computation is based on electron movement that obeys the laws of physics. Such an approach in this field began in the 1960s with Landauer theory regarding information principles and was continued with Feynman lectures in computation.

In similitude, in each spike a physical correspondence for inputs, set of rules and output can be revealed. We understood this issue after we performed several simulations on Hodgkin-Huxley (HH) model computing mutual information. Our analysis shows that mutual information between input signal and sodium flux is about two times that between input signal and output spikes during each spike (Aur et al., 2006). Since mutual information between input stimuli and sodium fluxes has these high values, then the incoming sodium fluxes can be considered during each spike to be the inputs. The set of rules in each AP are described by physical laws of motion that govern the movement of charges. Finally, the outputs can be considered to be in the form of outward K^+ fluxes.

For simplicity, in the above discussion we only considered the fluxes of sodium and potassium. However, in each spike several charges of Na^+, K^+, Cl^- and eventually Ca^{2+} perform complex computation obeying physical laws. The APs are generated by the opening and closing of channels that allow the flow of several charges. Channels are stochastic in nature and their conductances can also be reflected as a probability of their

opening. Since information-processing is based on ionic fluxes the "code" within each spike can be extremely complex and our approach is a step forward in understanding this computational mechanism.

Therefore, the main application of this method consists in associating computations with spatial electrical patterns in each spike. Since levels of electron movements have been already exploited in classical computing, here, the bio-physics of spike computation is reflected in spatial distribution of ions evidenced by the "image" of spatial patterns during each AP. The power of spike computation is given by high values of information transferred from stimulus to ionic fluxes. This analysis is a step forward in rethinking neuronal computation beyond the spike timing paradigm.

The complexity of the relationship between computation, information transfer and biological properties of neurons can indeed be seen to occur at various scales. At the most fundamental level, the computation and information transfer occurs on the basis of the dynamics and distribution of different ionic fluxes during the AP (Aur et al., 2006).

The second level at the cell scale involves spike coding usually viewed in the time domain. Known examples are well studied involving rate coding or spike coding (Gerstner and Kistler, 2002; Maass, 1997) that have been the premise of the strong development of artificial neural networks and artificial intelligence. This level of transfer can occur at the ensemble level where groups of neurons can be seen to encode for complex behavior (Barnes et al., 2005; Jog et al., 1999; Wilson and McNaughton, 1993).

A moderate analysis has been developed for the third level or "wave coding" as the final achievement of group of neurons in human fMRI studies (Cerf-Ducastel and Murphy, 2003; Poellinger et al., 2001).

There is a strong relationship between all these three observable levels of communication methods that confer strong information handling capabilities for neuronal networks. However this important and significant informational and computational power comes from the dynamics of different ionic fluxes during the APs.

Since multichannel data provides information from many neurons simultaneously, the properties of several neurons and the patterns of information processing within them can be studied over a time period, and potentially correlated to the behavioral paradigm. Investigation of learning may relate this variability of electric flow in neurons with behavior during freely behaving experiments in animals. Starting from this point of view, the analysis of electrical events in neurons during AP in vivo has potentially great significance and offers a new opportunity for improving our understanding of brain functions.

References

Amari S, Chen TP, Cichocki A. Stability analysis of learning algorithms for blind source separation. Neural Netw 1997;10(8):1345–51.

Aur D, Connolly CI, Jog MS. Computing spike directivity with tetrodes. J Neurosci 2005;149(1):57–63.

Aur D, Connolly CI, Jog MS. Computing information in neuronal spikes. Neural Process Lett 2006;23:183–99.

Barnes TD, Kubota Y, Hu D, Jin DZ, Graybiel AM. Activity of striatal neurons reflects dynamic encoding and recoding of procedural memories. Nature 2005;437(7062):1158–61.

Bell A, Sejnowski T. An information maximization approach to blind separation and blind deconvolution. Neural Comput 1995;7:1129–59.

Bierer D, Anderson J. Multi-channel spike detection and sorting using an array processing technique. Neurocomputing 1999;26–27:947–56.

Brenan KE, Campbell SL, Petzold LR. Numerical solution of initial-value problem in differential-algebraic equations. North-Holland, Amsterdam: Elsevier; 1989.

Buzsáki G. Large-scale recording of neuronal ensembles. Nat Neurosci 2004;7:5.

Cardoso JF. Super-symmetric decomposition of the fourth-order cumulant tensor, blind identification of more sources than sensors. In: Proceedings of the ICASSP'91; 1991. p. 3109–12.

Cerf-Ducastel B, Murphy C. FMRI brain activation in response to odors is reduced in primary olfactory areas of elderly subjects. Brain Res 2003;986:39–53.

Cover T, Thomas J. Elements of information theory. New York: Wiley and Sons; 1991.

De Boor C. A practical guide to splines. Springer-Verlag; 1978.

Fee MS. Active stabilization of electrodes for intracellular recording in awake behaving animals. Neuron 2000;27:461–8.

Gerstner W, Kistler WM. Spiking neuron models single neurons, populations. Plasticity Cambridge University Press; 2002.

Gray C, Maldonado P, Wilson M, McNaughton B. Tetrodes markedly improve the reliability and yield of multiple single-unit isolation from multi-unit recordings in cat striate cortex. J Neurosci Meth 1995;63(1–2):43–54.

Griffiths DJ. Introduction to electrodynamics. Prentice Hall; 1999.

Häusser M, Spruston N, Stuart GJ. Diversity and dynamics of dendritic signaling. Science 2000;290:739–44.

Helmchen F, Svoboda K, Tank DW. In vivo dendritic calcium dynamics in deep-layer cortical pyramidal neurons. Nat Neurosci 1999;2:989–96.

Holt GR, Koch C. Interactions via the extracellular potential near cell bodies. J Comput Neurosci 1999;6:169–84.

Hulata E, Segev R, Ben-Jacob E. A method for spike sorting and detection based on wavelet packets and Shannon's mutual information. J Neurosci Meth 2002;117:1–12.

Hyvärinen A, Karhunen J, Oja E. Independent component analysis. John Wiley and Sons; 2001.

Jog MS, Connolly CI, Kubota Y, Iyengar DR, Garrido L, Harlan R, et al. Tetrode technology: advances in implantable hardware, neuroimaging, and data analysis techniques. J Neurosci Meth 2002;117:141–52.

Jog MS, Kubota Y, Connolly CI, Hillegaart, Graybiel AM. Building neural representations of habits. Science 1999;286:1745–9.

Kasuga A, Enoki R, Hashimoto Y, Akiyama H, Kawamura Y, Inoue M, et al. Optical detection of dendritic spike initiation in hippocampal CA1 pyramidal neurons. Neuroscience 2003;118:899–907.

Kerr JND, Plenz D. Dendritic calcium encodes striatal neuron output during up-states. J Neurosci 2002;22:1499–512.

Lee TW, Girolami M, Bell AJ, Sejnowski T. A unifying information-theoretic framework for independent component analysis. Int J Comput Math Appl 2000;39(11):1–21.

Maass W. Networks of spiking neurons: the third generation of neural network models. Neural Netw 1997;10:1659–71.

Nolan MF, Malleret G, Dudman JT, Buhl DL, Santoro B, Gibbs E, et al. Behavioral role for dendritic integration: HCN1 channels constrain spatial memory and plasticity at inputs to distal dendrites of CA1 pyramidal neurons. Cell 2004;119:719–32.

Oesch N, Euler T, Taylor WR. Direction-selective dendritic action potentials in rabbit retina. Neuron 2005;47(5):739–50.

Oweiss KG, Anderson DJ. Spike sorting novel shift and amplitude invariant technique. Neurocomputing 2002;44–46:1133–9.

Poellinger A, Thomas R, Lio Lee PA, Makris N, Rosen BR, Kwong KK. Activation and habituation in olfaction—an fMRI study. Neuroimage 2001;13:547–60.

Quirk MC, Blum KI, Wilson MA. Experience-dependent changes in extracellular spike amplitude may reflect regulation of dendritic action poten-

tial back-propagation in rat hippocampal pyramidal cells. J Neurosci 2001;21(1):240–8.

Rebrik SP, Wright BD, Emondi AA, Miller KD. Cross-channel correlations in tetrode recordings: implications for spike-sorting. Neurocomputing 1999;2627:1033–8.

Sanchez VD. Frontiers of research in BSS-ICA. Neurocomputing 2002;49: 7–23.

Saraga F, Wu CP, Zhang L, Skinner FK. Active dendrites and spike propagation in multi-compartment models of oriens-lacunosum/molecular hippocampal interneurons. J Physiol 2003;552.3:673–89.

Scott A. Neuroscience, a mathematical primer. New York: Springer-Verlag; 2002.

Spencer L, Smith JW, Otis TS. An ultra small array of electrodes for stimulating multiple inputs into a single neuron. J Neurosci Meth 2004;133:1–2, 15, p. 109–114.

Takahashi S, Anzai Y, Sakurai Y. A new approach to spike sorting for multi-neuronal activities recorded with a tetrode /how ICA can be practical. Neurosci Res 2003;46:265–72.

Toth TI, Crunelli V. Solution of the nerve cable equation using Chebyshev approximations. J Neurosci Meth 1999;87:119–36.

Tian Y. Using rank formulas to characterize equalities for Moore–Penrose inverses of matrix products. Appl Math Comput 2004;147(2):581–600.

Wilson MA, McNaughton BL. Dynamics of the hippocampal ensemble code for space. Science 1993;261:1055–8.

Cogn Comput
DOI 10.1007/s12559-011-9106-3

From Neuroelectrodynamics to Thinking Machines

Dorian Aur

Received: 10 May 2011 / Accepted: 30 July 2011

Abstract Natural systems can provide excellent solutions to build artificial intelligent systems. The brain represents the best model of computation that leads to general intelligent action. However, current mainstream models reflect a weak understanding of computations performed in the brain that is translated in a failure of building powerful thinking machines. Specifically, temporal reductionist neural models elude the complexity of information processing since spike timing models reinforce the idea of neurons that compress temporal information and that computation can be reduced to a communication of information between neurons. The active brain dynamics and neuronal data analyses reveal multiple computational levels where information is intracellularly processed in neurons. New experimental findings and theoretical approach of neuroelectrodynamics challenge current models as they now stand and advocate for a change in paradigm for bio-inspired computing machines.

Keywords Artificial general intelligence · Brain computations · Machine learning · Neuroelectrodynamics · Neural correlates of consciousness

Introduction

At this moment, several scientists agree that an exponential increase in computer power or stored information does not automatically generate intelligent systems. Current artificial systems are far from matching human skills and intelligence. There are many questions regarding the link between neurophysiological processes, behavioral or cognitive aspects, and artificial intelligent systems. How is the world perceived in the brain, how do we store new memories? Can a current computer acquire a full range of mental capabilities? Is there a set of computational rules which can formalize human understanding? Are there truths only recognizable by the human mind? Can a direct equivalence between algorithm building and artificial intelligence be found? Can an intelligent system be built via detailed brain simulations? What is intelligence? Are there specific principles of AI that can be universal (general)? Is there a relationship between how computation is performed and intelligence? Finally, does computational capability or the models of computation count?

Many issues in understanding how computations are performed in the brain are generated by current reductionist models that mislead regarding computational power of neurons. This paper highlights a different paradigm, a different model of computation that shapes information processing in the brain.

Computation by Physical Interaction

Interactions can be often perceived in any natural system. From weak gravitational forces that keep the planets in their orbits to strong fundamental forces that bound the quarks together in protons, all these interactions model the world that we know today. The entire universe has been assimilated with a computing machine, a quantum computer [1], or a digital computer [2] that follows simple Turing machine rules [3]. Early theoretical ideas that computing is interaction came from Richard Feynman and Robin Milner [4–6] and have been further developed by Wegner and Goldin [7, 8]. However, these models have

D. Aur (✉)
Stanford University, Palo Alto, CA, USA
e-mail: DorianAur@gmail.com

Published online: 09 August 2011

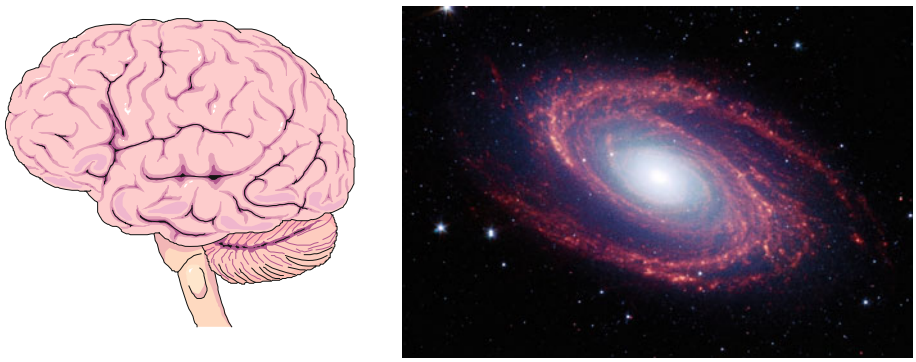

Fig. 1 The brain and the universe share similar physical laws where physical interaction defines a form of computation

received little attention from scientific community compared to Turing models. Since natural interactions lead to changes in physical fields, then alterations in electrical or gravitational field can be interpreted as states of an evolving computing machine (Fig. 1). All these natural models of computing by interaction allow stronger computability power than classical models [6, 9].

However, the mainstream of computational neuroscience and neural computational modeling focuses on spike timing dogma (STD) with well-known temporal features, firing rate [10] interspike interval (ISI) [11, 12] or spike timing-dependent plasticity (STDP) [13] where information is compressed in the temporal domain. The neurons simulated in networks as temporal computing machines represent strong reductionist models of developed computations in the brain.

The Failure of STD and Temporal Computing Machine

Regarded as a universal truth, STD does not need to be disputed or doubted in neuroscience. Extensive brain recordings and mathematical models are just needed to reinforce the temporal behavior of computing machine. However, the relationship between temporal patterns and information storage is missing (see the dilemma of synapses [14]). The neuron model becomes an information bottleneck that compresses any received information (Fig. 2a) [15]. Additionally, the integrate-and-fire model is "good enough" and even performs better in simulations than the Hodgkin Huxley model [16]. This incomplete knowledge from neuroscience misleads regarding several levels of computation that exist in neurons.

In a reductionist manner, all neural computational models compress temporal information. However, within biological cells, intracellular processes are always directly involved in information processing. The roots of intelligent action lie deep in information processing performed by single cells [17]. A classic example is Paramecium; it can swim around, avoid obstacles, and find food without any synaptic connections or spiking [18]. Without delivering spikes within a millisecond range, simple organisms show decision-making abilities [19]. Since electrophysiological recordings focus on temporal patterns, most analyses elude any subtle changes, electrical patterns that occur in neuronal spikes [20, 21]. However, these changes can be evidenced within sub-milliseconds during each generation of action potential [22]. While the role of computation in cognition is important [23], the failure of current neural models to provide an understanding of mind in computational terms is clear [24]. Contrary to the mainstream analysis of temporal patterns, recent models reveal complex electrical behavior of neurons at a subcellular scale directly involved in information processing [25–29]. This view is reinforced by experimental results [20–22, 30] and recent progress in understanding computations in the brain using a different paradigm [14]. The action potential (AP) is not so all-or-none event. The neuron "speaks" during a very short time, in less than a millisecond during AP generation. Therefore, in order to understand the neuron's language (meaning, semantics), one needs to carefully listen the "words" with adequate techniques. Spike directivity (SD) is a computational tool that provides information regarding spatial distribution of electrical processes developed in the neuron during a generated action potential [20, 21].The variability of recorded AP shapes is transformed into the variability of vectors that quantify changes in transient charge density during AP propagation [21]. Therefore, during a spike, the spike directivity vector reveals the electrical outcome determined by complex microscopic interactions inside the cell and therefore SD reflects changes in intracellular computations.

While temporal features carry little information about object categories, behavior, or semantics, the transient charge density within spikes and resulting spike directivity patterns (Fig. 4a) reveal hidden information and provide better results in discriminating behavioral changes during a procedural T-maze tasks [14, 22, 31] or categories of visual object recognition [30]. Since generated spikes from a single recorded cell can carry different information regarding behavioral semantics or presented objects spikes cannot be added, averaged (e.g., mean firing rate) without loosing meaningful information.

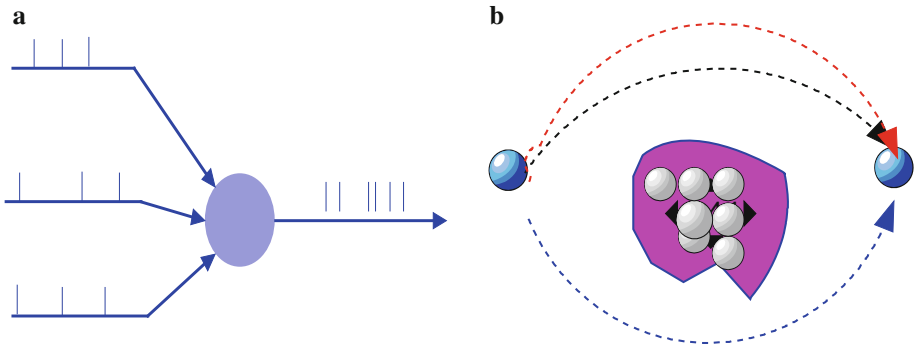

Fig. 2 Any computational system has to access the memory to write (code) and read (decode) information. **a** The spike timing neuron compresses temporal information. **b** The processing and exchange of information are intracellularly hidden; neurons do not compress information in temporal domain. Schematic representation of computing by interaction, the protein structure in the cell, and electric interactions provide "direct" access to stored memory. Information can be quickly read and written during electric interactions

Neuroelectrodynamics: Brain Computing is Interaction

The brain is a computing machine that uses electrical charges and their interaction to read, write, and process information. Since information can be stored in a distribution of electric charges, throughout the neuron within soma, dendrites, and axonal branches, most macromolecular structures (e.g., proteins) embed information [32].

The process of computation by interaction can be modeled on a digital computer using so-called computational cube (Fig. 3a) [14]. The dynamics of electric charges and their interaction are described by difference equations, and particle swarm algorithms required to perform optimization and discriminate between several presented images. This model of developed interaction shows that more information can be embedded in a spatial distribution of electric charges rather than in the temporal behavior of spikes. Therefore, the effect of changes in molecular structure, molecular interactions has to be reconsidered and incorporated as integral parts of "neural computations" in addition to extracellular fields. The electrostatic properties of biological molecules are important and are determined by their charge-density distribution. The electrostatic effects are "felt" by surrounding biomolecules, ions, and other macromolecular formations [27, 33]. While protein dipole moments can be obtained experimentally for small proteins, the calculation of dipole moments can be theoretically achieved knowing the three-dimensional position of all atoms [34, 35]. Therefore, during transitory events, information regarding the distribution of atoms/charges can be seen to be embedded in a vector representation of the dipole moment (Fig. 4b). Additionally, protein characteristics are sensitive to changes in the electric field generated in the surrounding environment, which can alter protein conformational characteristics, formation of complex protein aggregates, and intrinsic interactions with other molecules and bonding.

Neuroelectrodynamics describe computation as an ongoing process shaped by the dynamics and interactions of electric charges in the brain. The process of interaction can be evidenced during action potentials and synaptic spikes since transient electrical patterns occur in each generated spike. Intrinsic information processing is related to physical machinery able to alter the dynamics of electric charges and their spatial distribution at molecular level. The dynamic rearrangement of electric charges in space, in macromolecular formations can be seen as the "coding phase" where information is written in the structure. At molecular level, the spatial rearrangement of charges is regulated by changes in gene expression, protein folding, alterations in electric field, polarizations or the effect of hormones, and neurotransmitters. This new model of interactive computation developed intracellularly within every spike is fundamentally a non-Turing phenomenon. The occurrence of electrical patterns in spikes [20] is a result of different regulatory mechanisms from gene selection/expression, DNA computations to membrane properties involved in computation. Therefore, information processing in the neuron requires a combination of different forms of computation where electrical interactions have an integrative role bringing several mechanisms of information processing together.

There is a close relationship between coding and decoding information. Since a certain spatial distribution of electric charges alters the local electric field then, local dynamics of electric charges are influenced by these changes (Fig. 2b). A reciprocal relationship between coding (writing information) and decoding in terms of "reading" information does exist and is reinforced in neuroelectrodynamics. Therefore, the "decoding phase" can be revealed by a preferential spatial occurrence of electrical patterns and transient charge-density dynamics of neuronal or synaptic spikes. These transient changes occur selectively in neurons involved in information processing

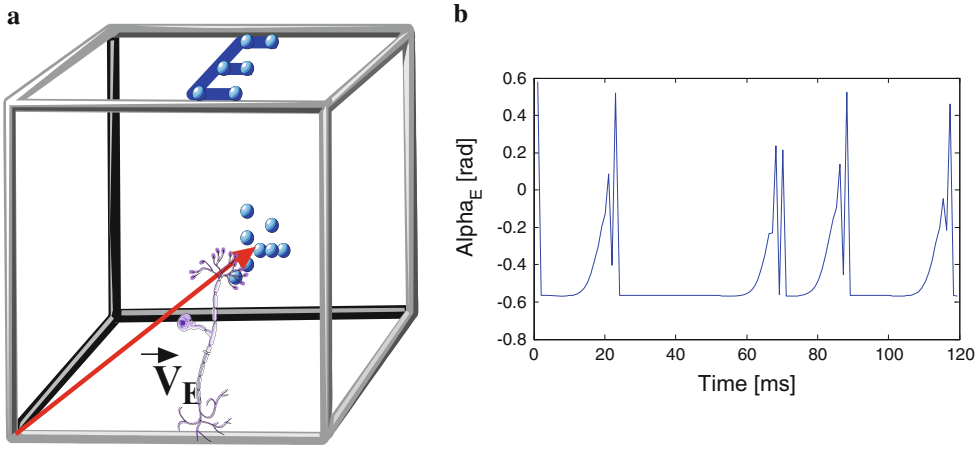

Fig. 3 The representation of computational cube and generated electrical patterns in space and in time adapted from [14]. **a** The transitory dynamics that occurs during a spike can be approximated with a vector and is a result of interaction between moving electrical charges (e.g., ions Na^+, K^+) and the distribution of charges within intracellular space (macromolecules, proteins). **b** The temporal spike-like behavior within a computational cube embeds little information regarding presented images

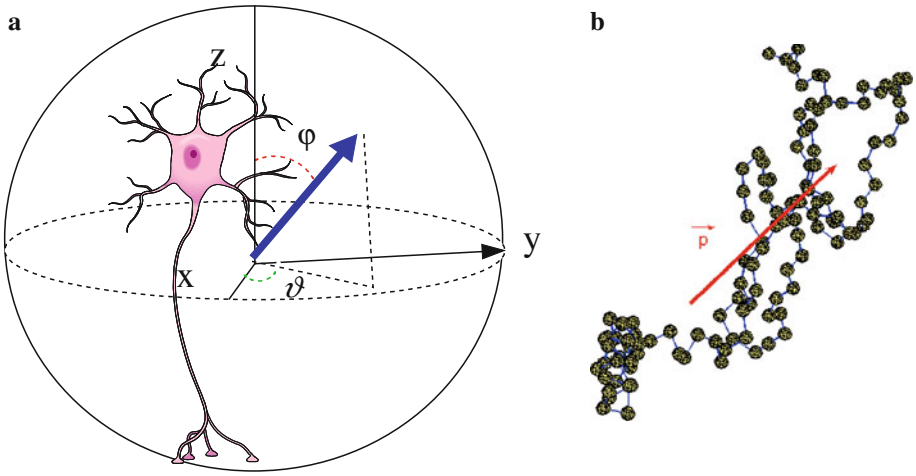

Fig. 4 Electrical patterns occur at different scales. In action potentials, electrical patterns are not random but they reflect intracellular information processing and are related to behavioral or cognitive events [22, 30]. **a** Schematic representation of a scaled neuron included in a unit sphere. Spike directivity vector in *red color* is a reflection of transient density distribution of electric charges during AP propagation. **b** Schematic representation of a protein and the generated dipole moment $\vec{p}$ in *red arrow* (Color figure online)

and provide significant evidence regarding changes in behavior or object recognition [14, 29].

Neuroelectrodynamics, Semantics, and Consciousness

The transient charge density that occurs during a millisecond time of AP generation is a result of local interactions within neuron and provides more information regarding behavioral semantics than temporal patterns [29, 30]. In this case, the resulting semantics are an outcome of computation by interaction. On the other hand, consciousness characterized as a "major puzzle confronting the neural view of the mind" [36] has received a lot of attention over the past years. Using fMRI signals, He and Raichle [37] hypothesized that slow cortical potentials (SCP) with frequency bandwidths below 1 Hz are determinant characteristic to the "emergence of consciousness". This view opposed to an earlier hypothesis advanced by Crick and Koch [36] where only frequencies close to 40 Hz are critical to awareness and consciousness. A later hypothesis [38] points to a different direction where "the exact timing" of spikes influences "the competition" and relates to neural correlates of consciousness.

Indeed, the phenomenon of consciousness requires a scientific explanation. However, the above explanation does not seem to come from spike timing models with millisecond precision, it involves an understanding of subtle significant changes of electrical interactions and charge dynamics in specific brain regions. In this case, the fundamental level of computation seems to be carried by the dynamics and interaction of electric charges and can be revealed using simultaneous recordings of action potentials and local field potentials from human patients or animal models of epilepsy [39].

The process of interaction between incoming information carried by electrical field, ionic fluxes in spikes, and preexisting polarizations within macromolecular structures

(where memories are stored) is strongly regulated. At different levels, the spiking activity is controlled and the fundamental frequency is locally continuously maintained. However, during or even before the seizure, in specific epileptogenic regions, reaction diffusion phenomena [40] and nonlinear electric interactions can lead to local internal resonances and chaos generation in the brain. Similar phenomena shape the planetary dynamics and can be expressed by using similar mathematical models [41]. The model of interaction in the brain can be simply described using the Hamiltonian formalism of electric charges motion [42]:

$$\frac{\mathrm{d}q}{\mathrm{d}t} = \frac{\partial H}{\partial p} \text{ and } \frac{\mathrm{d}p}{\mathrm{d}t} = -\frac{\partial H}{\partial q} \tag{1}$$

where $p = \dot{q}$ and can be rewritten in the form of action angle variable:

$$H = \sum_{I=1,N} H_0(I_i) + \varepsilon V(I_1, I_2, \ldots I_N, \theta_1, \theta_2, \ldots \theta_N) \tag{2}$$

N represents the degree of freedom and H_0 is the unperturbed dynamics (non-interacting charges) [43]. The presence of perturbation leads to the following condition for internal nonlinear resonances [43, 44]:

$$n_1\omega_1(I_{10}) + \cdots + n_N\omega_N(I_{N0}) = 0 \tag{3}$$

where n_1,…, n_N are natural numbers. If the perturbation energy is higher than the energy difference between the two closest unperturbed resonant orbits [45]:

$$\Delta H_i > E_{i+1} - E_i \tag{4}$$

chaotic dynamics develops. Indeed, chaos can naturally develop in Hamiltonian systems with many degrees of freedom that describe the motion of charged particles in electric field (Arnold diffusion, resonance overlap) and is locally maintained in the brain if neurons do not fire or have a very low firing rate [42].

Significant local changes in the dynamics of electric field precede and last after each seizure. Since significant changes in neuronal activity determine alterations in electric field that can be revealed using complexity measures, this phenomenon provides a scientific explanation for neural correlates of consciousness that may involve subtle quantum aspects [25, 46]. Close to random processes, longer periods of chaotic dynamics impair information processing and transmission during preictal and postictal states (Fig. 5a). The analysis of complexity measure shows that consciousness is a result of complex interactions that provide "integrated information" [47, 48]. If these interactions are too weak (the cells do not fire), information cannot be intracellularly "read" or "written" and therefore cannot be integrated. Excessive strong interactions determined by aberrant simultaneous firing during the epileptic seizures can generate excessive order that impairs information processing and integration. Altered states of consciousness can occur during the seizure when "excessive order" is generated by extended electrical resonances. Therefore, rhythmic neuronal firing that constrains the frequency range of oscillations is required to maintain the conscious state (Fig. 5b).

An increase in the amplitude of low-frequency bandwidths (<1 Hz) reflects local chaotic diffusion while higher frequencies characterize synchronous neuronal activity or abnormal extended electrical resonant regimes (>150 Hz). Therefore, maintaining and regulating a fundamental bandwidth of frequencies is critical (Fig. 5b). The occurrence of high-energy spectrum in different atypical rhythms, very slow cortical waves, or very strong high-frequency harmonics (>150 Hz) represents markers of dysfunction.

Toward Bio-Inspired Computers

The entire biophysical model of the brain is built to maintain continuous interactions in the system to integrate different sources of information. A simple analysis of biological neural networks identifies two different types of interactions. During spike activity, "strong" interactions intracellularly occur within dendrites, soma, axon while "weak" forms of interaction between neurons can be described by synaptic and non-synaptic interactions (e.g., electric field). These interactions that intracellularly occur can be related to the mechanism of neurotransmitters action or different activities in astrocytic glial cells. The general framework of temporal coding approximates only a small part of weak interactions and ignores strong interactions that occur within cells. In general, temporal patterns provide an approximation of "weak" interactions. In addition, not all interactions can be described by weight type connections [49]. Therefore, following the spike timing dogma, intracellular interactions were simplified to reinforce the temporal coding hypothesis. From a computational perspective, strong interactions have to be reconsidered. These intracellular interactions are built using at least three major regulatory loops that are strongly interconnected. The fundamental loop of electric interactions is modulated by neurotransmitter systems and genetic regulatory mechanisms of protein synthesis (Fig. 6) [12]. The process of gene regulation (transcription) involved in protein synthesis can be mathematically modeled by systems of differential equations:

$$\dot{x} = Nv(x) \tag{5}$$

where x are the concentration variables, v the reaction rates, and N is the stoichiometry matrix [50, 51]. The changes in gene regulation are essential to individual

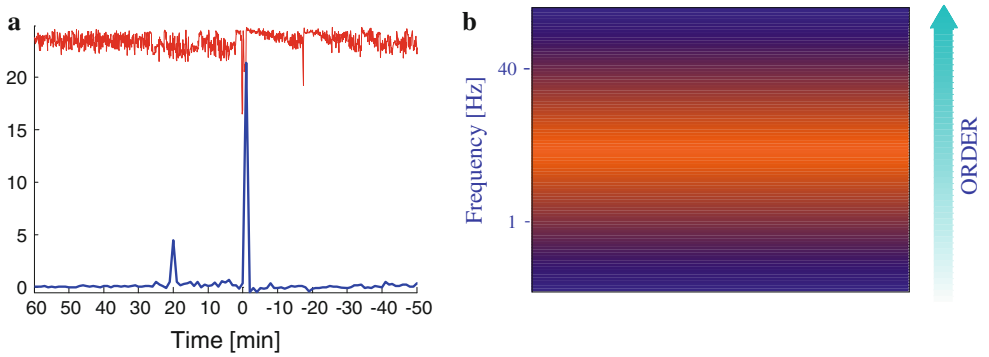

Fig. 5 The seizure generation becomes a window to understand consciousness in computational terms. **a** The power of high-frequency oscillations is represented in blue color (adapted from [42]). Changes in complexity are scaled and represented in *red color*. Chaotic diffusion is maintained before the epileptic seizure and is characterized by high values of complexity. The strongest peak (in *blue color*) occurs during the ictal state and represents "extreme" order detected in electric field with very low complexity values. **b** The conscious state is maintained as long as the dynamics of electric charges are regulated by rhythmic neuronal activity. The *arrow* points toward increased order. Very low frequencies are specific for chaotic dynamics (*bottom*), while high-frequency oscillations characterize excessive order in the dynamics of electric charges (*top*). Altered states of consciousness are related to "excessive" order during ictal phase or chaotic diffusion in the preictal or postictal phase (see changes in complexity measure **a**) (Color figure online)

neuron function, include enzymatic reactions and may determine protein synthesis and degradation. Slow variables are typically total protein concentrations, while fast variables describe metabolites and biochemical complexes. The Eq. 5 can be rewritten to include slow variables x^s, N^s, v^s, and fast variables x^f, N^f, v^f [51]. In general, important effects generated by fast and slow changes in electric field were neglected; however, experimental work has shown that gene expression and protein synthesis depend on electromagnetic interactions [52–54]. These results show that information encoded in DNA/RNA might have been selected and "written" in the molecular structure by changes in electromagnetic field.

Many neurotransmitters modulate neuronal activity and are involved in information processing by changing the nature of molecular interactions. Fast-acting neurotransmitters have effects via ionotropic receptors, which occur in milliseconds. Other neurotransmitters may determine slower, longer-lasting effects operating in minutes or even longer [55]. Similar systems of differential equations as in Eq. 5 can be written to include neurotransmitter regulation with their fast and slow dynamics. However, since the new synthesised proteins can be directly involved in the regulation of neurotransmitter release [56, 57], this system of differential equations that describes the neurotransmitter regulation has to be interconnected with the upper loop of protein synthesis (Fig. 6). In addition, the alterations of electrical and chemical gradients can modulate the neurotransmitter transporters [58]. Importantly, the entire system needs to include the regulation of endogenous electric field, the dynamics of electric charges. The electrical regulation can be modeled using the Hamiltonian formalism presented above. However, all these different interconnected levels provide just a basic model of complex regulatory mechanisms required to maintain the process of computing by interaction in biological neurons. Indeed, the ability to simulate these interactions using algorithmic models and Turing framework is limited. However, the recent progress in synthetic genomics [59, 60] could open the possibility to build bio-inspired computers that follow the architecture presented in Fig. 6. Small molecular computing machines can be built use genetic codes, synthetic proteins [60], and then interconnected together in a general framework as presented in NED. We already have shown that information can be "read" using simple techniques [20, 21]. The biological substrate can act within a biological context to store endogenously information in the molecular structure and can be interfaced with digital computers that may use different types of interactions to "read" or "write"

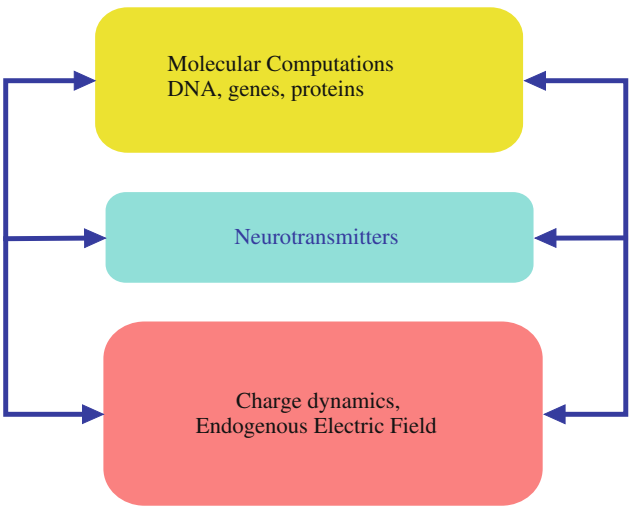

Fig. 6 The fundamental model of computation by interaction is maintained by at least three regulatory interconnected systems

information from or within molecular structures. Outside of the biological context, the synthetic biological substrate is physically realizable and could be used for purposes to build hybrid computers. Therefore, the future of computing structures may not necessarily rely solely on current silicon technology [61].

Discussion

There is a huge difference between human mind capabilities and the power of current computers that attempt to mimic human performance. The reductionist view of STD has lead to a failure in understanding intelligent computations in the brain. Neuroscience and neural computation have perpetuated the gimmick of spike timing and reductionist models that have lead nowhere in understanding the neural code. Indeed, using traditional optimization principles, artificial systems can adapt to environment requirements; however, they do not describe essential characteristics of computations performed in the brain. In order to perform intelligent action, many traditional approaches use reactive models, machine learning techniques, statistics combined with huge databases. Recent technical achievement at IBM, the artificial intelligent program developed and called Watson shows how difficult is to incorporate semantics in current computing machines even though the Jeopardy game provides an ideal environment to build interactions and acquire semantics [62]. However, Watson would need to be completely retrained to achieve different tasks in different environments. Moved in a real "environment," Watson would not be able to race former human competitors. The attempt to change what Watson is doing will increase the cost of design and probably the carried "memory". Therefore, Watson offers a clear view of current limitations in building AI systems. Indeed, Watson reflects the ingenuity of many engineers from IBM to embed algorithmically all sorts of interactions. In fact, this model shows our limits to understand and replicate bio-intelligent computations developed in the brain.

Neuroelectrodynamics brings a new, different path to build intelligent computations and points to a specific model of information by interaction developed in the brain [14]. These intrinsic computations intracellularly developed in the brain have no direct algorithmic solutions. Since computing by interaction is intrinsically a non-Turing model of computation, these computations can be hardly replicated on current computers. This model of computation has been previously hinted in computer science by few without pointing explicitly to brain processes since spike timing models did not allow such a link to be made. NED points to change in paradigm regarding computational systems required to understand cognitive events and build strong intelligent systems. Computing by interaction is necessary to embed semantics at the smallest level in order to perform intelligent action. Therefore, one can predict that understanding the brain language and biological substrate [60] "can change computing forever, even if most computer scientists don't know it yet".

Conclusion

Neurons do not seem to compress temporal information, they process, store, and exchange information. Information processing and exchange of information in neurons are hidden during a millisecond time frame of action potential propagation. The transitory electrical patterns in spikes are built upon the existing order in molecular structure [27, 32]. Indeed, information processing within neurons is continuous; however, every neuron "speaks" in less than a millisecond during AP generation and the action potentials are its "words". Therefore, the process of computation cannot be reduced to a synaptic communication of information between neurons. During computation, information can be simultaneously "read," "written," and integrated by electric interactions. Specific forms of computation by interaction define an intrinsic non-Turing (non-halting) model of information processing in the brain [8, 25, 27]. Indirectly, the measure of complexity provides the answer to the most intriguing question. Why do neurons always spike? Paraphrasing Schrödinger [63], neuronal firing is required to create order in the brain (disordered environment) against the second law of thermodynamics. The new model (NED) highlights brain computations, brain language instead of neural coding or neural computing [14]. NED points to a change in paradigm required to build more efficient bio-inspired computing machines by directly using the biological substrate. Once such computing models is built, and they can help us to better understand how perception is transformed into recognition almost instantaneously, how word-forms are transformed into meaning in computational terms. In these intelligent systems, understanding semantics and implementing awareness and consciousness may be vital to perform "general intelligent action". Understanding the new model of computation developed in the brain can be an important step to develop reliable artificial intelligent systems with general purpose.

References

1. Lloyd S. Programming the Universe: a quantum computer scientist takes on the cosmos. 1st ed. New York: Knopf; 2006.

2. Zuse K. Elektronische Datenverarbeitung. 1967; 8:336–44.
3. Schmidhuber J. Alle berechenbaren Universen, Spektrum der Wissenschaft (German edition of Scientific American), Spezial 3/07; 2007. pp. 75–9.
4. Feynman RP. Feynman lectures on computation. Perseus Books Group. ISBN 0738202967; 2000.
5. Hey Tony. Richard Feynman and computation. Contemp Phys. 1999;40(4):257–65.
6. Milner R. Computing is interaction. In Proc. IFIP Congress (1); 1994. p. 232–3.
7. Wegner P. Why interaction is more powerful than algorithms. Commun ACM. 1997;40(5):80–91.
8. Goldin D, Wegner P. The interactive nature of computing: refuting the strong church-Turing thesis. Minds Mach. 2008;18(1):17–38.
9. Siegelmann HT. The simple dynamics of super Turing theories. Comput Sci. 1996;168:461–72.
10. McClelland JL, Rumelhart DE. Exploration in parallel distributing processing. Cambridge: Brandford Books, MIT Press; 1988.
11. Gerstner W, Kistler WM. Spiking neuron models single neurons, populations, plasticity. Cambridge, UK: Cambridge University Press; 2002.
12. Izhikevich EM. Resonate-and-fire neurons. Neural Netw. 2001; 14:883–94.
13. Caporale N, Dan Y. Spike timing-dependent plasticity: a Hebbian learning rule. Annu Rev Neurosci. 2008;31:25–46.
14. Aur D, Jog M. Neuroelectrodynamics—understanding the brain language. Amsterdam, Netherland: IOS Press; 2010.
15. Buesing L, Maass W. A spiking neuron as information bottleneck. Neural Comput. 2010;22(8):1961–92.
16. Lazar AA. Population encoding with Hodgkin-Huxley neurons. IEEE Trans Inf Theory. 2010;56:821–37.
17. Ford BJ. The secret power of the single cell. The New Scientist 2010;206(2757):26–7.
18. Kung C. The physiological basis of taxes in paramecium. Ann Rev Physiol. 1982;44:519–34.
19. Ford BJ. On Intelligence in Cells: the case for whole cell biology. Interdisc Sci Rev. 2009;34(4):350–65.
20. Aur D, Jog MS. Building spike representation in tetrodes. J Neurosci Methods. 2006;157(2):364–73.
21. Aur D, Connolly CI, Jog MS. Computing spike directivity with tetrodes. J Neurosci Methods. 2005;149(1):57–63.
22. Aur D, Jog MS. Neuronal spatial learning. Neural Process Lett. 2007;25(1):31–47.
23. Chalmers DJ. A computational foundation for the study of cognition (unpublished manuscript); 1997.
24. Horst S. Symbols, computation and intentionality: a critique of the computational theory of mind. Berkeley and Los Angeles: University of California Press; 1996.
25. Hameroff S, Nip A, Porter M, Tuszynski J. Conduction pathways in microtubules, biological quantum computation, and consciousness. Biosystems. 2002;64:149–68.
26. Pidaparti RM, Primeaux D, Saunders B. Modeling and simulation of biological self-assembly structures from nanoscale entities. J Nanosci Nanotechnol. 2007;7(12):4248–53.
27. Woolf NJ, Priel A, Tuszynski JA. Nanoscience: structural and functional roles of the neuronal cytoskeleton in health and disease. Heidelberg: Springer; 2009.
28. Poznanski RR. Towards an integrative theory of cognition. J Integr Neurosci. 2002;1:145–56.
29. Craddock TJA, Tuszynski JA, Priel A, Freedman H. Microtubule ionic conduction and its implications for higher cognitive functions. J Integr Neurosci. 2010;9(2):103–22.
30. Aur D. Where is the 'Jennifer Aniston neuron'? available from Nature Precedings. http://dx.doi.org/10.1038/npre.2010.5345.2 (2010).
31. Aur D, Jog M. Reading the neural code: what do spikes mean for behavior?. Available from Nature Precedings http://dx.doi.org/10.1038/npre.2007.61.1 (2007).
32. Levitt M, Chothia C. Structural patterns in globular proteins. Nature. 1976;261:552–8.
33. Tuszynski JA, Luchko T, Carpenter EJ, Crawford E. Results of molecular dynamics computations of the structural and electrostatic properties of tubulin and their consequences for microtubules. J Comput Theor Nanosci. 2004;1(4):392–7.
34. Antosiewicz J. Computation of the dipole moments of proteins. Biophys J. 1995;69(4):1344–54.
35. Takashima S. Measurement and computation of the dipole moment of globular proteins III: chymotrypsin. Biophys Chem. 1996;58(1–2):13–20.
36. Crick F, Koch C. Towards a neurobiological theory of consciousness. Seminars Neurosci. 1990;2:263–75.
37. He BJ, Raichle ME. The fMRI signal, slow cortical potential and consciousness. Trends Cogn Sci. 2009;13(7):302–9.
38. Crick F, Koch C. A framework for consciousness. Nat Neurosci. 2003;6(2):119–26.
39. Aur D. Understanding the physical mechanism of transition to epileptic seizures. J Neurosci Methods. 2011; doi:10.1016/j.jneumeth.2011.05.028.
40. Conrad M, Kampfner RR, Kirby KG, Rizki EN, Schleis G, Smalz R, Trenary R, Hastings HM. Towards an artificial brain. BioSystems. 1989;23(2–3):175–218.
41. Voyatzis G. Chaos, order, and periodic orbits in 3:1 resonant planetary dynamics. Astrophys J. 2008;675(1):802–16.
42. Aur D. The physical mechanism in epilepsy—understanding the transition to seizure submitted, available also from Nature Precedings. http://hdl.handle.net/10101/npre.2010.5398.1 (2010).
43. Chirikov BV. A universal instability of many-dimensional oscillator systems. Phys Rep. 1979;52(5):263–379.
44. Reichl LE. The transition to chaos: conservative classical systems and quantum manifestations. New York: Springer Verlag; 2004.
45. Luo ACJ. Singularity and dynamics on discontinuous vector fields, monograph book series in nonlinear science and complexity (physics). Amsterdam: Elsevier; 2006.
46. Pereira Alfredo Jr. Astrocyte-trapped calcium ions: the hypothesis of a quantum-like conscious protectorate. Quantum Biosyst. 2007;2:80–92.
47. Balduzzi D, Tononi G. Integrated information in discrete dynamical systems: Motivation and theoretical framework. PLoS Comput Biol. 2008;4(6):e1000091.
48. Tononi G. An information integration theory of consciousness. BMC Neurosci. 2004;5:42.
49. McClelland JL, Rumelhart DE. Explorations in parallel distributed processing: A handbook of models, programs, and exercises. Cambridge: MIT Press; 1988.
50. Heinrich R, Schuster S. The regulation of cellular systems. New York: Chapman & Hall; 1996.
51. Berthoumieux S, Brilli M, de Jong H, Kahn D, Cinquemani E. Identification of metabolic network models from incomplete high-throughput datasets. Bioinformatics. 2011;27(13):i186–95. art. no. btr225.
52. Rao S, Henderson AS. Regulation of c-fos is affected by electromagnetic fields. J Cell Biochem. 1996;63(3):358–65.
53. Hirai T, Yoneda Y. Transcriptional regulation of neuronal genes and its effect on neural functions: gene expression in response to static magnetism in cultured rat hippocampal neurons. J Pharmacol Sci. 2005;98(3):219–24.
54. Goodman R, Blank M. Insights into electromagnetic interaction mechanisms. J Cell Physiol. 2002;192(1):16–22.
55. Kandel E, Schwartz J, Jessell T. Principles of neural science. 4th ed. McGraw-Hill Medical; 2000. ISBN: 0838577016.

56. Cheetham JJ, Murray J, Ruhkalova M, Cuccia L, McAloney R, Ingold KU, Johnston LJ. Interaction of synapsin I with membranes. Biochem Biophys Res Commun. 2003;309(4):823–9.
57. Haase J, Killian A-M, Magnani F, Williams C. Regulation of the serotonin transporter by interacting proteins. Biochem Soc Trans. 2001;29(6):722–8.
58. Mortensen OV, Amara SG. Dynamic regulation of the dopamine transporter. Eur J Pharmacol. 2003;479(1–3):159–70.
59. Wooley JC, Lin HS. Catalyzing inquiry at the interface of computing and biology, report of the National Research Council of the National Academies. Washington: National Academy Press; 2005.
60. Gibson DG, Glass JI, Lartigue C, Noskov VN, Chuang R-Y, Algire MA, Benders GA, et al. Creation of a bacterial cell controlled by a chemically synthesized genome. Science. 2010; 329(5987):52–6.
61. Parker AC, Joshi J, Hsu C–C, Singh NAD. A carbon nanotube, implementation of temporal and spatial dendritic computations. In: Proceedings of the 51st IEEE midwest symposium on circuits and systems. 2008; pp. 818–21, 10–13.
62. Frenkel KA. Schooling the Jeopardy! champ: far from elementary. Science. 2011;331(6020):999.
63. Schrödinger E. What is life? The physical aspect of the living cell. New York: Macmillan; 1945.

ELSEVIER

Journal of Neuroscience Methods 149 (2005) 57–63

JOURNAL OF NEUROSCIENCE METHODS

www.elsevier.com/locate/jneumeth

Computing spike directivity with tetrodes

Dorian Aur [a,*], Christoper I. Connolly [b], Mandar S. Jog [a]

[a] *Department of Clinical Neurological Sciences, Movement Disorders Program, London Health Sciences Centre, 339 Windermere Rd., London, Ont., Canada N6A 5A5*

[b] *SRI International, Menlo Park, CA, USA*

Received 6 January 2005; received in revised form 4 May 2005; accepted 5 May 2005

Abstract

The ability of neurons to generate electrical signals is strongly dependent on the evolution of ion-specific pumps and channels that allow the transfer of charges under the influence of electric fields and concentration gradients. This paper presents a novel method by which flow of these charge fluxes may be computed to provide directivity of charge movement. Simulations of charge flow as well as actual electrophysiological data recorded by tetrodes are used to demonstrate the method. The propagation of charge fluxes in space in data from simulation and actual recordings during action potential can be analyzed using signals recorded by tetrodes. Variation in spike directivity can be estimated by computing singular value decomposition of the estimated 3D trajectory data. The analysis of the spike model can be accomplished by performing simulations of presumed equivalent moving charges recorded by the tetrode tips. For in vivo spike recordings, the variation of spike directivity could be obtained using several spikes of selected neurons considering the charge movement model (CMM). The relationship between computer simulation results and tetrode data recordings is examined. The paper concludes by showing that the method for calculating directivity in actual spike recordings is robust. The method allows for improved filtering of data and more importantly may shed light on furthering the study of spatio-temporal encoding in neurons.

Keywords: Tetrode; Spike modelling; Singular value decomposition; Newton–Raphson

1. Introduction

The brain is composed of a large number of electrically active cells that communicate with each other. Starting from the early work of Hebb (1949), understanding of brain function was directed toward the coding properties of groups of neurons named “cell assemblies”. Few studies focused on the spatial properties of the action potential (AP). In this context plasticity changes have been related to overall connection strength between the pre- and postsynaptic neurons.

The origins of the problems regarding view of cell functioning at an electrophysiological level currently and in the past may arise from the limited ability of single cell recordings that primarily analyze mainly stereotyped waveforms. In addition, most research that has studied large populations of neurons (Zhang et al., 1998) hoping to find pattern of activities, has largely ignored the study of spatial distribution of electrical events from single spikes as a method of information coding. Current thinking holds that, since the spike is considered to be a reasonably stereotyped waveform for individual cells, information flow from cell to cell is supposed to be carried by the occurrence of the AP at particular times or rates. In this respect, the spike is felt to be a passive event that does not itself code for anything. Indeed physiologists often reduce the spike to a discrete scalar event in time and analyze behavior in this context alone.

It is therefore possible that the flow of information with spike events may be communicated within the milieu of the extracellular space and such information to the surrounding neurons is intrinsic and important in determining the flow of information outside of what is communicated through the spike event alone. However, spatial features of spikes are an essential part of the surrounding milieu of a biological cell. Processing of information received from neighboring

* Corresponding author. Tel.: +1 519 685 8300x32758.
E-mail address: daur2@uwo.ca (D. Aur).

0165-0270/$ – see front matter © 2005 Elsevier B.V. All rights reserved.
doi:10.1016/j.jneumeth.2005.05.006

neurons involve activities in several synapses, ionic channels, changes in membrane potential that usually have a spatial distribution.

In order to study the spatial properties of individual neurons and how they affect the spatio-temporal spread of information requires the collection of multi-dimensional data for every spike. Tetrode recordings that utilize four tips allow such a 4D view of the spike. The goal of much tetrode-based research is to study these interactions by assigning spikes to different neurons. Several spike-detection and sorting methods have been proposed in the literature (Gray et al., 1995; Jog et al., 1999, 2002; Sahani et al., 1998). The method developed by Takahashi et al. (2003) combines an independent component analysis and *k*-means clustering to solve the spike-overlapping problem within tetrode recordings. Recently Emondi et al. (2004) developed a reliable procedure for tracking neurons across files for non-overlapping data sets.

Based on four measured signals from tetrode our paper provides a computational approach for determining variability of spikes' spatial directivity. This paper is not another spike sorting method, nor is it a technique for tracking neurons over days, from tetrode recordings (Chelaru and Jog, 2005; Emondi et al., 2004). The paper presents a method of computing the directivity of charge flow during action potentials and its variability in successive spikes within extracellular space. This charge flow directivity may have a substantial impact on the milieu within which a neuron is active and therefore should not be ignored. This interesting and important approach of the dynamics of the spikes generated by neurons, its impact on the extracellular milieu and their possible intricate relationship, does not yet exist in the literature.

In the first step of the algorithm, a simplified spike model based on charges in movement is constructed. For the "charge movement model", the trajectory of charge is computed using a Newton–Raphson algorithm followed by a singular value decomposition algorithm that is performed to determine the directivity of the artificially generated spike. The trajectory gives the overall direction of AP propagation from start to finish. However, since the spike trajectory is a curve, it is not so easy to compare trajectories of several spikes. A linear approximation of the trajectory is needed for easier spatial variability investigation for which singular value decomposition (SVD) is performed. The computed components are the largest singular value and its corresponding right singular vector represents, in fact, the main directivity tendency for the spike in the computational space.

2. Charge movement model

Neurons are enclosed by plasma membranes whose primary function is to control the passage of ions and molecules. Diffusion of ions from high to low concentration is the effect of concentration differences between intracellular and extracellular space. Ion-specific pumps allow the transfer of charges up and down gradients over a finite volume. Several ions like K^+, Na^+, Cl^-, Ca^{2+} carry electric charges and their movement is influenced not only by concentration gradients but also by electrical fields. Therefore, ionic flux J under the influence of an electric field and concentration gradient can be written using the Nernst–Planck equation:

$$J = -\mu z C \frac{\partial V}{\partial x} - D \frac{\partial C}{\partial x} \tag{1}$$

where V is the electric potential, μ the mobility, z the valence of the ion, C the concentration and D is the diffusion coefficient (Schwartz, 1971).

A model of collective ionic motion is proposed for analysis (Fig. 1). The movement of charged particles during AP will generate an electrostatic field $\vec{E}$. For analysis, a simplified spike model includes a single charge in movement that generates potential variation in the four tips that simulate a tetrode. The electrostatic potential $V_A(x, y, z)$ in point A due to charge distribution is a 3D scalar field that can be computed:

$$V_A(r) = \frac{1}{4\pi\varepsilon} \sum_{i=1}^{n} \frac{q_i}{r_i} \tag{2}$$

where ε is the medium permittivity, q_i and r_i the charges and their distances to point A.

The electrostatic field is a quantity that varies in space and is determined by the configuration of source charges. The lines of the electrostatic field, $\vec{E}$ point in the direction of maximum increase of electrostatic potential $\vec{E} = -\nabla V$ or:

$$\vec{E}(\vec{r}) = \frac{1}{4\pi\varepsilon} \sum_{i=1}^{n} \frac{q_i}{r_i^3} \vec{r}_i \tag{3}$$

If these charges are moving in space and if a conductor is in the field the drop of potential in a length Δl of conductor can be computed by:

$$V_b(t) - V_a(t) = \frac{I(t)\Delta l}{\sigma A} \tag{4}$$

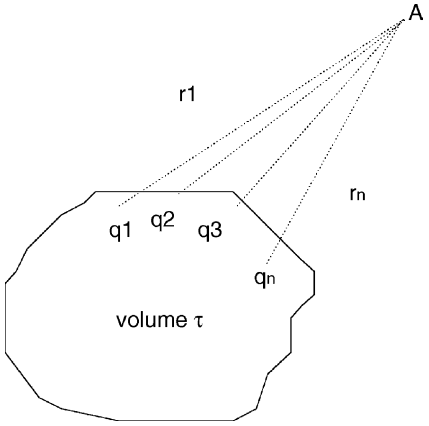

Fig. 1. Example of distributed discrete charges in space and their distances from the point A where the electrostatic potential is computed.

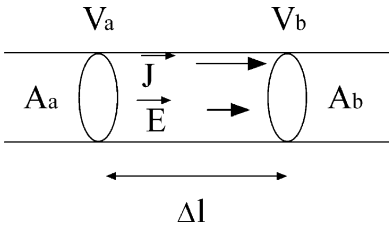

Fig. 2. The electrostatic field $\vec{E}$ generated by charges in movement in a conductor with length Δl.

where A is the area, σ the conductivity and Δl the length of the conductor and $\vec{E}$ could be considered constant (Fig. 2).

Since conductivity σ, area A and the length Δl are the same for every tetrode tip equation (3) can be written:

$$V_b^i(t) - V_a^i(t) = \frac{I_i(t)\Delta l}{\sigma A}, \quad i = 1, 2, 3, 4 \tag{5}$$

where I_i is the current generated in the tip i of tetrode by drop of potential in a length Δl of the conductor.

Substituting Eq. (2) into Eq. (5) one can write:

$$\frac{1}{4\pi\varepsilon}\sum_{i=1}^{n}\frac{q_i}{r_{ij}^a(t)} - \frac{1}{4\pi\varepsilon}\sum_{i=1}^{n}\frac{q_i}{r_{ij}^b(t)} = \frac{I_i(t)\Delta l}{\sigma A}, \quad j = 1, 2, 3, 4 \tag{6}$$

This is equivalent to a point charge $\sum_{i=1}^{n} q_i$ at distance $R_j^a = \sum_{i=1}^{n}\frac{1}{r_{ij}^a}$ and $R_j^b = \sum_{i=1}^{n}\frac{1}{r_{ij}^b}$. Therefore, Eq. (6) can be written:

$$\frac{1}{4\pi\varepsilon}\left(\frac{q}{R_j^a} - \frac{q}{R_j^b}\right) = kI_j(t), \quad j = 1, 2, 3, 4 \tag{7}$$

where $k = \frac{\Delta l}{\sigma A}$.

The left side of Eq. (7) is the potential of a physical electric dipole that consists of two equal and opposite charges q. From the law of cosines in the dipole case (Griffiths, 1999) Eq. (7) can be written:

$$\frac{1}{4\pi\varepsilon}\left(\frac{qd_j\cos\theta_j}{R_j^2}\right) = kI_j(t), \quad j = 1, 2, 3, 4 \tag{8}$$

where d_j is the distance between charges and θ_j is the angle between R_j and the dipole direction. That is equivalent to a single charge at distance R_j. Therefore, the trajectory of the charge q can be obtained using the following approach.

3. Computing the trajectory

Let us consider $s_0(k)$, $s_1(k)$, $s_2(k)$ and $s_3(k)$, $k \in \mathbf{N}$ to be the signals recorded from the four tips of the tetrode. Since the term $d_j(t)\cos\theta_j(t)$ can be considered to be approximately the same for each tetrode tip one may write the following nonlinear system of equations:

$$\begin{aligned}
\frac{s_0(k)}{s_1(k)} &= \frac{(x(k)-x_1)^2 + (y(k)-y_1)^2 + (z(k)-z_1)^2}{x(k)^2 + y(k)^2 + z(k)^2},\\
\frac{s_0(k)}{s_2(k)} &= \frac{(x(k)-x_2)^2 + (y(k)-y_2)^2 + (z(k)-z_2)^2}{x(k)^2 + y(k)^2 + z(k)^2},\\
\frac{s_0(k)}{s_3(k)} &= \frac{(x(k)-x_3)^2 + (y(k)-y_3)^2 + (z(k)-z_3)^2}{x(k)^2 + y(k)^2 + z(k)^2}
\end{aligned} \tag{9}$$

where x_i, y_i, z_i ($i = 1, 4$) are the positions in the space of the tetrode. The same equations could be obtained from the hypothesis that the position of source q is at intersection of four spheres (Jog et al., 2002). The equations in (9) can be written as a nonlinear system $f_j(x, y, z) = 0, j = 1, \ldots, 3$ where $\mathbf{F} = (f_1, f_2, f_3)$. An iterative Newton–Raphson scheme is used to find solution for the nonlinear system:

$$d_{n+1} = d_n - \mathbf{J}^{-1}\mathbf{F}(d_n), \quad n \in \mathbf{N} \tag{10}$$

where the Jacobian $\mathbf{J}$ of function $\mathbf{F}$ is:

$$\mathbf{J} = \begin{pmatrix} \frac{\partial f_1}{\partial x} & \frac{\partial f_1}{\partial y} & \frac{\partial f_1}{\partial z} \\ \frac{\partial f_2}{\partial x} & \frac{\partial f_2}{\partial y} & \frac{\partial f_2}{\partial z} \\ \frac{\partial f_3}{\partial x} & \frac{\partial f_3}{\partial y} & \frac{\partial f_3}{\partial z} \end{pmatrix} \tag{11}$$

Therefore, at each discrete moment k, from recorded signals, $s_1(k)$, $s_2(k)$, $s_3(k)$, $s_4(k)$ the spatial trajectory ($x(k)$, $y(k)$, $z(k)$) is determined when there is a solution d_{n+1} for the nonlinear system (Brenan et al., 1989). Having the trajectory data, the next step is to determine the spike directivity.

4. Computing spike directivity

In order to obtain spike directivity one has to write the matrix $\mathbf{P} \in \Re^{nx3}$ composed by trajectory coordinates ($x(k)$, $y(k)$, $z(k)$):

$$\mathbf{P} = \begin{pmatrix} x(1) & y(1) & z(1) \\ \cdots & \cdots & \cdots \\ x(n) & y(n) & z(n) \end{pmatrix} \tag{12}$$

where $k = 1, 2, \ldots, n$. For each spike one may compute the centroid of the data $\mu = E(\mathbf{P}^{\mathrm{T}})$ forming the matrix $\mathbf{P}_{\mathrm{tr}}$ of translated points $\mathbf{P}_{\mathrm{tr}} = p_i - \mu_i$, $i = 1,2, \ldots, n$.

Writing singular value decomposition (Stewart, 1993):

$$\mathbf{P}_{\mathrm{tr}\,nx3} = \mathbf{U}_{nxn}\mathbf{S}_{nx3}\mathbf{V}_{3x3}^{\mathrm{T}} \tag{13}$$

where

$$\mathbf{S} = \begin{pmatrix} s_1 & & \\ & s_2 & \\ & & s_3 \\ \ldots & \ldots & \ldots \end{pmatrix}; \qquad \mathbf{U} = (u_1, u_2, \ldots, u_n);$$

$$\mathbf{V} = (v_1, v_2, v_3); \tag{14}$$

it is possible to find the largest singular value for **S** and extract from **V** the corresponding right singular vector that represents direction cosines of the best linear approximation.

An important consideration in such computations is the stability of the angle of moving charge. In order to measure the deviation of computed trajectories when the angle of the moving charge is changed, a separate computation specific to this alteration in the angle of the charge, is performed. The angle between two computed directions can be determined using the right singular vector:

$$\Delta\theta = \arccos\left(\frac{\langle v, v'\rangle}{|v||v'|}\right) \tag{15}$$

Even in the simplified case of a single moving charge, the overall computation becomes essentially manually unsolvable. For this reason a series of simulations have been performed on a PC computer (Pentium 4, 1.6 GHz, 512 MB RAM) with Matlab Version 6.0—MathWorks, Inc. All the routines were custom developed or are freely available on the world-wide-web.

In the section below we describe the applications of the methods discussed above. Simulation of charges moving across tetrode tips induces voltage in tetrode tips. Computations for calculating the trajectory and the subsequent directivity are then performed. The impact variables such as tetrode tip geometry and system noise on the directivity computations is discussed. Finally the method is applied to real recorded neuronal spikes and directivity of charge flow in the data is demonstrated.

5. Simulations and analysis

Since directivity and trajectory calculations are performed for spikes within the same frame of reference, a relative change in these parameters can be computed using the system described above. It is assumed that tetrodes do not change their tip configurations during the recordings. As discussed above, when a charge is moved across the tetrode tips, a voltage is induced in the four channels. The act of measurement using the tetrode transforms the actual "real" direction. This is clearly presented in Fig. 3 where the actual trajectories are straight while the computed trajectories are curvilinear. Therefore, when analyzing recorded signal from tetrodes, it is not possible to provide directivity in real space, only in this transformed so-called "tetrode" space. However, since the analysis of all recorded data is performed in this space, the computations of the relative spatial directivity remain valid.

The difference in the relative positions in space of the charge linear trajectory and the directivity can be explained as follows. Imagine a concave or convex mirror and a small ball moving near the mirror that follows a linear trajectory in 3D space. In the mirror one may see a bent image of the ball trajectory during the movement. In our case instead of light reflection that provides the image trajectory of the ball on the mirror, a charge trajectory "image" is obtained from induced

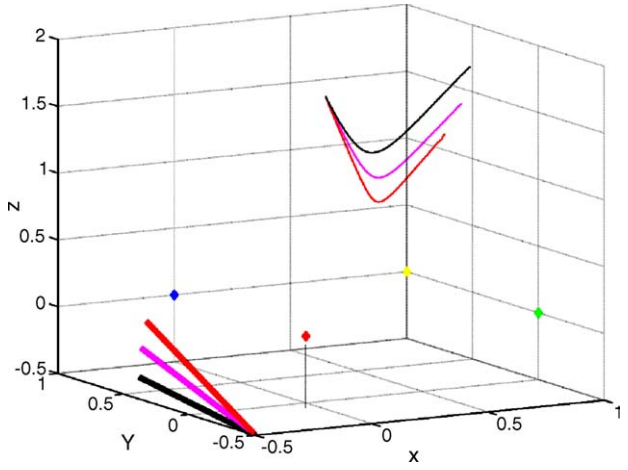

Fig. 3. The changes in the linear trajectory of charge (bold, red, magenta, black lines) and computed trajectory modifications (red, magenta, black trajectories) are shown. Each division is approximately 20 μm. For display purposes approximately 60 μm of charge movement is shown. The "mirror" effect is visible for computed trajectories. (For interpretation of the references to color in this figure legend, the reader is referred to the web version of the article.)

currents by the described computational process. In the simulated experiment the charge is the object moving in 3D space with initial conditions (initial position, speed, etc.) provided by the software user, while the computed trajectory is equivalent to "image" from the mirror. Thus, the trajectory and indeed the relative position computed will be a transformed version of the "real" trajectory or image.

In the computations described above, the knowledge of absolute tetrode tip geometry and distances appears to be important. However, in relative terms, as long as the tip geometry does not change between recorded spikes, the computations of relative directivity-change between spikes remain unaffected. In order to compute a trajectory in real space (Eq. (9)) one would need to know the actual position of tetrode tips in 3D Cartesian space. Measurements of inter-tip distances from tetrodes show that the average spacing between tips is approximately 20 μm with a measurement error of approximately 3 μm for each tip (Chelaru and Jog, 2005; Jog et al., 2002). Charges are then launched simultaneously or in successive trials. The speed of movement of the charge as well as the distance from the midpoint of the tetrode tips to the charge (approximately 30 μm) is held relatively constant. However, this distance varied slightly as the input angles is changed (Fig. 3). For an easier analysis charge trajectories are constrained to describe lines in 3D space. In the simulation, the charge movement is about 260 μm, and successive trials are performed. In the figure however, only a small portion of the actual charge movement distance is displayed. For three successive trials (Fig. 3) the linear charge trajectory is deviated by 10° and this deviation is represented by red, magenta and black bold lines.

Coordinates of tetrode tips are represented by colored diamonds starting with red for the first channel, green, blue

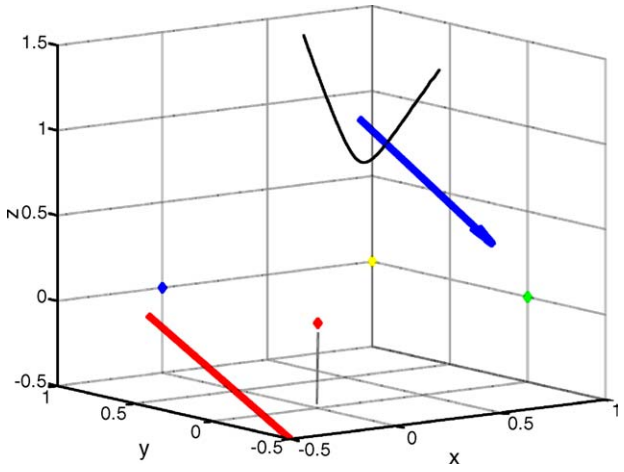

Fig. 4. An example of linear trajectory of a single charge (bold, red line) and the computed trajectory (black curve) and estimated directivity (blue line) are shown. Each division is approximately 20 μm. For display purposes approximately 60 μm of charge movement is shown. The positions are clearly different (see text). (For interpretation of the references to color in this figure legend, the reader is referred to the web version of the article.)

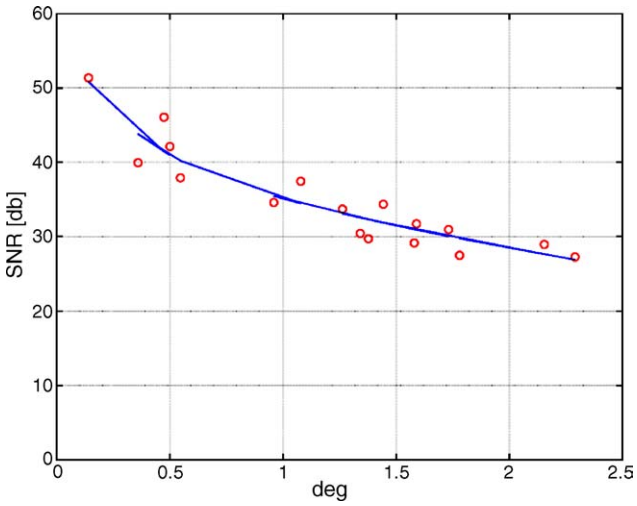

Fig. 5. The graph shows an estimation of dependence between signal to noise ratio and the error in computing deviation angle. Red circles are data obtained from several simulations with decreasing SNR while the blue curve represents the optimal nonlinear approximation. (For interpretation of the references to color in this figure legend, the reader is referred to the web version of the article.)

and yellow for the second, third and fourth channel of the tetrode respectively. Computed trajectories are curves in red, magenta and black. Each division on the axes is approximately 20 μm. One such trajectory is then used to further display computed directivity of the charge flow using the method presented above (Fig. 4). The computed charge directivity is shown by a blue bold line. Although the computed directivity does not map the actual charge directivity, it is clear that the proposed method provides a robust way to analyze variations of directivity in spike recordings between neuronal spikes. Importantly, one can observe that this computing approach can be performed without the full knowledge of actual tip positions.

Additionally, despite modern, high performance acquisition systems and filtering methods, all physiological recordings are susceptible to noise that occurs from various sources such as distant neurons, external electrical noise and animal behavioral artifacts.

In order to better understand the impact of this additional noise on the method for computing directivity, we added such noise to the data. In our simulations these sources of noise are modeled by Gaussian noise added to the "induced" signals in tetrode tips by the moving charges. Dependence of computed deviation in directivity and noise level is displayed in Fig. 5. For a signal noise ratio greater than 25 dB (SNR > 25 dB) the errors in computing deviations are usually less than 3° (Fig. 5). In case of higher noise levels, errors in computing deviation angle may increase. However, spikes that are very noisy should be eliminated from computing spike directivity. One way to perform this spike filtering is to analyze the computed trajectory from nonlinear equation system (Eq. (9)) and eliminate spikes that have trajectory points far away from tetrode tips coordinates. Thus our method can be used as an additional filtering mechanism to eliminate spikes that would randomly contaminate the data.

For real recorded spikes directivity is obtained in two main steps (Fig. 6). The trajectory is computed from recorded data in the first step with the Newton–Raphson algorithm. Then in the second step a linear approximation of the trajectory is performed by a singular value decomposition that gives the overall direction of AP propagation in "tetrode space".

We started our simulations with movements of simple charges that describe linear trajectories in 3D space to show how the method works. The reader may see that by applying this method, simple but curved trajectories are obtained from the computation. These curves (Figs. 3 and 4) that show trajectories of single charges in movement are far less complex than usual trajectories obtained from processing real spikes. The reader may have a false impression regarding the application of the presented method for real recorded data. The propagation of ionic fluxes within biological spikes implies simultaneous movement of several charges during the occurrence of an action potential. Therefore, we provide an example where several charges that are moving in space could generate similar trajectories to computed trajectories from real recorded spikes. We show an example where

Fig. 6. This shows a quick reference diagram for the method. The spatial trajectory $x(k)$, $y(k)$, $z(k)$ is firstly determined with Newton–Raphson algorithm. Spike directivity is then computed using trajectory coordinates and singular value decomposition.

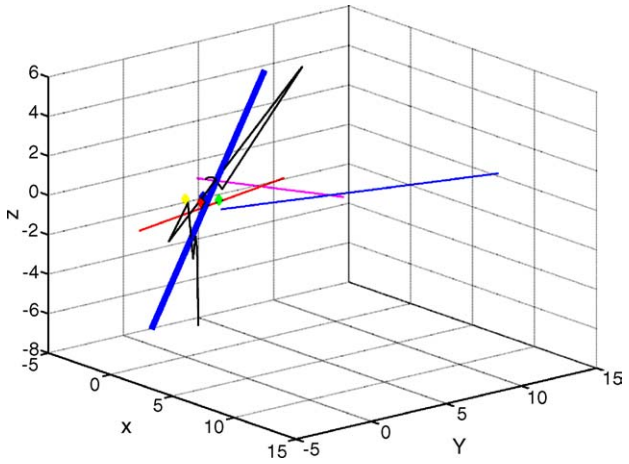

Fig. 7. Linear simultaneous movements of three charges (red, magenta, blue lines), computed trajectory (black curve) and computed directivity (bold blue line). Each division is approximately 20 μm. For display purposes approximately 60 μm of charge movement is shown. (For interpretation of the references to color in this figure legend, the reader is referred to the web version of the article.)

three identical charges with different angles of movement are represented in three different colors (Fig. 7). The simultaneous movement of charges (red, magenta and blue lines) is simulated in the presence of Gaussian noise (SNR = 25 dB). The overall computed trajectory (black curve) and computed directivity (bold blue line) are represented.

Finally, Fig. 8 shows the application of the method to a real recorded spike. Note the similarity of the computed trajectory from the recorded spike to the simulated multi-charge flow trajectory from Fig. 7. The black curve represents the trajectory while and computed directivity is the bold blue line.

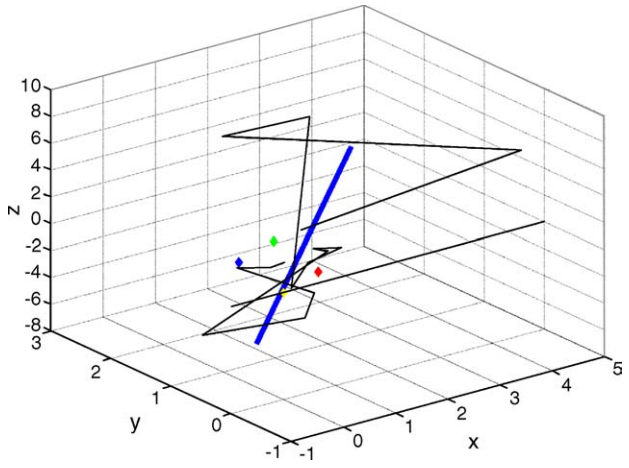

Fig. 8. An example of real spike trajectory (black curve) and computed directivity (bold blue line). Each division is approximately 20 μm. (For interpretation of the references to color in this figure legend, the reader is referred to the web version of the article.)

6. Conclusion

Neuronal spikes recorded in extracellular space by electrodes represent propagation of several electric charges. The alterations caused in the electric field within the extracellular space are recorded by the electrodes. Tetrodes have the ability to observe this phenomenon in four dimensions. However, a further analysis of the spike profile itself can be used to understand whether the process of action potential transmission along a conductor can itself be seen as a directed flow of charge that alters the extracellular milieu in a specific way.

This paper uses simulated charge movement in space and the induced voltages on a conductor as a model to understand whether it is possible to obtain information regarding directivity of such flow of charges. Simulated tetrodes perceive the charge movement as voltage that mimics the action potentials in spiking neurons. A process for computing the directivity of this charge flow is then proposed within the paper. This process of the induction of AP is then applied to the actual data obtained from tetrode recordings and a profile of spike directivity from these recordings is presented.

The weakness of the present method is that it relies on the quality of the electrical recordings. Factors common to all electrode recordings techniques which consist of noise level and number of days that a tetrode can be kept in the brain to record data contribute to this data recording quality. A discussion related to noise analysis was presented in the above simulations. Since new modern, high performance acquisition systems for in vivo recordings provide increased values of signal to noise ratio, the errors in computing deviations are usually small and the method works well in practice.

In addition, it is possible that the changes in directivity that could be seen occurring by the application of our method could result simply due to tetrode drift and movement. Firstly, the internal consistency of this method relies on the fact that the tetrodes are not actually physically moved during the analysis period. The hardware used to implant the drives has to be reliable enough to also avoid inadvertent movement. Additionally, we describe a method of demonstrating directivity changes that are expected to occur in the tens or hundreds of millisecond range. Natural tetrode movement around the brain would be at a much lower frequency.

There are various important applications of this work. First, action potentials can now be seen and analyzed as charge flow that may have directivity. This concept could have a direct impact on the understanding of the extracellular milieu within which electrical events such as the action potential are occurring. Second, the traditional methods of electrophysiology use only spike timing as a way of describing information coding by neurons. However, neurons may also code information in a true “spatial” way by dynamically altering the propagation of charge direction over time. It is possible that both the reception of information and the output of neurons could exhibit directivity. Such changes, over time may be behaviorally dependent. This may become a powerful method for selecting sources of input and output by

neuronal ensembles, thereby possibly determining the state of the space within which neural activity is occurring. Such a phenomenon of change of directivity can be thought of as a dynamical alteration of the spatial receptive field of neuronal ensembles. Such receptive field modulation has been observed often, without an adequate explanation of the mechanism (Mehta et al., 2004). The method proposed in our paper and the implications of behaviorally dependent spatial directivity changes are therefore important.

Third, in the larger sense, computations of directivity can be used a possible filtering technique where outlying spikes that have trajectory points that are unreasonably distant, could be eliminated from the data set.

The ability to compute trajectory and directivity of charge flow by tetrode recordings use the spike as a reflection of this flow and gives us a glimpse of the complexity of milieu within which neurons function. Our results show that besides improved spike sorting procedures, tetrodes can be used in computing the trajectory of equivalent electrical charges that model electrical events during AP. Based on obtained trajectory, estimation of changes in spike directivity over an arbitrary reference system in real recordings could be achieved. This is a new potentially powerful application of tetrode recording methodology.

References

Brenan KE, Campbell SL, Petzold LR. Numerical solution of initial-value problem in differential-algebraic equations. North-Holland, Amsterdam: Elsevier; 1989.

Chelaru MI, Jog MS. Spike source localization with tetrodes. J Neurosci Meth 2005;142(2):305–15.

Emondi AA, Rebrik SP, Kurgansky AV, Miller KD. Tracking neurons recorded from tetrodes across time. J Neurosci Meth 2004;135:95–105.

Gray C, Maldonado P, Wilson M, McNaughton B. Tetrodes markedly improve the reliability and yield of multiple single-unit isolation from multi-unit recordings in cat striate cortex. J Neurosci Meth 1995;63(1/2):43–54.

Griffiths DJ. Introduction to electrodynamics. Prentice-Hall; 1999.

Hebb DO. The organization of behavior. New York: John Wiley; 1949.

Jog MS, Kubota Y, Connolly CI, Hillegaart, Graybiel AM. Building neural representations of habits. Science 1999;286:1745–9.

Jog MS, Connolly CI, Kubota Y, Iyengar DR, Garrido L, Harlan R, Graybiel AM. Tetrode technology: advances in implantable hardware, neuroimaging, and data analysis techniques. J Neurosci Meth 2002;117:141–52.

Mehta MR, Lee AK, Wilson MA. Response to Melamed et al.: coding and learning of behavioral sequences—open questions and potential solutions. Trends Neurosci 2004;27(1):14–5.

Sahani M, Pezaris JS, Andersen RA. On the separation of signals from neighboring cells in tetrode recordings. In: Jordan I M, Kearns MJ, Solla SA, editors. Advances in neural information processing systems 10. Cambridge, MA: MIT Press; 1998.

Schwartz TL. The thermodynamic foundations of membrane physiology. In: Adelman Jr W, editor. Biophysics and physiology of excitable membranes. New York: Van Nostrand Reinhold Company; 1971. p. 47–95.

Stewart GW. The early history of the SVD. SIAM Rev 1993;35:558–61.

Takahashi S, Sakurai Y, Tsukada M, Anzai Y. A new approach to spike sorting for multi-neuronal activities recorded with a tetrode. Neurosci Res 2003;46:265–72.

Zhang K, Ginzburg I, McNaughton BL, Sejnowski TJ. Interpreting neuronal population activity by reconstruction: Unified framework with application to hippocampal place cells. J Neurophysiol 1998;79:1017–44.

Journal of Neuroscience Methods 200 (2011) 80–85

Contents lists available at ScienceDirect

Journal of Neuroscience Methods

journal homepage: www.elsevier.com/locate/jneumeth

Understanding the physical mechanism of transition to epileptic seizures

Dorian Aur

Dept of Comparative Medicine, Stanford University, Palo Alto, CA, United States

ARTICLE INFO

Article history:
Received 10 January 2011
Received in revised form 11 May 2011
Accepted 27 May 2011

Keywords:
Epilepsy
Seizure generation
KAM theory
Seizure prediction
Neuroelectrodynamics

ABSTRACT

The mechanisms of generating epileptic seizures are still unknown. To identify the mechanisms that underlie the transition to seizure a combination of features that include firing rate, power spectrum and complexity measures were simultaneously analyzed. Pre-ictal periods are characterized by large fluctuations of firing rate which reflect local dysfunctional regulation of neuronal activity. This local dysfunction in neuronal activity is translated in changes of endogenous electric field within clustered regions with high frequency oscillations (HFO) that act at fundamental level of charge dynamics and lead to chaotic dynamics followed by electrical resonances. Right before the onset of seizures the presence of chaotic behavior becomes persistent and leads all types of cells to fire simultaneously and generate the transition to ictal state. The alteration in neuronal regulation and the nature of physical phenomena involved in this transition supports some models of seizure generation and rules out others.

1. Introduction

Epilepsy is a multifaceted neurological disorder where the occurrence of seizures leads to alterations in normal electric rhythms that can be recorded and analyzed. The hippocampus plays a central role in the generation and propagation of seizures (Parent et al., 1997; Buzsaĭki, 2006) in both human and rodent models of temporal lobe epilepsy. Current models show that several factors which govern neuronal excitability and intrinsic neurochemistry (Farrant and Nusser, 2005) are involved in seizure generation, however little is yet known about how these factor operate and determine the seizure onset. Distinct electrophysiological phenomena originating from different epileptic brain regions precede the ictal discharge.

The presence of interictal spikes is associated with an increased risk for spontaneous seizure (Gotman, 1991; Staley et al., 2005). During interictal periods in epileptic focal regions quasi-localized clusters of high-frequency oscillations (HFO) have been previously revealed based on EEG analysis (Bragin et al., 1999; Buzsáki, 2002; Staba et al., 2002; Worrell et al., 2004; Bragin et al., 2010). These high frequency oscillations appear periodically in the epileptic brain and they manifest on a scale of centimeters generated by abnormal hyper-synchronization of large neuronal ensembles (Crépon et al., 2010). The formation of HFO clusters that become broader after the application of $GABA_A$ receptor antagonist bicuculine was firstly reported in (Bragin et al., 2002). The presence of HFO in the seizure-generating structures is highly related to temporal and spatial location of seizure onset (Crépon et al., 2010). On the other hand few analyses have highlighted the presence of focal low frequency oscillations that precede ictal discharge in EEG or MEG data (Adeli et al., 2003; Csercsa et al., 2010). While alterations at different levels can always facilitate abnormal neuronal activities, the occurrence of seizures is a rare event with a very low probability of occurrence.

From gene to gliogenesis (Bonni et al., 1997) and neurotransmitter release (Cartmell and Schoepp, 2000) to neurogenesis (Zhao et al., 2008) all mechanisms are highly regulated in the brain. This regulation further extends to synaptic activity (Newman, 2003) and firing activity of neurons in different brain regions. Therefore, changes in regulation at different levels can have broad consequences and influence rhythmic patterns of neuronal activity. The electric field generated by a population of neurons that fire was termed endogenous electric field by Jefferys (1995). Changes in endogenous electric field alter the dynamics of electric charges, the diffusion of ions as well as the neurotransmitter release (Fröhlich and McCormick, 2010). All these changes can significantly influence local neuronal activity. Therefore, we hypothesize that dysfunctional regulation of neuronal activity inside epileptogenic regions changes relevant characteristics of endogenous electric field and leads to seizure generation. To test this hypothesis recorded local field potentials from the dentate gyrus and unit data from putative granule cells in epileptic pilocarpine-treated rats were analyzed before and during spontaneous seizures. A combination of features that include firing rate, power spectrum and complexity measures were simultaneously analyzed.

E-mail address: DorianAur@gmail.com

0165-0270/$ – see front matter © 2011 Elsevier B.V. All rights reserved.
doi:10.1016/j.jneumeth.2011.05.028

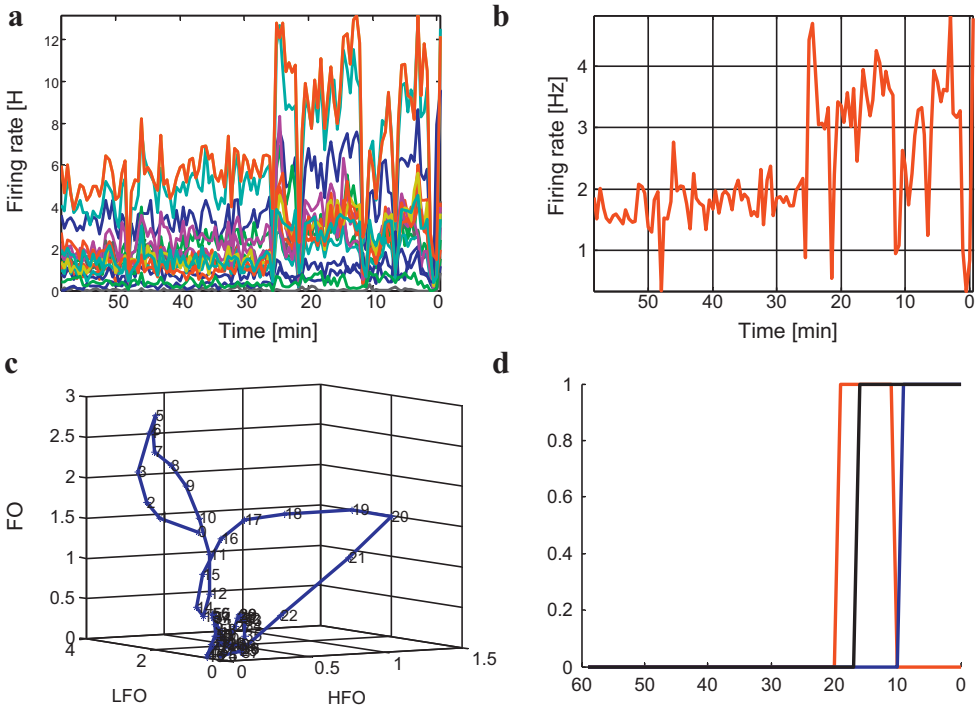

Fig. 1. Strong fluctuations of firing rate in the HFO region precede the seizure onset and determine significant changes in power spectrum. (a) The evolution of changes in firing rate in granule cell layer 1 h prior to seizure represented in different colors. The high values of firing rate represented in red color are generated by interneurons (mean firing rate >5 Hz) while lower firing rates are generated by granule cells. (b) The average of firing rate of neurons represented in (a). (c) The corresponding trajectory in LFO, HFO, FO space during 60 min before seizure. Most of the time the trajectory is bounded, rarely is highly perturbed (see min 20 and min 6). (d) The windowed *t*-test shows that statistically significant changes in HFO (in red) that occur 20 min before seizure followed by significant changes in LFO and in the main frequency band. The *t*-test outcome for LFO is represented in black and for FO in blue color. (For interpretation of the references to color in this figure legend, the reader is referred to the web version of the article.)

2. Data collection materials and methods

All experiments were performed in accordance with the National Institutes of Health Guide for the Care and Use of Laboratory Animals and were approved by the Stanford University Institutional Animal Care and Use Committee. Tetrode implants, data acquisition and histological verification of the tetrodes position were previously performed by Bower and Buckmaster and the details of the protocol were published in Bower and Buckmaster (2008).

The seizure onset was identified electrographically from one of the tetrodes based on changes in the spectral power following the techniques presented in Bower and Buckmaster (2008). Recorded local field potentials from the dentate gyrus of four pilocarpine-treated, epileptic rats were analyzed using FFT power spectrum 1 h prior to spontaneous seizure onset. The power spectrum was computed for three different bandwidths: (high frequency oscillations HFO, $200 < f < 300$ Hz, main frequency oscillations (FO) 2–100 Hz and low frequency oscillations (LFO) $0.1 < f < 2$ Hz). The harmonic components within these specific frequency bands where extracted and then averaged. Further the envelope is extracted from four different electrodes by using principal component analysis (PCA) and a zero phase-shift band pass digital filter is used to suppress the noise and improve the signal-to-noise ratio (Urbach and Pratt, 1986). The envelope of the first principal component of HFO, LFO or FO events is statistically analyzed using a windowed *t*-test or one-way ANOVA for all seizures with window size of 5 min. The widowed *t*-test is used to detect the existence of rare events in activity compared to a baseline period of the first 10 min. In each case the *t*-test indicates a rejection of the null hypothesis at the 5% significance level. For recorded local field potentials Kolmogorov complexity measure is estimated using techniques described in Small (2005). Tetrodes recording of unit data from putative granule cells during 12 spontaneous seizures were selected from HFO epileptogenic regions. An automated unsupervised classification of multidimensional data in the tetrode setup was used (KlustaKwik, Harris K.D. et al., Rutgers University) followed by manual selection of final clusters was performed (MClust-3.5, Redish A.D. et al., University of Minnesota).

3. Results

A selected example presents changes that occur during 60 min before the seizure (Fig. 1). Significant fluctuations of firing rate in an ensemble of neurons display wide uprising trend 20 min before the seizure onset (Fig. 1a and b). The high values of firing rate represented in top red color are generated by interneurons (mean firing rate > 5 Hz) while lower firing rates are generated by granule cells (Fig. 1a). Changes of high frequency oscillations (HFO, $200 < f < 300$ Hz), main frequency oscillations (FO, 2–100 Hz) and low frequency oscillations (LFO-$0.01 < f < 2$ Hz) display a relevant trajectory in LFO, HFO, FO space during 60 min before seizure (Fig. 1b). Large amplitudes of HFO with local maxima (peaks) or minima (valleys) can be observed in HFO envelope determined by concomitant increase/decrease "kicks" in the firing rate of granule cell units that precede the seizure onset (Fig. 1a–c). Most of the time this trajectory in frequency domain remains bounded, only rarely is highly perturbed (see min 20 and min 6). The analysis of HFO data with a windowed *t*-test shows that a statistically significant change in HFO (in red) occurs 20 min before seizure followed by significant changes in LFO (in black) and main frequency (in blue color) band that correspond to strong firing rate fluctuations (Fig. 1d).

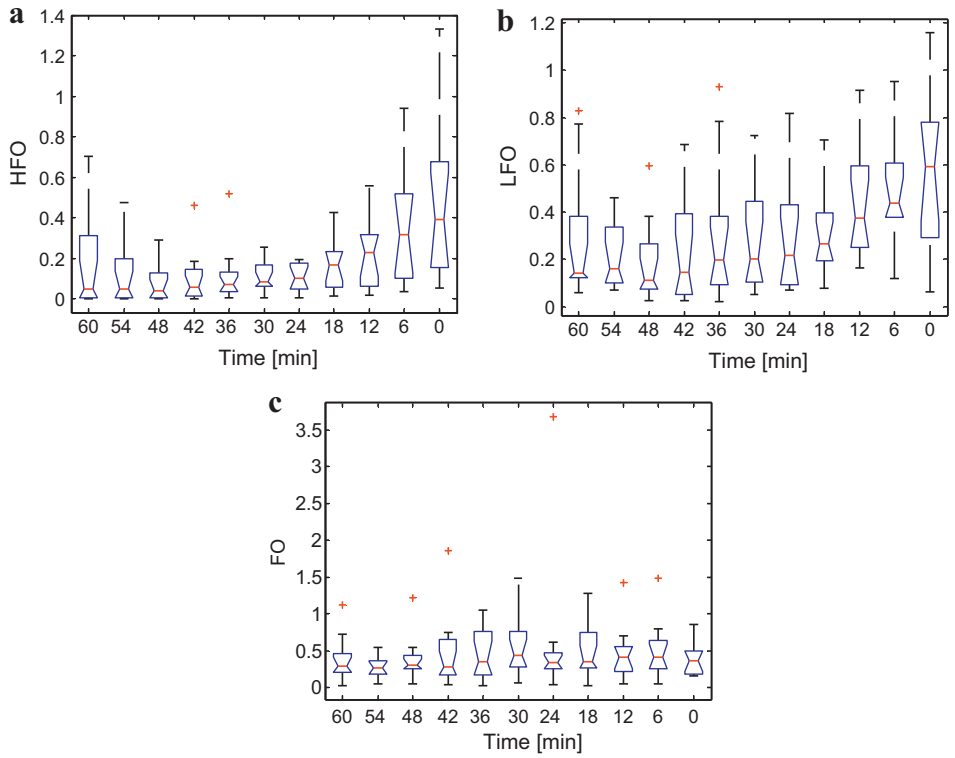

Fig. 2. One-way ANOVA analysis of changes in the amplitude of harmonics using a 5 min window. For each column the lines of the box display the lower quartile, median and upper quartile values. The red crosses mark data outliers with values not included between the whiskers. ANOVA displays statistically significant difference in case of (a), HFO ($F = 5.76$, $p = 3.78 \times 10^{-7}$) (b), LFO ($F = 2.52$; $p = 0.0091$) and does not provide statistical difference (c), for FO ($F = 0.58$, $p = 0.821$). (For interpretation of the references to color in this figure legend, the reader is referred to the web version of the article.)

The presence of HFO was detected in 12 selected seizures recorded from four pilocarpined treated rats. These data were statistically analyzed and one–way ANOVA test was performed during 60 min before seizure assuming independent estimates for groups of 5 min window. The estimated F-ratio and p-values summarize the result of statistical analysis. Statistically, significant changes in the amplitude of power spectrum harmonics precede the seizure onset. The ANOVA analysis shows a statistically significant change in HFO ($p = 3.78e{-}7$, $F = 5.76$) and LFO ($p = 0.0091$, $F = 2.52$). A post hoc pairwise comparison is performed in order to reveal where in time these differences are significant. On average the significant change in HFO and LFO harmonics occurs between 5 and 10 min before the seizure onset (Fig. 2a and b). However, there is no significant trend in the main frequency bandwidth ($p = 0.821$, $F = 0.58$, Fig. 2c).

Indeed, averaging data from several seizures can show a certain trend of HFO characteristics and firing rate (Bower and Buckmaster, 2008) however this type of analysis hides significant details regarding nonlinear dynamics and transitory regimes that occur in every seizure (Fig. 1a and b).

A representative example of HFO propagation between granule cell layer (GCL), hilus and CA3 during 60 min before the seizure onset is shown in Fig. 3a. The statistically significant change in HFO occurs first in GCL layer then expands to CA3 region and hilus (Fig. 3b). The trajectory in frequency domain remains bounded and starts to be perturbed only during the preictal period.

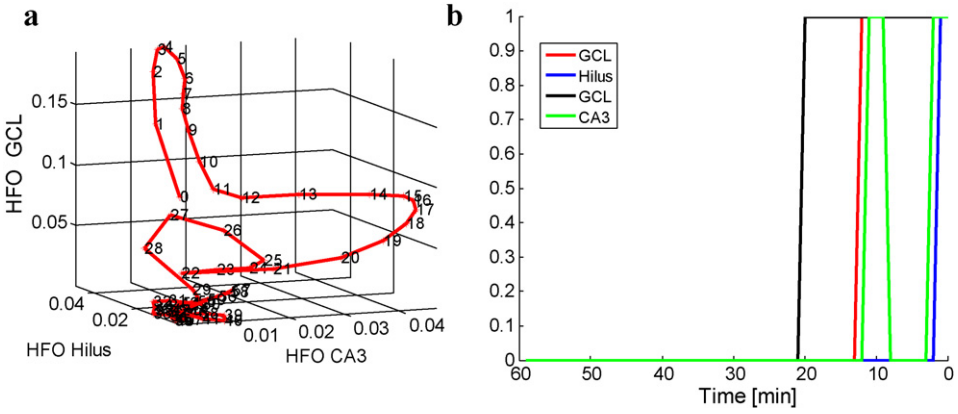

Fig. 3. Statistically significant changes in HFO envelope occur 20 min before seizure. (a) The propagation of HFO between (GCL), hilus and CA3 region. (b) Statistically significant changes in HFO occur first in GCL (black and red color for two different tips of tetrodes implanted in GCL) and they expand to CA3 region and hilus. (For interpretation of the references to color in this figure legend, the reader is referred to the web version of the article.)

The periods when chaotic dynamics become persistent show continuous high values of complexity that can be easily detected. The scaled measure of complexity, in red color and normalized changes of firing rate, in blue color, are both represented 1 h prior to seizure (Fig. 4a). Marked in yellow color are regions that correspond to low firing rate periods and exhibit persistent chaotic dynamics. The occurrence of persistent chaotic dynamics is followed by an increase of firing rate which correspond to peaks in HFO envelope (Fig. 1c). During inter-ictal period the duration of persistent chaotic dynamics is short. Right before the seizure an unusual longer period with abnormal persistent chaotic dynamics precedes the seizure (Fig. 4b). In (Fig. 4c) the presence of periods with persistent chaotic dynamics is displayed 1 h before the seizure.

The representation of regulatory system (Fig. 5a) schematically shows the relation between neuronal activity, electric field and dynamics of electric charges. The transitory regime represents a general outcome after a perturbation. A comparison between a theoretical model of response to impulse perturbation and changes that occur in HFO envelope and average firing rate before, during and after spontaneous seizures are displayed in (Fig. 5). Globally, the impulse response of a regulatory system can be approximated with a sinc function and is represented in Fig. 5b. If the system is nonlinear this response and the resulting shape can become more complex. Remarkable, the shape of HFO envelope and average firing rate (Fig. 5c and d) follow this theoretical model where three main phases can be identified. The raising phase (preictal) shows an increasing trend in the average firing rate and HFO amplitude. The ictal phase is characterized by peak HFO and firing rate values and the postictal period is characterized by a decrease in HFO and firing rate fluctuations. The transitory regime that precedes seizure generation (preictal state) is characterized by brief periods when chaotic dynamics occur (Fig. 5c and d). These periods display increased values of signal complexity. The period after the seizure (postictal phase) shows a longer transition with prolonged chaotic diffusion regimes over 20 min when high values of complexity characterize the dynamics.

4. Discussion

The power spectrum analyses show that the regulatory mechanism is present in the frequency domain. Most of the time there are small fluctuations in frequency (Figs. 1c and 3a) which reflect a regulatory process that rarely is altered even in the epileptogenic regions. Dominant frequency oscillations of electric field (FO) are continuously maintained by neuronal activities. However, 10–20 min before the seizure in the focal epileptogenic region the broadband power spectrum occurs. Strong HFO and LFO harmonics reflect significant changes in the dynamics of endogenous electric field, the presence of electrical resonances and chaotic dynamics. Specifically, the increase in amplitude of LFO harmonics is related to chaos generation and reflects a universal behavior of nonlinear systems (Cvitanovic, 1995; Pritchard and Duke, 1992). Chaotic diffusion can develop and its presence becomes evident during the decrease, or absence of firing and corresponds to periods when high values of complexity are estimated (Fig. 4a). Abrupt changes in firing rate translate to significant changes in endogenous electric fields that generate alterations in the dynamics and interactions of electric charges. Chaotic dynamics correspond to periods of lower firing activity which are marked in yellow and magenta color. Large peaks of the HFO envelope or firing rate characterize electrical resonant regimes with low values of complexity (Figs. 4a–c and 5c, d).

The severe dysfunctional regulation of local neuronal activity represents the biological substrate of transition to seizure. Right before the seizure the decrease in firing rate, the absence of firing becomes unusual longer and is translated in a prolonged period

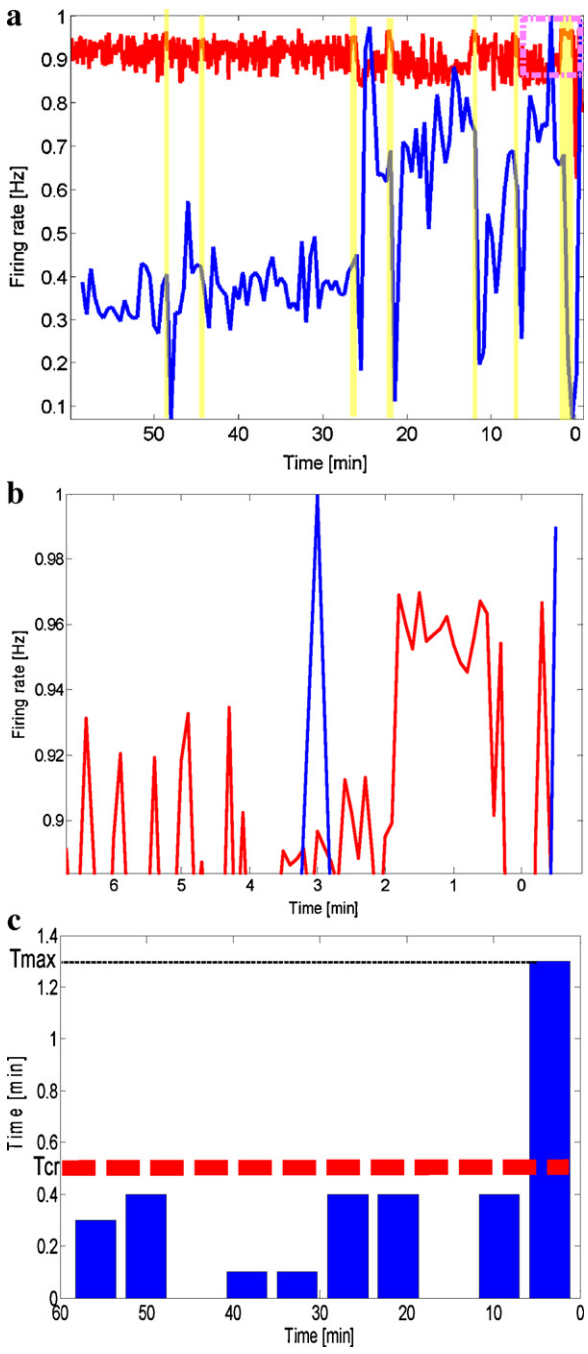

Fig. 4. Specific transitory behavior precedes the seizure onset and reveals a severe dysfunction in local neuronal activity regulation. (a) The normalized change of firing rate is represented in blue color and the measure of complexity is scaled and represented in red color 1 h prior to seizure. The changes that occur in firing rate correlate with alterations in the dynamics of electric charges. High values of complexity correspond to increased chaotic dynamics (yellow marked regions). (b) The detail of chaos persistence represents the rectangle from (a). Right before the seizure onset high values of complexity in red color reveal an unusual longer period with abnormal persistent chaotic dynamics that marks the transition to seizure. (c) The presence of persistent chaotic dynamics represented 1 h before the seizure. Right before the seizure onset unusual persistent chaotic dynamics is detected. Each bar in blue color represents the duration of persistent chaotic. The horizontal dashed red line marks the critical time ($T_{cr} \cong 0.5$ min). The seizure is a rare event that occurs only if chaotic dynamic lasts longer than T_{cr}. (For interpretation of the references to color in this figure legend, the reader is referred to the web version of the article.)

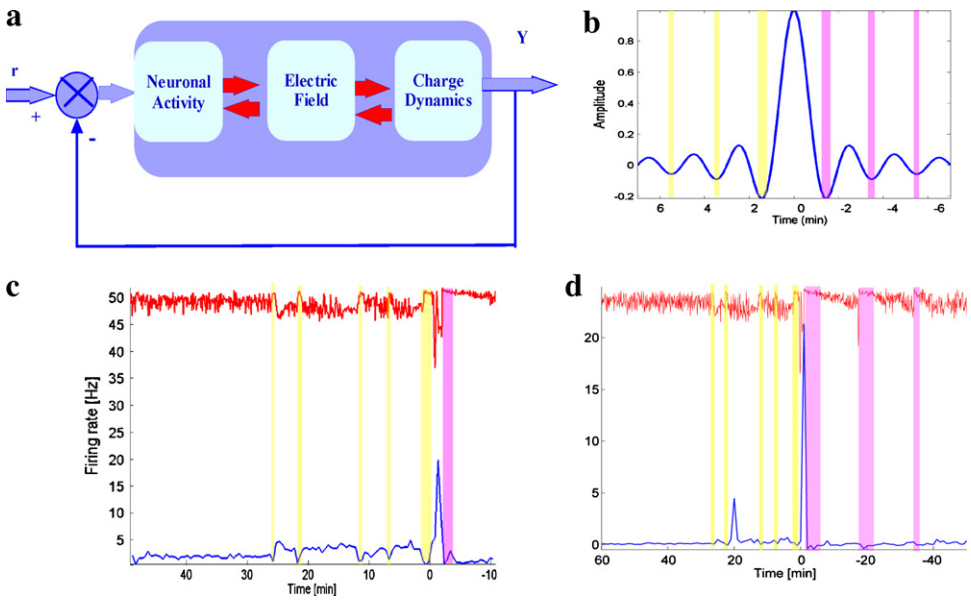

Fig. 5. A comparison between theoretical model of response to perturbation in a linear system and the transition to seizure represented by changes in HFO and average firing rate before, during and after spontaneous seizures. (a) Schematic representation of regulatory system where changes in neuronal activity, electric field and dynamics of electric charges are strongly related. (b) The response of regulatory linear system to impulse is the sinc function. (c) Fluctuations of average firing rate 1 h before the seizure represented in blue color show periods with lower neuronal activity characterized by increased chaotic dynamics revealed by high values of signal complexity plotted in red color. Chaotic dynamics develops during preictal periods (marked in yellow) and postictal periods (marked in magenta). (d) The changes in HFO envelope 1 h before the seizure represented in blue color includes brief periods when chaos develops and characterizes low HFO values. During postictal phase similar chaotic periods are developed (marked in magenta color). The peaks in HFO amplitude define elevated neuronal firing rates. (For interpretation of the references to color in this figure legend, the reader is referred to the web version of the article.)

of persistent chaotic diffusion (Fig. 4a–c). If chaotic dynamics lasts over 30 s the transition to ictal state is certain. Therefore, this prolonged persistent chaotic regime is a specific feature, characterizes dysfunctional regulation and marks the transition to seizure. Once the resonant regime occurs in the focal region it expands very fast in larger areas and generates the seizure. Since only a severe alteration of neuronal activity leads to seizure then the ictal state is a rare event.

The nature of regulation mechanisms and physical phenomena involved in this transition supports some models of seizure generation and rules out others. Before the seizure onset different types of neurons including granule cell units and interneurons display similar increasing fluctuations of firing rate (Fig. 1a). In the focal region 10–20 min in advance the process of recruitment of different types of neurons that perform similar dynamics is essential to generate the seizure. Therefore, independent of their type all neurons have similar active role in seizure generation. Under extensive, persistent chaotic diffusion relevant differences between different types of neurons disappear and all types of cells start to fire together and generate the transition to ictal state.

Since different types of neurons do not seem to reveal distinct role in seizure generation, a more general model is required to explain the transition to seizure. Specifically, these analyses suggest that impaired regulation of local neuronal activity significantly changes the characteristics of endogenous electrical field in the focal region and is the fundamental source of seizure generation. Since dysfunctional regulation does not always occur, then indeed the ictal state is a rare event.

The increased fluctuations of firing rate during pre-ictal period is equivalent to a response to a 'perturbation' that changes local endogenous electric field and the dynamics of electric charges in the epileptogenic region. This approach offers a required framework to relate nonlinear dynamics of Kolmogorov Arnold Moser theory (KAM) (Kolmogorov, 1954; Arnold, 1963; Moser, 1967) and its extensions to explain essential changes in the characteristics of electric field and charge dynamics. In this case the KAM theory refers to Hamiltonian systems with many degrees of freedom that describe the motion of charged particles in electric field. The theoretical aspects involved in a transition to chaotic behavior were presented in Chirikov (1979), Reichl (2004). A perturbation with higher energy determines diffusion across the resonances lines (resonance interference) and a fast transition to chaotic dynamics. The interaction between resonances in perturbed and unperturbed orbits generates transitory regimes that lead to chaotic behavior (Luo, 2006). The prolonged period of chaotic diffusion (postictal phase) follows strong resonant regimes developed during the seizure and is maintained if neurons have low firing rates (Fig. 5c). Since in a nonlinear system, the resonance frequency depends on action, then changes in action (perturbations) are reflected in alterations of power spectrum harmonics. This phenomenon explains significant changes in the amplitude of power spectrum harmonics that precede the seizure onset (Fig. 2). In addition in systems with many degrees of freedom (e.g. charges in electric field) diffusion can occur *along the resonance lines* (Arnold diffusion) and determine a gradual transition to chaotic behavior.

Many factors that include changes in morphological and molecular basis can act together or separately and alter local regulation of neuronal activity. Genetic mutations of ion channels (Claes et al., 2001; Escayg and Goldin, 2010) failure of glutamate reuptake from the extracellular space (Moritani et al., 2005), aberrant synaptic connectivity(Jacobs et al., 1999), terminal sprouting (Tauck and Nadler, 1985), potassium lateral diffusion (Park and Durand, 2006) glial buffering on extracellular potassium are only few phenomena that can lead to impaired regulation of local neuronal activity.

This result strongly suggests that the regulation of neuronal activity (firing rate homeostasis) is required to avoid the persistent chaotic dynamics in the focal epileptogenic region. Therefore, maintaining a sustained neuronal activity in every brain region is required to control chaotic dynamics. However 'excessive order' needs also to be also avoided. During the seizure (about 2 min, Fig. 5b) loss of consciousness can occur followed by confusion and lack of responsiveness (Fagan et al., 1990). Both phenomena

suggests that information processing is altered either due to "excessive" order during the ictal state or due increased periods with abnormal low firing rate and persistent chaotic dynamics (disordered states) in the post-ictal phase. These results point to a relationship between altered conscious experience and intrinsic characteristics of endogenous electric field and reveal a general physical model of computation previously presented in neuroelectrodynamics (Aur and Jog, 2010).

5. Conclusion

The paper presents a combination of several methods applied together to analyze data recordings that brings a cross-disciplinary understanding of the mechanisms involved in seizure generation. Experimental data analysis and analytical models show that the process underlying seizure generation is a rare event, the effect of a severe dysfunctional regulation of neuronal activity inside epileptogenic region. This dysfunctional regulation of neuronal activity in the epileptogenic region is translated in significant changes in endogenous electric field that determines the occurrence of electrical resonances and chaotic dynamics that lead to seizure.

The result of this analysis rules out a precise long term seizure forecasting. However, it clarifies the possibility of accurate short time seizure prediction and effective close loop neuromodulation (Aur et al., 2010). The regularity of the motion and transitory regimes are specific characteristics of multi-dimensional physical systems. These results show that underlying physical principles are universal in nature, they can be observed and transferred between different fields and may reveal the secrets of disturbing neurological condition.

Acknowledgements

The author wishes to thank especially to Paul Buckmaster for continuous excellent feedback and Izumi Toyoda, Mark Bower and Anatol Bragin for suggestions to improve the manuscript. This work was supported by Epilepsy Foundation Award 161096.

References

Adeli H, Zhou Z, Dadmehr N. Analysis of EEG records in an epileptic patient using wavelet transform. J Neurosci Methods 2003;123(1):69–87.
Arnold VI. Proof of a Theorem by A.N. Kolmogorov on the invariance of quasi-periodic motions under small perturbations of the Hamiltonian. Russian Math Surv 1963;18:13–40.
Aur, D., Toyoda, I., Bower M.R. Buckmaster, P.S., 2010, System and Method for Seizure Prediction and Treatment of Epileptic Seizures, S10-419-prov. Patent, http://otlportal.stanford.edu/techfinder/technology/ID=28515.
Aur D., Jog, M., 2010. Neuroelectrodynamics- Understanding The Brain Language, IOS Press 2010. http://dx.doi.org/10.3233/978-1-60750-473-3-i.
Bonni A, Sun Y, Nadal-Vicens M, Bhatt A, Frank DA, Rozovsky I, et al. Regulation of gliogenesis in the central nervous system by the JAK-STAT signaling pathway. Science 1997;278(5337):477–83.
Bower MR, Buckmaster PS. Changes in granule cell firing rates precede locally recorded spontaneous seizures by minutes in an animal model of temporal lobe epilepsy. J Neurophysiol 2008;99(5):2431–42.
Bragin A, Engel J, Staba RJ. High-frequency oscillations in epileptic brain. Curr Opin Neurol 2010;23(2):151–6.
Bragin A, Engel Jr J, Wilson CL, Fried I, Buzsaïki G. High-frequency oscillations in human brain. Hippocampus 1999;9(2):137–42.
Bragin A, Mody I, Wilson CL, Engel Jr J. Local generation of fast ripples in epileptic brain. J Neurosci 2002;22(5):2012–21.
Buzsáki G. Theta oscillations in the hippocampus. Neuron 2002;33(3):325–40.
Buzsaïki G. Rhythms of the Brain. Oxford University Press; 2006.
Cartmell J, Schoepp DD. Regulation of neurotransmitter release by metabotropic glutamate receptors. J Neurochem 2000;75(3):889–907.
Chirikov BV. A universal instability of many-dimensional oscillator systems. Phys Rep 1979;52(5):263–379.
Claes L, Del-Favero J, Ceulemans B, Lagae L, Van Broeckhoven C, De Jonghe P. De novo mutations in the sodium-channel gene SCN1A cause severe myoclonic epilepsy of infancy. Am J Hum Genet 2001;68(6):1327–32.
Crépon B, Navarro V, Hasboun D, Clemenceau S, Martinerie J, Baulac M, et al. Mapping interictal oscillations greater than 200 Hz recorded with intracranial macroelectrodes in human epilepsy. Brain 2010;133(1):33–45.
Csercsa R, Dombovári B, Fabó D, Wittner L, Erss L, Entz L, et al. Laminar analysis of slow wave activity in humans. Brain 2010;133(9):2814–29.
Cvitanovic P. Classical and quantum chaos: a cyclist treatise. Lecture notes, preprint, 1995.
Escayg A, Goldin AL. Sodium channel SCN1A and epilepsy: mutations and mechanisms. Epilepsia 2010;51(9):1650–8.
Fagan KJ, Soo Ik, Lee. Prolonged confusion following convulsions due to generalized nonconvulsive status epilepticus. Neurology 1990;40(11):1689–94.
Farrant M, Nusser Z. Variations on an inhibitory theme: Phasic and tonic activation of GABA A receptors. Nat Rev Neurosci 2005;6(3).
Fröhlich F, McCormick DA. Endogenous electric fields may guide neocortical network activity. Neuron 2010;67(1):129–43.
Gotman J. Relationships between interictal spiking and seizures: human and experimental evidence. Can J Neurol Sci 1991;18(4 Suppl):573–6.
Jefferys JG. Nonsynaptic modulation of neuronal activity in the brain: electric currents and extracellular ions. Physiol Rev 1995;75:689–723.
Jacobs KM, Mogensen M, Warren E, Prince DA. Experimental microgyri disrupt the barrel field pattern in rat somatosensory cortex. Cereb Cortex 1999;9(October–November (7)):733–44.
Luo ACJ. Singularity and Dynamics on Discontinuous Vector Fields, Monograph Book Series in Nonlinear Science and Complexity (Physics). Elsevier; 2006.
Moritani T, Smoker WRK, Sato Y, Numaguchi Y, Westesson P-LA. Diffusion-weighted imaging of acute excitotoxic brain injury. Am J Neuroradiol 2005;26(2):216–28.
Moser JK. Convergent series expansions for quasi-periodic motions. Math Ann 1967;169:136–76.
Kolmogorov AN. On the conservation of conditionally periodic motions under small perturbation of the Hamiltonian. Dokl Akad Nauk SSR 1954;98:527–30.
Newman EA. New roles for astrocytes: regulation of synaptic transmission. Trends Neurosci 2003;26(10):536–42.
Parent JM, Yu TW, Leibowitz RT, Geschwind DH, Sloviter RS, Lowenstein DH. Dentate granule cell neurogenesis is increased by seizures and contributes to aberrant network reorganization in the adult rat hippocampus. J Neurosci 1997;17(10):3727–38.
Park EH, Durand DM. Role of potassium lateral diffusion in non-synaptic epilepsy: a computational study. J Theor Biol 2006;238:666–82.
Pritchard WS, Duke DW. Measuring chaos in the brain: a tutorial review of nonlinear dynamical EEG analysis. Int J Neurosci 1992;67(1–4):31–80.
Reichl LE. The Transition to Chaos: Conservative Classical Systems and Quantum Manifestations. Springer Verlag; 2004.
Small M. Applied Nonlinear Time Series Analysis: Applications in Physics and Physiology. World Scientific; 2005.
Staba RJ, Wilson CL, Bragin A, Fried I. Quantitative analysis of high-frequency oscillations (80–500 Hz) recorded in human epileptic hippocampus and entorhinal cortex. J Neurophysiol 2002;88(4):1743–52.
Staley K, Hellier JL, Dudek FE. Do interictal spikes drive epileptogenesis? Neuroscientist 2005;11(4):272–6.
Tauck DL, Nadler JV. Evidence of functional mossy fiber sprouting in hippocampal formation of kainic acid-treated rats. J Neurosci 1985;5(4):1016–22.
Urbach D, Pratt H. Application of finite impulse response digital filters to auditory brain-stem evoked potentials. Electroencephalogr Clin Neurophysiol 1986;64(3):269–73.
Worrell GA, Parish L, Cranstoun SD, Jonas R, Baltuch G, Litt B. High-frequencyoscillations and seizure generation in neocortical epilepsy. Brain 2004;127:1496–506.
Zhao C, Deng W, Gage FH. Mechanisms and functional implications of adult neurogenesis. Cell 2008;132(4):645–60.

Journal of Neuroscience Methods xxx (2012) xxx–xxx

Contents lists available at SciVerse ScienceDirect

Journal of Neuroscience Methods

journal homepage: www.elsevier.com/locate/jneumeth

A comparative analysis of integrating visual information in local neuronal ensembles

Q1 Dorian Aur*

Department of Mathematics and Statistics, University of Victoria, Victoria, BC, V8W 3R4 Canada

ARTICLE INFO

Article history:
Received 9 February 2012
Received in revised form 19 March 2012
Accepted 20 March 2012

Keywords:
Biological neuron
Information processing
Spike directivity
Neural code
Nanoneuroscience
Neuroelectrodynamics

ABSTRACT

Spike directivity, a new measure that quantifies the transient charge density dynamics within action potentials provides better results in discriminating different categories of visual object recognition. Specifically, intracranial recordings from medial temporal lobe (MTL) of epileptic patients have been analyzed using firing rate, interspike intervals and spike directivity. A comparative statistical analysis of the same spikes from *a local ensemble of four selected neurons* shows that electrical patterns in these neurons display higher separability to input images compared to spike timing features. If the observation vector includes data from all four neurons then the comparative analysis shows a highly significant separation between categories for spike directivity ($p = 0.0023$) and does not display separability for interspike interval ($p = 0.3768$) and firing rate ($p = 0.5492$). Since electrical patterns in neuronal spikes provide information regarding different presented objects this result shows that related information is intracellularly processed in neurons and carried out within a millisecond-level time domain of action potential occurrence. This significant statistical outcome obtained from a local ensemble of four neurons suggests that meaningful information can be electrically inferred at the network level to generate a better discrimination of presented images.

1. Introduction

One important function of the brain is to represent, transform and integrate information received from sensory inputs. Large populations of neurons are commonly involved in information processing in the nervous system. How is this information processed by every cell in the network and how is information integrated in the brain remained unexplained.

Traditional approaches to neural coding hypothesize that information is represented in the spike rate of neurons (Shadlen and Newsome, 1994) or precise timing or of individual spikes (Bialek et al., 1991). More recently besides firing frequency data, interspike interval (ISI) has been assumed to characterize stimuli inputs and provide an accurate representation of distributed neural code (Gerstner and Kistler, 2002). The classical coding model highlights the importance of temporal patterns in large-scale brain networks (Shadlen and Newsome, 1994; Abbott et al., 1997; Honey et al., 2007; Felleman and Van Essen, 1991; Softky and Koch, 1993). Therefore, the main idea of recordings and current analyses in neuroscience is to analyze and decode temporal patterns.

The neuronal activity in the temporal lobe is related to visual recognition of different objects (Liu et al., 2009). In particular these neurons can show selective, invariant, and explicit responses to a set of images. We know from Kreiman et al. (2000) that the same neurons are activated during vision and visual imagery and that firing rate is able to separate between various categories. Quiroga et al. (2005) showed that single MTL neurons fire selectively in response to a particular face, animal, object or scene since single neurons may encode features of particular objects. Almost always responses in single units outlast stimulus presentation and can be associated with conscious recognition (Quiroga et al., 2005).

However, these analyses have raised many new questions. How are categories identified, classified and remembered in these neurons? Are specific neurons or network modules dedicated to face perception? What is the relationship between temporal patterns (firing rate, ISI) and memory formation?

In this paper we try to provide some answers using 'spike directivity', a new measure that captures electrical features during action potential (AP) propagation. Contrary to common belief action potentials are not uniform (stereotyped) pulses of electricity. The digital-like uniformity of action potentials is not validated by experimental data (Quirk et al., 2001; Aur et al., 2005; Aur and Jog, 2006, 2007, 2010; Sasaki et al., 2011). Simple computational techniques can be used to extract information from small changes in APs waveforms (Aur et al., 2005; Aur and Jog, 2006). For every recorded spike, a new measure spike directivity (SD) can be computed using extracellular recordings. Multiple monopoles can describe the current source density of a spike and provide

* Tel.: +1 250 853 3289.
E-mail address: DorianAur@gmail.com

0165-0270/$ – see front matter © 2012 Published by Elsevier B.V.
doi:10.1016/j.jneumeth.2012.03.008

information regarding spatial distribution of electrical processes developed in the cell. If a reference in space is considered (e.g. one tip of tetrodes) then changes in transient charge density that occur intracellularly during action potential (AP) propagation can be represented and monitored (Aur et al., 2005).

Indeed, various characteristics can be used to analyze neuronal activity however, here only three hypotheses are considered. The first hypothesis assumes that firing rate characteristics can provide accurate measures of information processed by neurons during object presentation. The second hypothesis is that interspike interval distributions can provide accurate measures of information processed by neurons during object presentation and the third hypothesis states that spike directivity characteristics provide accurate measures of information processed by neurons during object presentation. Therefore, the main idea is to test statistical significance of these hypotheses in providing information regarding object category. In order to test above hypotheses, the activity of a relatively small subset of neurons from MTL that responded to series of presented images is analyzed. Only three categories of images are analyzed, images of faces, images of animals and images of landscapes. Each category includes five presented images.

2. Data collection materials and methods

The data was previously recorded from patients with pharmacologically intractable epilepsy that have been implanted as described in Kreiman et al. (2000) with depth electrodes to detect the area of seizure onset. The placement of the depth electrodes in the MTL followed limited clinical requirements. Images of faces, animals, and landscapes were presented for 1 s, with 1 s pause after each presentation, in pseudo-random order on a laptop computer in multiple recording sessions, six times each. During all sessions patients were asked to indicate whether a human face was presented. All patients were able to identify human faces with the error rate less than 1%. Majority of these neurons responded to several presented images. Spike detection and sorting were performed and applied to recorded data using well established algorithms. Three main categories of presented images are considered for analysis. The firing rate characteristics, interspike interval distributions and spike directivity characteristics are computed.

The raw cross-correlations of recorded data indicate the presence of similar APs recorded from at least four implanted electrodes. Therefore, the same APs were detected in at least four electrodes that can be considered to form a 'tetrode' framework. An automated unsupervised classification of multidimensional data in the tetrode setup was used (KlustaKwik, Harris et al., Rutgers University). The default values of KlustaKwik from Mclust along with energy features are used to cluster the recordings. Pre-clustered spikes with similar means were merged together and from 17 clusters and only 9 clusters were further considered, about 2000 spikes. The selection of neurons was determined by the requirements to compute spike directivity from recorded AP shapes. Since spike directivity analysis requires extracting information from the variability of AP shapes, action potentials (APs) from neurons that generate smaller amplitudes are not included. Therefore, neurons that generate small AP amplitudes (max values <0.1 mV) were not considered and also one cluster with very high amplitudes was not further included. Four neurons represent the maximum number of neurons that have amplitudes >0.1 mV and can be well separated using the same group of electrodes. This procedure was followed by a manual selection of spikes. The final result shows four well separated clusters with signal amplitudes >0.1 mV which provided four neurons (N_1–N_4) with their APs that were further analyzed (Fig. 1). For each category and for all four analyzed neurons the peristimulus time histogram (PSTH) with equal bin size (20 ms) shows the times at which the neurons fire APs. The response in these neurons did not disappear with stimulus offset and continued up to 2 s after stimulus offset. Therefore, the entire period between

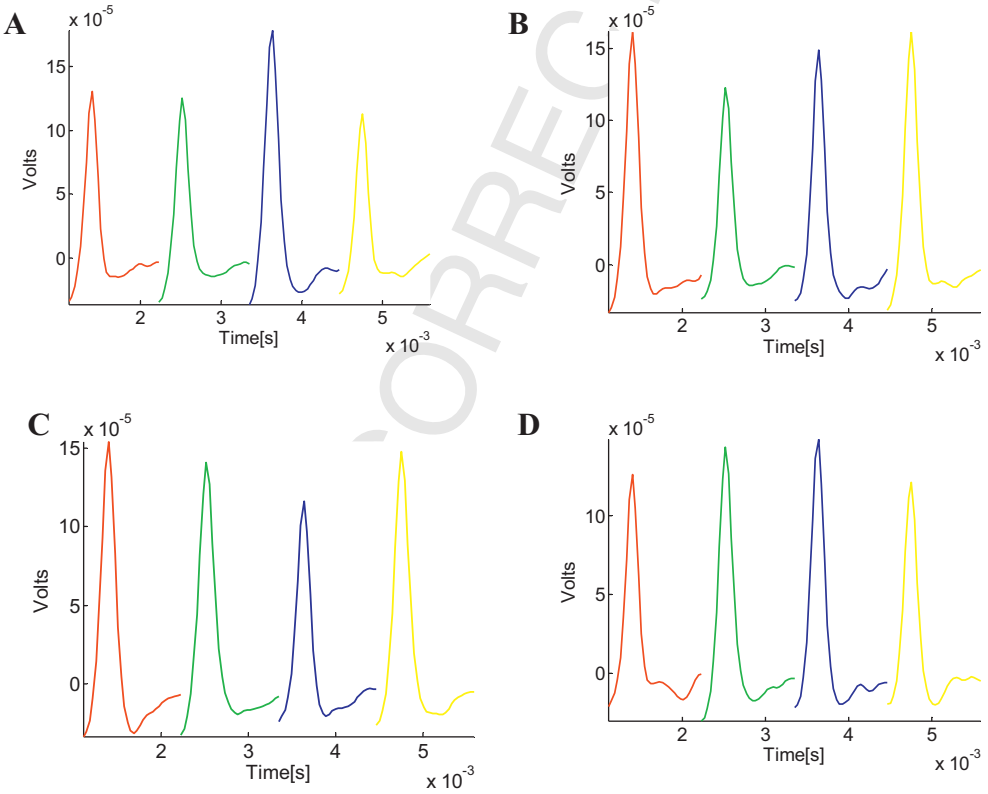

Fig. 1. The mean amplitudes of waveforms recorded from four selected neurons (A) N_1, (B) N_2, (C) N_3 and (D) N_4.

Please cite this article in press as: Aur D. A comparative analysis of integrating visual information in local neuronal ensembles. J Neurosci Methods (2012), doi:10.1016/j.jneumeth.2012.03.008

Table 1
The maximum values for the means of amplitudes for all 4 selected neurons.

	Channel 1 [μV]	Channel 2 [μV]	Channel 3 [μV]	Channel 4 [μV]
N_1	130.2	125.0	177.7	161.3
N_2	161.6	122.8	149.1	161.3
N_3	154.2	140.7	116.1	147.7
N_4	126.4	143.7	148.4	121.5

200 ms and 2000 ms after stimulus onset is considered in these analyses. The presence of a refractory period in single units has been checked (less 1% spikes within <3-ms ISI). The maximum values of the means of APs amplitudes provide the difference between four channels in a tetrode configuration where about 550 spikes are generated by 4 neurons (Fig. 1 and Table 1). Without performing complex cell membrane recordings or intracellular recordings the extracellulary recorded potentials can be used to estimate changes in charge density that occur inside neurons using the charge movement model (Aur et al., 2005). Multiple monopoles can describe the current source density of a spike (Aur and Jog, 2006, 2010; Gold et al., 2006). The monopole technique was experimentally tested (Lee et al., 2011). For each clustered spike we computed spike directivity using the algorithm presented in Aur et al. (2005). To maintain a correct search direction, a test for positive definiteness of J matrix is required and corrections are introduced if necessary (Dennis and Schnabel, 1983) using plausible convergence criteria to stop the algorithm (Isaacson and Keller, 1994; Mittelhammer et al., 2000). Since the sample size is similar ($n > 40$) and the same spikes are used, then statistical methods can well capture the difference between different methods of analysis.

2.1. Image presentation and hypotheses

The set of images includes five faces with corresponding features $f^{FACES} = \{f^{Face1}, f^{Face2}, f^{Jennifer}, f^{Ander}, f^{Drew}\}$, five animals with features $f^{ANIM} = \{f^{Monkey}, f^{Horse}, f^{Eleph}, f^{Spider}, f^{Tiger}\}$ and five landscapes $f^{LAND} = \{f^{Out10}, f^{Out12}, f^{Out20}, f^{Out26}, f^{Out28}\}$ where $f^{FACES} \in F^{FACES}$, $f^{ANIM} \in F^{ANIM}$ and $f^{OUT} \in F^{OUT}$. The presentation of each image category generates neural activity which is the response considered to be the 'output space' with corresponding characteristics for faces $h^{FACES} = \{h^{Face1}, h^{Face2}, h^{Jennifer}, h^{Ander}, h^{Drew}\}$, animals $h^{ANIM} = \{h^{Monkey}, h^{Horse}, h^{Eleph}, h^{Spider}, h^{Tiger}\}$ and landscapes $h^{LAND} = \{h^{Out10}, h^{Out12}, h^{Out20}, h^{Out26}, h^{Out28}\}$ where $h^{FACES} \in H^{FACES}$, $h^{ANIM} \in H^{ANIM}$ and $h^{OUT} \in H^{OUT}$. The set of features f_i varies from image to image, however objects from a certain category have to share specific features. This set of features that characterize presented images contains relevant attributes which may include semantic aspects or other particular characteristics. The neural response can be measured by estimating the firing rate. Given a set of features $f_i \in F$ the neuron transforms (maps) the set of input features in series of action potentials (APs) in such way that $h_{firing_i} \in H_F$ represents the image feature f_i:

$$F \xrightarrow{T_F} H_F \tag{1}$$

where T_F is the transformation from image feature to firing characteristics. Since images are repeatedly presented, then the estimation of firing rate can be obtained if this value is averaged. The mean firing rate response to a picture is computed as the median number of spikes across trials between 200 and 2000 ms after stimulus onset. The probability density of ISI can be also considered a measure of neural activity which embeds information. Therefore, given the same set of features $f_i \in F$ the neuron transforms (maps) this set of features in interspike interval characteristics $h_{ISI_i} \in H_{ISI}$

$$F \xrightarrow{T_{ISI}} H_{ISI} \tag{2}$$

where T_{ISI} is the transformation from image feature to ISI data. The probability density of ISI is obtained using a kernel density estimator that generates the characteristics h_{ISI}^{FACES} for faces, h_{ISI}^{ANIM} for animals and h_{ISI}^{LAND} for landscapes.

The existence of patterns of activation (micro-maps) determined by different spatial charge densities has been recently evidenced in APs (Aur et al., 2005; Aur and Jog, 2006). Since APs are spatially modulated in a meaningful way (Aur and Jog, 2010) then it is expected that electrical patterns within spikes contain information from presented images. Therefore, given a set of features f_i the neuron transforms (maps) these features in electrical patterns and spike directivity characteristics $f_i \in F$

$$F \xrightarrow{T_{SD}} H_{SD} \tag{3}$$

where $h(x_i, y_i, z_i)$ represents the distribution of electrical charges in Cartesian coordinates (x_i, y_i, z_i) and T_{SD} is the transformation from object feature into a distribution of electric patterns within spikes. Since spike directivity characterizes the transient density of electrical charges, then the third hypothesis is that the relationship between object presentation and the presence of electrical patterns (micro-maps) is not random and can be captured by an analysis of spike directivity. Since every spike directivity vector points on a sphere surface (Fig. 2a) the corresponding output features $h_{SD_i} \in H_{SD}$ are determined by estimating spike directivity and corresponding representation as distinct points on the unit sphere (Fig. 2b):

$$S^2 = \{r \in R^3 : ||r|| = 1\} \tag{4}$$

In order to analyze the resulting distribution of the head of arrows on the unit sphere all three-dimensional Cartesian coordinates (x_i, y_i, z_i) are mapped into spherical coordinates θ_i and φ_i where:

$$\theta_i = a \tan\left(\frac{y_i}{x_i}\right) \tag{5}$$

and

$$\varphi_i = a \tan\left(\frac{z_i}{\sqrt{x_i^2 + y_i^2}}\right) \tag{6}$$

The density of mapped features (only θ_i angle is considered) can be estimated using a kernel density estimator:

$$\widehat{h}(\theta) = \frac{1}{ns}\sum_{i=1}^{n}\left(\frac{K(\theta - \theta_i)}{s}\right) \tag{7}$$

where K is a Gaussian kernel and s is the smoothing parameter Terrell and Scott (1992). These electric patterns represented on the unit sphere map specific features of faces h_{SD}^{FACES}, animals h_{SD}^{ANIM} or landscapes h_{SD}^{LAND}.

3. Results

All four analyzed neurons responded primarily to all different images. Two different spikes recorded from the same neuron can display different spike directivities (Fig. 3). The electrical activity appears mirrored (Aur et al., 2005). Since the entire device is

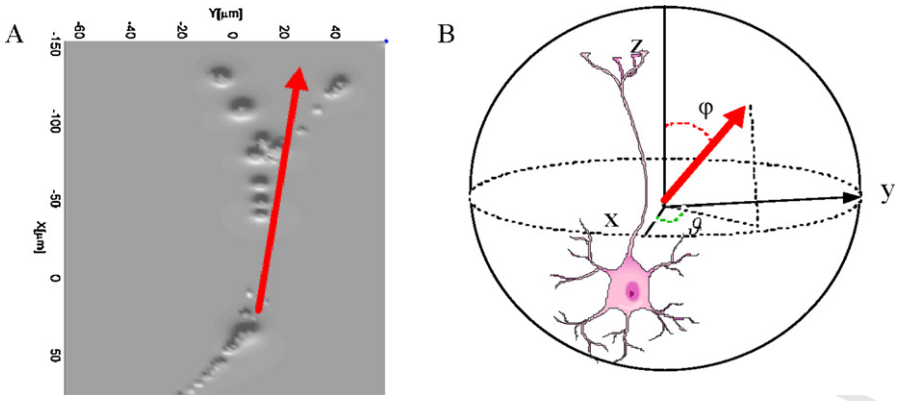

Fig. 2. (A) The representation of spike directivity as a vector in red color when electrical patterns occur simultaneously in two axonal branches (adapted from Aur and Jog (2010)). X and Y represent the coordinates in microns of 2D-view of recorded spike. (B) A schematic representation of scaled neuron in the unit sphere. The spike directivity is represented in red color. The arrow head points on the 2-sphere surface. In a spherical coordinate system the angles θ and φ characterize the orientation of spike directivity vector (θ values range from 0 to 2π while φ values range from 0 to π). (For interpretation of the references to color in figure legend, the reader is referred to the web version of the article.)

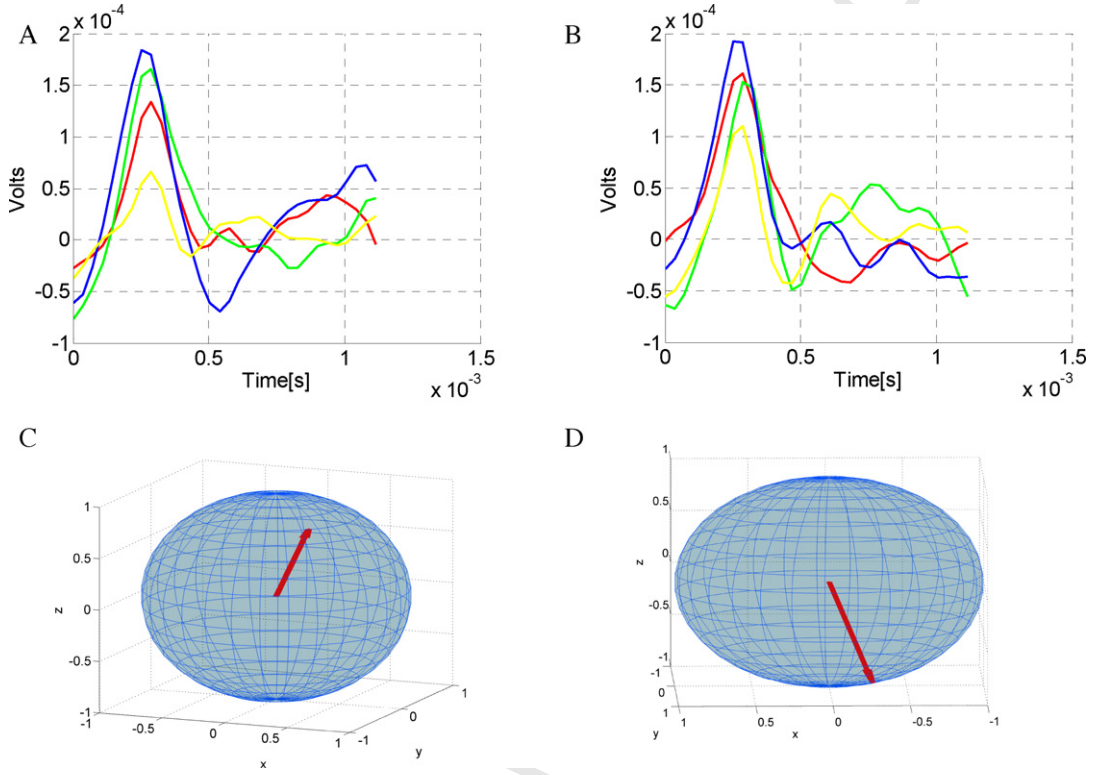

Fig. 3. Two different spikes from the same neuron recorded by four electrodes represented in blue, red, green and yellow display two different spike directivities. The panels C and D are estimates from panels A and B. The differences of recorded voltages within these two spikes represented in A and B are mapped into corresponding changes of spike directivity in C and D. The head of the arrow points on a sphere with radius one ($\|r\| = 1$). (A) Four recorded waveforms and their corresponding spike directivity represented on the north hemisphere (C). (B) Four recorded waveforms and their corresponding spike directivity represented on the South hemisphere (D).

asymmetric, the representation of spike directivity on the north hemisphere provides a better resolution and displays in an explicit topographic manner the relationship with encoded categories (Fig. 4). Assuming normality of data, one way ANOVA statistics can be used to determine if these characteristics of faces, animals and landscapes are well separated. A similar analysis is performed for firing rate and ISI probability densities and then compared.

The estimated *F*-ratio and *p*-values summarize the result of comparative statistical analysis (see Table 2). Larger values of *F*-ratio show that the variation among group means do not occur by chance. In the first two neurons one way ANOVA statistics of firing rate characteristics does not provide any separation between

Table 2
A comparative analysis one way ANOVA test.

	Firing rate		ISI		SD	
	p	*F*	*p*	*F*	*p*	*F*
N_1	0.678	0.4	0.3196	1.15	0.028	3.62
N_2	0.248	1.57	0.0008	7.3	0.0012	6.87
N_3	0.09	2.95	9.9749e-007	14.48	0.065	2.75
N_4	0.0261	5.01	0.1723	1.77	0.011	4.57

Please cite this article in press as: Aur D. A comparative analysis of integrating visual information in local neuronal ensembles. J Neurosci Methods (2012), doi:10.1016/j.jneumeth.2012.03.008

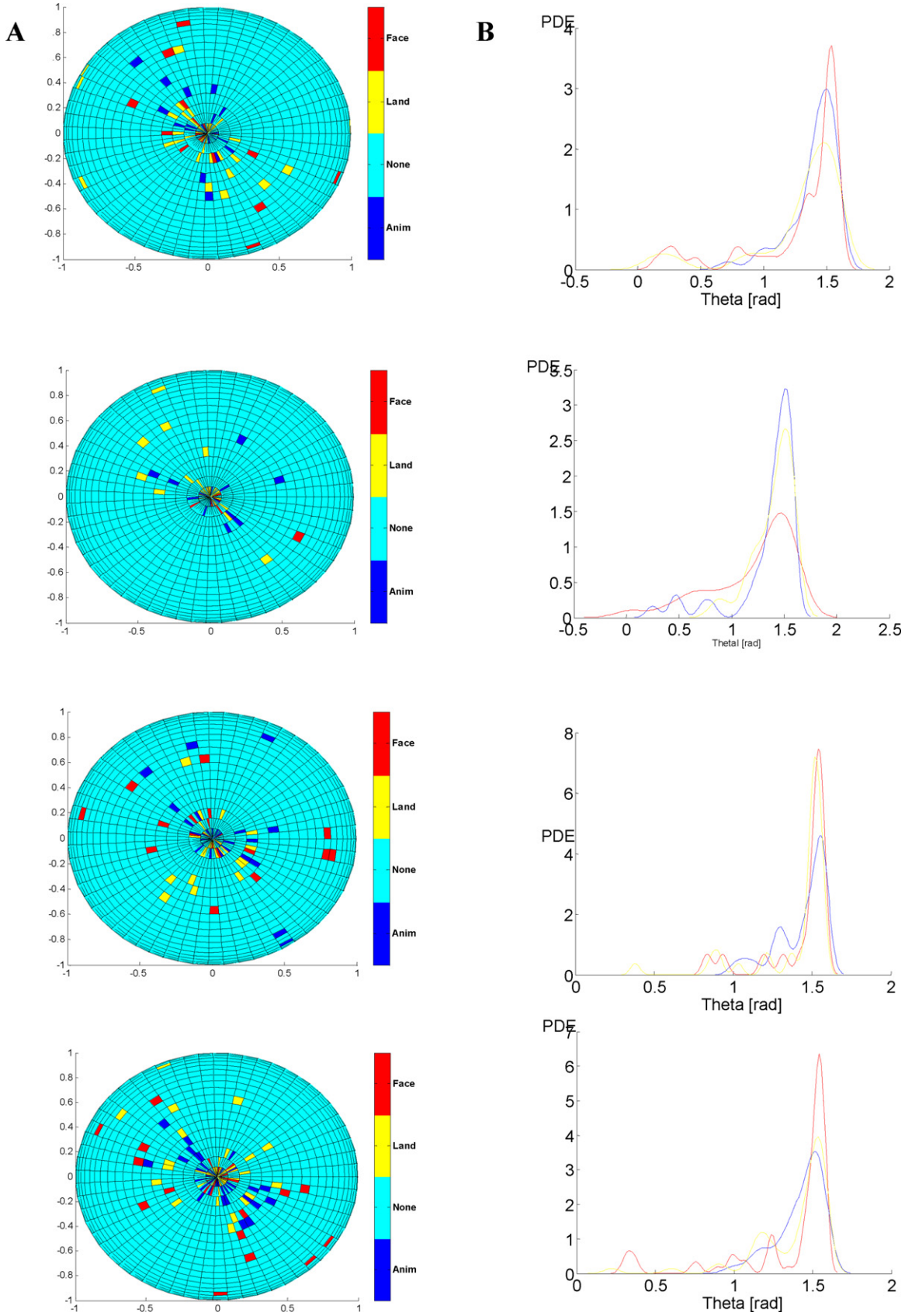

Fig. 4. The representation of spike directivity features is mapped on the north hemisphere of four neurons. The corresponding probability density estimate of spike directivity (θ_i angles) of faces in red color, animals in blue color and landscapes are represented in yellow color. (A) The representation of spike directivity head arrows on the unit sphere; (B) The probability density estimates of spike directivity (θ_i angles) display clustering effects in all four neurons (faces in red color, animals in blue color, landscapes in blue color). (For interpretation of the references to color in figure legend, the reader is referred to the web version of the article.)

Please cite this article in press as: Aur D. A comparative analysis of integrating visual information in local neuronal ensembles. J Neurosci Methods (2012), doi:10.1016/j.jneumeth.2012.03.008

categories (p-values >0.1) N_1: $p = 0.678$, N_2: $p = 0.248$). However, the observed difference is significant ($p < 0.05$) in the neuron N_4: $p = 0.0261$ and marginally significant ($p < 0.1$) in the neuron N_3: $p = 0.09$. Similar analysis carried on using probability density of ISI displays highly significant category separability ($p < 0.001$) in two neurons (N_2: $p = 0.0008$; N_3: $p = 9.9749e\text{-}007$) and does not provide any separation in the other two neurons (N_1: $p = 0.3196$; N_4: $p = 0.1723$). Interestingly, the neuron where the firing rate shows high separability between ISI characteristics (N_2: $p = 0.0008$) is the one where firing rate does not provide any separation (N_2: $p = 0.248$). Additionally, for firing rate the difference is significant in N_4 (N_4: $p = 0.0261$) and does not display separability if ISI is analyzed in N_4 (N_4: $p = 0.1723$). However, one way ANOVA statistics of probability density function of the θ angle shows that electric characteristics generated during AP propagation in these neurons significantly separate these categories with p-values: N_1: $p = 0.028$, N_2: $p = 0.0012$; N_4: $p = 0.011$ and the difference is marginally significant in one neuron (N_3: $p = 0.065 < 0.1$).

If the observation vector includes data from all 4 neurons, then the comparative analysis shows a highly significant separation between categories for spike directivity ($F = 6.09$, $p = 0.0023$) and does not display separability for ISI ($F = 0.98$, $p = 0.3768$) and firing rate ($F = 0.61$, $p = 0.5492$). The normality of data is not an issue and does not change the significant difference between firing rate, ISI and spike directivity. The application of Kruskal–Wallis method shows similar significant differences between temporal coding (firing rate, ISI) and spike directivity (Table 3). In addition, the Kruskal–Wallis method does not require the assumption of a normal distribution. If the observation vector includes data from all 4 neurons, the comparative analysis with Kruskal–Wallis displays even a higher separation between categories than ANOVA ($p_{KW} = 2.629 \times 10^{-7}$). Also, in this small local network, the Kruskal–Wallis test does not display separability for ISI ($p_{KW} = 0.8904$) or firing rate ($p_{KW} = 0.4888$). A post hoc pairwise comparison shows that the difference between animals and other groups (faces and landscapes) is relevant. The firing rate and ISI

Table 3
Both tests ANOVA and Kruskal–Wallis show similar differences.

	Firing rate		ISI		SD	
	p	p_{KW}	p_{ANOVA}	p_{KW}	p_{ANOVA}	p_{KW}
N_1	0.678	0.5398	0.3196	0.2116	0.028	0.0439
N_2	0.248	0.2350	0.0008	0.0347	0.0012	0.0068
N_3	0.09	0.0743	9.9749×10^{-7}	0.2099	0.065	4.692×10^{-9}
N_4	0.0261	0.0331	0.1723	0.2358	0.011	1.26×10^{-5}

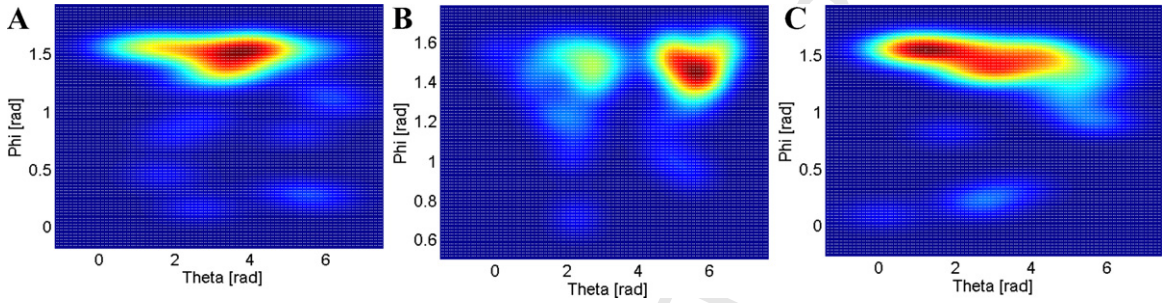

Q4 **Fig. 5.** The electrical activity of selected neuron (N_1) displays a direct relationship to encoded categories in a topographic manner. The two dimensional probability density estimate of arrowhead positions of spike directivities on the north hemisphere across θ and φ angles for (A) faces, (B) animals and (C) landscape.

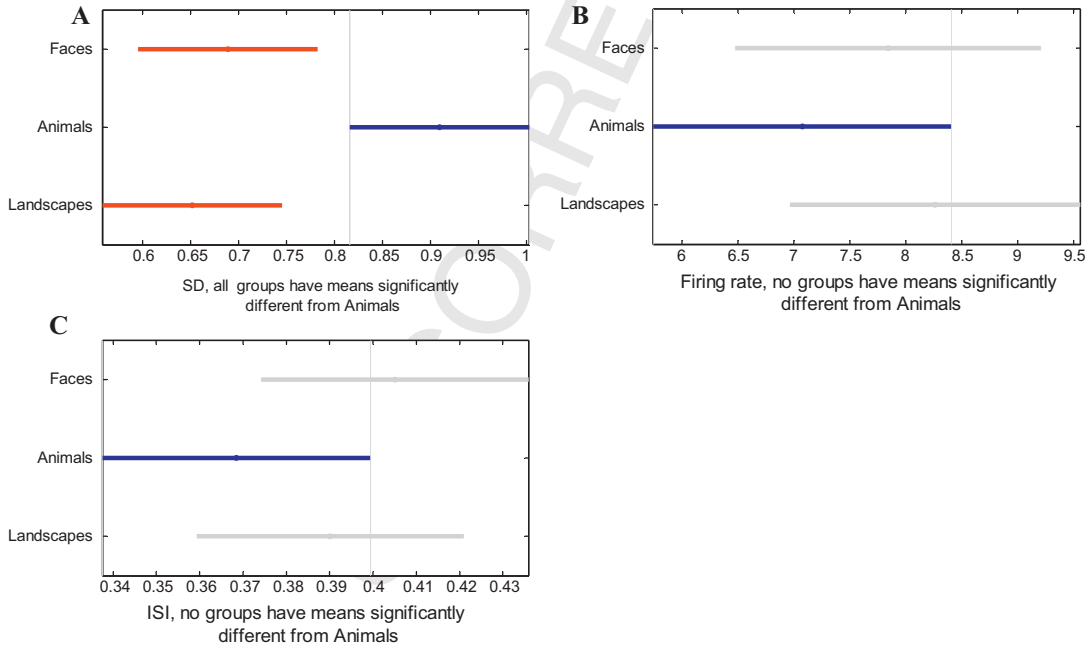

Fig. 6. A post hoc pairwise comparison shows differences between SD, firing rate and ISI analyses in four selected neurons (A) If spike directivity is considered then a significant difference occurs between animals and the other two categories (faces and landscapes). (B) There is no significant difference between categories if firing rate is considered. (C) There is no significant difference between categories if ISI is considered.

Please cite this article in press as: Aur D. A comparative analysis of integrating visual information in local neuronal ensembles. J Neurosci Methods (2012), doi:10.1016/j.jneumeth.2012.03.008

analysis do not provide a significant difference between the groups (Fig. 6).

4. Discussion

In these four selected neurons spike directivity analysis outperforms firing rate and ISI outcome in relating neuronal activity with category presentation. Statistical analysis shows that spatial distribution of electrical patterns is not random, it caries information regarding presented images and their categories (Fig. 5). The change in electrical patterns follows the anatomical model of the cell, the geometry and topology of active regions involved in spike generation (Fig. 2). The comparative analysis of spike directivity data from all four neurons together provides a highly significant separation between categories in both tests (ANOVA: $F = 6.09$, $p = 0.0023$; Kruskal–Wallis, $p_{KW} = 2.629 \times 10^{-7}$) while firing rate and interspike interval data recorded from the same group of neurons do not display statistical significant separability. The occurrence of electrical patterns and spatial modulation of action potential is determined by presented objects and shaped by specific morphological characteristics of neurons (Figs. 2 and 4). Since all four neurons respond to analyzed categories and provide highly significant separation between categories in both tests, these results suggest that information regarding presented images is intracellularly processed in many neurons and electrically inferred during AP generation. Within a millisecond-level time domain of AP generation the transient charge density dynamics provides meaningful information regarding object category representation. These neurons behave as 'weak learners' that attend to preferred spatial directions in the probably approximately correct sense (Aur and Jog, 2007).

Indeed, statistical analysis of electrical patterns in neuronal ensemble can tell more about the image class than using a separate analysis in single cells. A different spatial propagation of action potentials can determine a change in synaptic connectivity which may alter the communication of information in the network. Therefore, a different spatial propagation will target different synapses, change proximity interactions and ephaptic coupling (Anastassiou et al., 2011). A spatial modulation of AP propagation can alter the synaptic function via Ca^{2+} signaling that may increase the release of neurotransmitters with direct effects on ion channels in the postsynaptic neuron. The selection of neurons with APs (max values >0.1 mV) is solely required to accurately estimate spike directivity and does not limit the generality of results.

This fundamental approach in perceiving information in electrical patterns within spikes connects changes in electrical patterns with molecular machinery (Wang et al., 1998; LaFerla, 2002; Woolf et al., 2009; Guan et al., 2009; Aur, 2011; Aur et al., 2011) and complex electrochemical processes that spatially modulate AP propagation (Aur et al., 2011). If only few neurons are analyzed (e.g. four), firing rate and ISI do not always display statistical significant relationship with presented objects categories (Fig. 6). In addition, the analysis of temporal patterns (ISI, firing rate) shows that the local ensemble does not seem to perform significantly better than individual neurons ($p_{KW} = 0.8904$, $p_{KW} = 0.4888$). Therefore, the fundamental aspects of information processing, communication and computation may be hidden to temporal analysis (firing rate, ISI).

Indeed, the roots of intelligent action seem to lie deep in information processing performed by single cells (Ford, 2009, 2010). These simple cells have evolved to carry electric signals 'became' neurons in order to electrically integrate various information in the brain. Earlier theoretical models have revealed complex intracellular phenomena where molecular structures are directly involved in information processing (Barlow, 1996; Hameroff et al., 2002, 2010; Pidaparti et al., 2007; Woolf et al., 2009; Craddock et al., 2010). All of them have suggested the existence of sub-cellular platforms for information processing which preferentially regulate protein signaling pathways required to store fragments of information at the level of individual proteins.

5. Conclusion

The response of a local ensemble of four neurons to different presented images is captured by temporal coding features (firing rate, ISI) and spike directivity. Importantly, this small subset of neurons recorded by the same group of electrodes form together a local ensemble. If information from electrical patterns is considered the ensemble shows a better outcome in category recognition than any separate neuron. This property cannot be extended to temporal coding features. In fact, these experimental results confirm the existence of an important sub-cellular level for information processing. In this small local network, estimated electrical patterns provide enhanced discrimination of presented images. Meaningful changes in electrical patterns reveal that information regarding presented objects is processed within cells and electrically integrated in the brain. This outcome highlights a neuroelectrodynamic model of computation by interaction which brings back the strength of physical laws to explain the complexity of information processing in the brain (Aur, 2011; Aur and Jog, 2010; Aur et al., 2011). In addition the interaction between neurons including connectivity seems to be influenced by intracellular processes which can spatially modulate the propagation of APs. The all or none AP allows a fast interaction inside the cell when information stored within molecular structure (e.g. proteins) is carried out and integrated within the generated electric flux. Overall, this fast process (action potential-1 ms) is more energy efficient than a graded response since it provides stronger interaction with less energy. With adequate computational methods (e.g. spike directivity) this meaningful information that occurs during AP generation can be directly extracted from spikes. Spike directivity is a vector that quantifies changes in transient charge density during action potential propagation and reflects the interaction between charge densities embedded within molecular structures (e.g. proteins) and the transient developed flow of electrical charges. The presence of information regarding presented objects in the extracellular space suggests that various informations can be electrically integrated in the brain. These phenomena that occur within APs may provide a step forward in understanding the fundamental gap between molecular description, information processing, memory, neuronal function and actual framework in cognitive computation.

Acknowledgment

The author wish to thank Peter N. Steinmetz for providing data recordings and excellent feedback to improve the manuscript.

References

Abbott LF, Varela JA, Sen K, Nelson SB. Synaptic depression and cortical gain control. Science 1997;275(5297):220–4.
Anastassiou CA, Perin R, Markram H, Koch C. Ephaptic coupling of cortical neurons. Nat Neurosci 2011;14(2):217.
Aur D, Connolly CI, Jog MS. Computing spike directivity with tetrodes. J Neurosci Methods 2005;149(1):57–63.
Aur D, Jog MS. Building spike representation in tetrodes. J Neurosci Methods 2006;157(2):364–73.
Aur D, Jog MS. Neuroelectrodynamics, understanding the brain language. IOS Press; 2010.
Aur D. From neuroelectrodynamics to thinking machines. Cogn Comput 2011., doi:10.1007/s12559-011-9106-3, http://www.springerlink.com/content/x1l7388475323758/.
Aur D, Jog MS, Poznanski R. Computing by physical interaction in neurons. J Integr Neurosci 2011;10(4):413–22.

Please cite this article in press as: Aur D. A comparative analysis of integrating visual information in local neuronal ensembles. J Neurosci Methods (2012), doi:10.1016/j.jneumeth.2012.03.008

Aur D, Jog MS. Neuronal spatial learning. Neural Process Lett 2007;25(1):31–47, http://dx.doi.org/10.1007/s11063-006-9029-2.
Barlow H. Intraneuronal information processing, directional selectivity and memory for spatio-temporal sequences. Netw: Comput Neural Syst 1996;7(2):251–9.
Bialek W, Rieke F, De Ruyter Van Steveninck RR, Warland D. Reading a neural code. Science 1991;252(5014):1854–7.
Craddock TJA, Tuszynski JA, Priel A, Freedman H. Microtubule ionic conduction and its implications for higher cognitive functions. J Integr Neurosci 2010;9(2):103–22.
Dennis JE, Schnabel RB. Numerical methods for unconstrained optimization and nonlinear equations. Prentice-Hall, Inc; 1983.
Felleman DJ, Van Essen DC. Distributed hierarchical processing in the primate cerebral cortex. Cereb Cortex 1991;1(1):1–47, 1864.
Ford BJ. The secret power of the single cell. New Sci 2010;206:26–7.
Ford BJ. On intelligence in cells: the case for whole cell biology. Interdiscip Sci Rev 2009;34:350–65.
Gerstner W, Kistler WM. Spiking neuron models – single neurons, populations, plasticity. Cambridge Univ. Press; 2002.
Gold C, Henze DA, Koch C, Buzsáki G. On the origin of the extracellular action potential waveform: a modeling study. J Neurophysiol 2006;95:3113–28.
Guan JS, Haggarty SJ, Giacometti E, Dannenberg JH, Joseph N, Gao J, et al. HDAC2 negatively regulates memory formation and synaptic plasticity. Nature 2009;459(7243):55–60.
Hameroff S, Nip A, Porter M, Tuszynski J. Conduction pathways in microtubules, biological quantum computation, and consciousness. Biosystems 2002;64:149–68.
Hameroff SR, Craddock TJA, Tuszynski JA. 'Memory bytes' – a molecular match for CaMKII phosphorylation encoding of microtubule lattices. J Integr Neurosci 2010;9:253–67.
Honey CJ, Kötter R, Breakspear M, Sporns O. Network structure of cerebral cortex shapes functional connectivity on multiple time scales. Proc Natl Acad Sci U S A 2007;104(24):10240–5.
Isaacson E, Keller HB. Analysis of numerical methods. New York: Dover Publications; 1994.
Kreiman G, Koch C, Fried I. Imagery neurons in the human brain. Nature 2000;408(6810):357–61.
LaFerla FM. Calcium dyshomeostasis and intracellular signalling in Alzheimer's disease. Nat Rev Neurosci 2002;3(11):862–72.
Lee CW, King CE, Wu SC, Swindlehurst L, Nenadic Z. Signal source localization with tetrodes: experimental verification. In: Proceedings of 33rd Annual International Conference of the IEEE EMBS; 2011. p. 67–70.
Liu H, Agam Y, Madsen JR, Kreiman G. Timing, timing, timing: fast decoding of object information from intracranial field potentials in human visual cortex. Neuron 2009;62(2):281–90.
Mittelhammer RC, Judge GG, Miller D. Econometric foundations, vol. 1. Cambridge University Press; 2000.
Pidaparti RM, Primeaux D, Saunders B. Modeling and simulation of biological self-assembly structures from nanoscale entities. J Nanosci Nanotechnol 2007;7:4248–53.
Quiroga RQ, Reddy L, Kreiman G, Koch C, Fried I. Invariant visual representation by single neurons in the human brain. Nature 2005;435(7045):1102–7.
Quirk MC, Blum KI, Wilson MA. Experience-dependent changes in extracellular spike amplitude may reflect regulation of dendritic action potential back-propagation in rat hippocampal pyramidal cells. J Neurosci 2001;21:240–8.
Sasaki T, Matsuki N, Ikegaya Y. Action-potential modulation during axonal conduction. Science 2011;331(6017):599–601.
Shadlen MN, Newsome WT. Noise, neural codes and cortical organization. Curr Opin Neurobiol 1994;4(4):569–79, 511.
Softky WR, Koch C. The highly irregular firing of cortical cells is inconsistent with temporal integration of random EPSPs. J Neurosci 1993;13(1):334–50.
Terrell GR, Scott DW. Variable kernel density estimation. Ann Stat 1992;20(3):1236–65.
Wang HS, Pan Z, Shi W, Brown BS, Wymore RS, Cohen IS, et al. KCNQ2 and KCNQ3 potassium channel subunits: molecular correlates of the M-channel. Science 1998;282(5395):1890–3.
Woolf NJ, Priel A, Tuszynski JA. Nanoneuroscience: structural and functional roles of the neuronal cytoskeleton in health and disease. Springer Verlag; 2009.

Please cite this article in press as: Aur D. A comparative analysis of integrating visual information in local neuronal ensembles. J Neurosci Methods (2012), doi:10.1016/j.jneumeth.2012.03.008

ELSEVIER

Journal of Neuroscience Methods 149 (2005) 57–63

JOURNAL OF NEUROSCIENCE METHODS

www.elsevier.com/locate/jneumeth

Computing spike directivity with tetrodes

Dorian Aur [a,*], Christoper I. Connolly [b], Mandar S. Jog [a]

[a] *Department of Clinical Neurological Sciences, Movement Disorders Program, London Health Sciences Centre, 339 Windermere Rd., London, Ont., Canada N6A 5A5*

[b] *SRI International, Menlo Park, CA, USA*

Received 6 January 2005; received in revised form 4 May 2005; accepted 5 May 2005

Abstract

The ability of neurons to generate electrical signals is strongly dependent on the evolution of ion-specific pumps and channels that allow the transfer of charges under the influence of electric fields and concentration gradients. This paper presents a novel method by which flow of these charge fluxes may be computed to provide directivity of charge movement. Simulations of charge flow as well as actual electrophysiological data recorded by tetrodes are used to demonstrate the method. The propagation of charge fluxes in space in data from simulation and actual recordings during action potential can be analyzed using signals recorded by tetrodes. Variation in spike directivity can be estimated by computing singular value decomposition of the estimated 3D trajectory data. The analysis of the spike model can be accomplished by performing simulations of presumed equivalent moving charges recorded by the tetrode tips. For in vivo spike recordings, the variation of spike directivity could be obtained using several spikes of selected neurons considering the charge movement model (CMM). The relationship between computer simulation results and tetrode data recordings is examined. The paper concludes by showing that the method for calculating directivity in actual spike recordings is robust. The method allows for improved filtering of data and more importantly may shed light on furthering the study of spatio-temporal encoding in neurons.

Keywords: Tetrode; Spike modelling; Singular value decomposition; Newton–Raphson

1. Introduction

The brain is composed of a large number of electrically active cells that communicate with each other. Starting from the early work of Hebb (1949), understanding of brain function was directed toward the coding properties of groups of neurons named “cell assemblies”. Few studies focused on the spatial properties of the action potential (AP). In this context plasticity changes have been related to overall connection strength between the pre- and postsynaptic neurons.

The origins of the problems regarding view of cell functioning at an electrophysiological level currently and in the past may arise from the limited ability of single cell recordings that primarily analyze mainly stereotyped waveforms. In addition, most research that has studied large populations of neurons (Zhang et al., 1998) hoping to find pattern of activities, has largely ignored the study of spatial distribution of electrical events from single spikes as a method of information coding. Current thinking holds that, since the spike is considered to be a reasonably stereotyped waveform for individual cells, information flow from cell to cell is supposed to be carried by the occurrence of the AP at particular times or rates. In this respect, the spike is felt to be a passive event that does not itself code for anything. Indeed physiologists often reduce the spike to a discrete scalar event in time and analyze behavior in this context alone.

It is therefore possible that the flow of information with spike events may be communicated within the milieu of the extracellular space and such information to the surrounding neurons is intrinsic and important in determining the flow of information outside of what is communicated through the spike event alone. However, spatial features of spikes are an essential part of the surrounding milieu of a biological cell. Processing of information received from neighboring

* Corresponding author. Tel.: +1 519 685 8300x32758.
E-mail address: daur2@uwo.ca (D. Aur).

0165-0270/$ – see front matter © 2005 Elsevier B.V. All rights reserved.
doi:10.1016/j.jneumeth.2005.05.006

neurons involve activities in several synapses, ionic channels, changes in membrane potential that usually have a spatial distribution.

In order to study the spatial properties of individual neurons and how they affect the spatio-temporal spread of information requires the collection of multi-dimensional data for every spike. Tetrode recordings that utilize four tips allow such a 4D view of the spike. The goal of much tetrode-based research is to study these interactions by assigning spikes to different neurons. Several spike-detection and sorting methods have been proposed in the literature (Gray et al., 1995; Jog et al., 1999, 2002; Sahani et al., 1998). The method developed by Takahashi et al. (2003) combines an independent component analysis and *k*-means clustering to solve the spike-overlapping problem within tetrode recordings. Recently Emondi et al. (2004) developed a reliable procedure for tracking neurons across files for non-overlapping data sets.

Based on four measured signals from tetrode our paper provides a computational approach for determining variability of spikes' spatial directivity. This paper is not another spike sorting method, nor is it a technique for tracking neurons over days, from tetrode recordings (Chelaru and Jog, 2005; Emondi et al., 2004). The paper presents a method of computing the directivity of charge flow during action potentials and its variability in successive spikes within extracellular space. This charge flow directivity may have a substantial impact on the milieu within which a neuron is active and therefore should not be ignored. This interesting and important approach of the dynamics of the spikes generated by neurons, its impact on the extracellular milieu and their possible intricate relationship, does not yet exist in the literature.

In the first step of the algorithm, a simplified spike model based on charges in movement is constructed. For the "charge movement model", the trajectory of charge is computed using a Newton–Raphson algorithm followed by a singular value decomposition algorithm that is performed to determine the directivity of the artificially generated spike. The trajectory gives the overall direction of AP propagation from start to finish. However, since the spike trajectory is a curve, it is not so easy to compare trajectories of several spikes. A linear approximation of the trajectory is needed for easier spatial variability investigation for which singular value decomposition (SVD) is performed. The computed components are the largest singular value and its corresponding right singular vector represents, in fact, the main directivity tendency for the spike in the computational space.

2. Charge movement model

Neurons are enclosed by plasma membranes whose primary function is to control the passage of ions and molecules. Diffusion of ions from high to low concentration is the effect of concentration differences between intracellular and extracellular space. Ion-specific pumps allow the transfer of charges up and down gradients over a finite volume. Several ions like K^+, Na^+, Cl^-, Ca^{2+} carry electric charges and their movement is influenced not only by concentration gradients but also by electrical fields. Therefore, ionic flux J under the influence of an electric field and concentration gradient can be written using the Nernst–Planck equation:

$$J = -\mu z C \frac{\partial V}{\partial x} - D \frac{\partial C}{\partial x} \tag{1}$$

where V is the electric potential, μ the mobility, z the valence of the ion, C the concentration and D is the diffusion coefficient (Schwartz, 1971).

A model of collective ionic motion is proposed for analysis (Fig. 1). The movement of charged particles during AP will generate an electrostatic field $\vec{E}$. For analysis, a simplified spike model includes a single charge in movement that generates potential variation in the four tips that simulate a tetrode. The electrostatic potential $V_A(x, y, z)$ in point A due to charge distribution is a 3D scalar field that can be computed:

$$V_A(r) = \frac{1}{4\pi\varepsilon} \sum_{i=1}^{n} \frac{q_i}{r_i} \tag{2}$$

where ε is the medium permittivity, q_i and r_i the charges and their distances to point A.

The electrostatic field is a quantity that varies in space and is determined by the configuration of source charges. The lines of the electrostatic field, $\vec{E}$ point in the direction of maximum increase of electrostatic potential $\vec{E} = -\nabla V$ or:

$$\vec{E}(\vec{r}) = \frac{1}{4\pi\varepsilon} \sum_{i=1}^{n} \frac{q_i}{r_i^3} \vec{r}_i \tag{3}$$

If these charges are moving in space and if a conductor is in the field the drop of potential in a length Δl of conductor can be computed by:

$$V_b(t) - V_a(t) = \frac{I(t)\Delta l}{\sigma A} \tag{4}$$

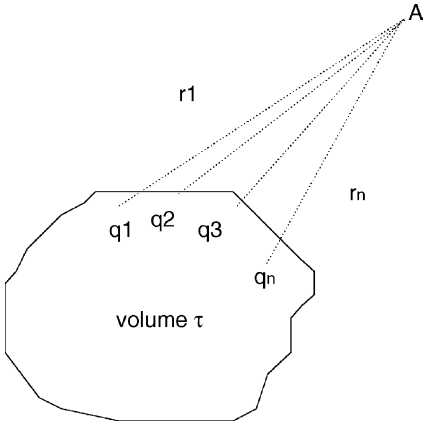

Fig. 1. Example of distributed discrete charges in space and their distances from the point A where the electrostatic potential is computed.

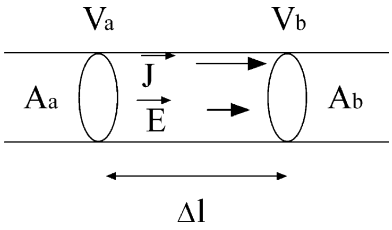

Fig. 2. The electrostatic field $\vec{E}$ generated by charges in movement in a conductor with length Δl.

where A is the area, σ the conductivity and Δl the length of the conductor and $\vec{E}$ could be considered constant (Fig. 2).

Since conductivity σ, area A and the length Δl are the same for every tetrode tip equation (3) can be written:

$$V_b^i(t) - V_a^i(t) = \frac{I_i(t)\Delta l}{\sigma A}, \quad i = 1, 2, 3, 4 \tag{5}$$

where I_i is the current generated in the tip i of tetrode by drop of potential in a length Δl of the conductor.

Substituting Eq. (2) into Eq. (5) one can write:

$$\frac{1}{4\pi\varepsilon}\sum_{i=1}^{n}\frac{q_i}{r_{ij}^a(t)} - \frac{1}{4\pi\varepsilon}\sum_{i=1}^{n}\frac{q_i}{r_{ij}^b(t)} = \frac{I_i(t)\Delta l}{\sigma A}, \quad j = 1, 2, 3, 4 \tag{6}$$

This is equivalent to a point charge $\sum_{i=1}^{n} q_i$ at distance $R_j^a = \sum_{i=1}^{n}\frac{1}{r_{ij}^a}$ and $R_j^b = \sum_{i=1}^{n}\frac{1}{r_{ij}^b}$. Therefore, Eq. (6) can be written:

$$\frac{1}{4\pi\varepsilon}\left(\frac{q}{R_j^a} - \frac{q}{R_j^b}\right) = kI_j(t), \quad j = 1, 2, 3, 4 \tag{7}$$

where $k = \frac{\Delta l}{\sigma A}$.

The left side of Eq. (7) is the potential of a physical electric dipole that consists of two equal and opposite charges q. From the law of cosines in the dipole case (Griffiths, 1999) Eq. (7) can be written:

$$\frac{1}{4\pi\varepsilon}\left(\frac{qd_j\cos\theta_j}{R_j^2}\right) = kI_j(t), \quad j = 1, 2, 3, 4 \tag{8}$$

where d_j is the distance between charges and θ_j is the angle between R_j and the dipole direction. That is equivalent to a single charge at distance R_j. Therefore, the trajectory of the charge q can be obtained using the following approach.

3. Computing the trajectory

Let us consider $s_0(k)$, $s_1(k)$, $s_2(k)$ and $s_3(k)$, $k \in \mathbf{N}$ to be the signals recorded from the four tips of the tetrode. Since the term $d_j(t)\cos\theta_j(t)$ can be considered to be approximately the same for each tetrode tip one may write the following nonlinear system of equations:

$$\begin{aligned}
\frac{s_0(k)}{s_1(k)} &= \frac{(x(k)-x_1)^2 + (y(k)-y_1)^2 + (z(k)-z_1)^2}{x(k)^2 + y(k)^2 + z(k)^2},\\
\frac{s_0(k)}{s_2(k)} &= \frac{(x(k)-x_2)^2 + (y(k)-y_2)^2 + (z(k)-z_2)^2}{x(k)^2 + y(k)^2 + z(k)^2},\\
\frac{s_0(k)}{s_3(k)} &= \frac{(x(k)-x_3)^2 + (y(k)-y_3)^2 + (z(k)-z_3)^2}{x(k)^2 + y(k)^2 + z(k)^2}
\end{aligned} \tag{9}$$

where x_i, y_i, z_i ($i = 1, 4$) are the positions in the space of the tetrode. The same equations could be obtained from the hypothesis that the position of source q is at intersection of four spheres (Jog et al., 2002). The equations in (9) can be written as a nonlinear system $f_j(x, y, z) = 0, j = 1, \ldots, 3$ where $\mathbf{F} = (f_1, f_2, f_3)$. An iterative Newton–Raphson scheme is used to find solution for the nonlinear system:

$$d_{n+1} = d_n - \mathbf{J}^{-1}\mathbf{F}(d_n), \quad n \in \mathbf{N} \tag{10}$$

where the Jacobian $\mathbf{J}$ of function $\mathbf{F}$ is:

$$\mathbf{J} = \begin{pmatrix} \frac{\partial f_1}{\partial x} & \frac{\partial f_1}{\partial y} & \frac{\partial f_1}{\partial z} \\ \frac{\partial f_2}{\partial x} & \frac{\partial f_2}{\partial y} & \frac{\partial f_2}{\partial z} \\ \frac{\partial f_3}{\partial x} & \frac{\partial f_3}{\partial y} & \frac{\partial f_3}{\partial z} \end{pmatrix} \tag{11}$$

Therefore, at each discrete moment k, from recorded signals, $s_1(k)$, $s_2(k)$, $s_3(k)$, $s_4(k)$ the spatial trajectory ($x(k)$, $y(k)$, $z(k)$) is determined when there is a solution d_{n+1} for the nonlinear system (Brenan et al., 1989). Having the trajectory data, the next step is to determine the spike directivity.

4. Computing spike directivity

In order to obtain spike directivity one has to write the matrix $\mathbf{P} \in \Re^{nx3}$ composed by trajectory coordinates ($x(k)$, $y(k)$, $z(k)$):

$$\mathbf{P} = \begin{pmatrix} x(1) & y(1) & z(1) \\ \cdots & \cdots & \cdots \\ x(n) & y(n) & z(n) \end{pmatrix} \tag{12}$$

where $k = 1, 2, \ldots, n$. For each spike one may compute the centroid of the data $\mu = E(\mathbf{P}^{\mathrm{T}})$ forming the matrix $\mathbf{P}_{\mathrm{tr}}$ of translated points $\mathbf{P}_{\mathrm{tr}} = p_i - \mu_i$, $i = 1,2, \ldots, n$.

Writing singular value decomposition (Stewart, 1993):

$$\mathbf{P}_{\mathrm{tr}\,nx3} = \mathbf{U}_{nxn}\mathbf{S}_{nx3}\mathbf{V}_{3x3}^{\mathrm{T}} \tag{13}$$

where

$$\mathbf{S} = \begin{pmatrix} s_1 & & \\ & s_2 & \\ & & s_3 \\ \ldots & \ldots & \ldots \end{pmatrix}; \qquad \mathbf{U} = (u_1, u_2, \ldots, u_n);$$

$$\mathbf{V} = (v_1, v_2, v_3); \tag{14}$$

it is possible to find the largest singular value for **S** and extract from **V** the corresponding right singular vector that represents direction cosines of the best linear approximation.

An important consideration in such computations is the stability of the angle of moving charge. In order to measure the deviation of computed trajectories when the angle of the moving charge is changed, a separate computation specific to this alteration in the angle of the charge, is performed. The angle between two computed directions can be determined using the right singular vector:

$$\Delta\theta = \arccos\left(\frac{\langle v, v'\rangle}{|v||v'|}\right) \tag{15}$$

Even in the simplified case of a single moving charge, the overall computation becomes essentially manually unsolvable. For this reason a series of simulations have been performed on a PC computer (Pentium 4, 1.6 GHz, 512 MB RAM) with Matlab Version 6.0—MathWorks, Inc. All the routines were custom developed or are freely available on the world-wide-web.

In the section below we describe the applications of the methods discussed above. Simulation of charges moving across tetrode tips induces voltage in tetrode tips. Computations for calculating the trajectory and the subsequent directivity are then performed. The impact variables such as tetrode tip geometry and system noise on the directivity computations is discussed. Finally the method is applied to real recorded neuronal spikes and directivity of charge flow in the data is demonstrated.

5. Simulations and analysis

Since directivity and trajectory calculations are performed for spikes within the same frame of reference, a relative change in these parameters can be computed using the system described above. It is assumed that tetrodes do not change their tip configurations during the recordings. As discussed above, when a charge is moved across the tetrode tips, a voltage is induced in the four channels. The act of measurement using the tetrode transforms the actual "real" direction. This is clearly presented in Fig. 3 where the actual trajectories are straight while the computed trajectories are curvilinear. Therefore, when analyzing recorded signal from tetrodes, it is not possible to provide directivity in real space, only in this transformed so-called "tetrode" space. However, since the analysis of all recorded data is performed in this space, the computations of the relative spatial directivity remain valid.

The difference in the relative positions in space of the charge linear trajectory and the directivity can be explained as follows. Imagine a concave or convex mirror and a small ball moving near the mirror that follows a linear trajectory in 3D space. In the mirror one may see a bent image of the ball trajectory during the movement. In our case instead of light reflection that provides the image trajectory of the ball on the mirror, a charge trajectory "image" is obtained from induced

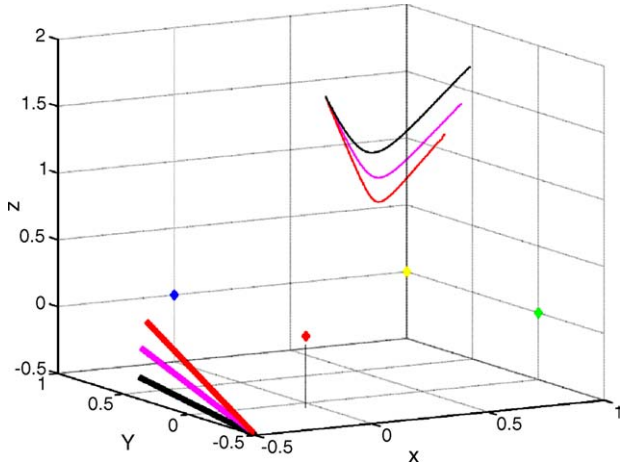

Fig. 3. The changes in the linear trajectory of charge (bold, red, magenta, black lines) and computed trajectory modifications (red, magenta, black trajectories) are shown. Each division is approximately 20 μm. For display purposes approximately 60 μm of charge movement is shown. The "mirror" effect is visible for computed trajectories. (For interpretation of the references to color in this figure legend, the reader is referred to the web version of the article.)

currents by the described computational process. In the simulated experiment the charge is the object moving in 3D space with initial conditions (initial position, speed, etc.) provided by the software user, while the computed trajectory is equivalent to "image" from the mirror. Thus, the trajectory and indeed the relative position computed will be a transformed version of the "real" trajectory or image.

In the computations described above, the knowledge of absolute tetrode tip geometry and distances appears to be important. However, in relative terms, as long as the tip geometry does not change between recorded spikes, the computations of relative directivity-change between spikes remain unaffected. In order to compute a trajectory in real space (Eq. (9)) one would need to know the actual position of tetrode tips in 3D Cartesian space. Measurements of inter-tip distances from tetrodes show that the average spacing between tips is approximately 20 μm with a measurement error of approximately 3 μm for each tip (Chelaru and Jog, 2005; Jog et al., 2002). Charges are then launched simultaneously or in successive trials. The speed of movement of the charge as well as the distance from the midpoint of the tetrode tips to the charge (approximately 30 μm) is held relatively constant. However, this distance varied slightly as the input angles is changed (Fig. 3). For an easier analysis charge trajectories are constrained to describe lines in 3D space. In the simulation, the charge movement is about 260 μm, and successive trials are performed. In the figure however, only a small portion of the actual charge movement distance is displayed. For three successive trials (Fig. 3) the linear charge trajectory is deviated by 10° and this deviation is represented by red, magenta and black bold lines.

Coordinates of tetrode tips are represented by colored diamonds starting with red for the first channel, green, blue

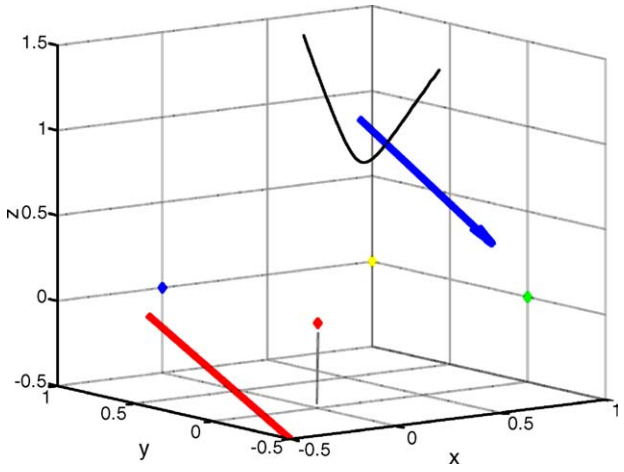

Fig. 4. An example of linear trajectory of a single charge (bold, red line) and the computed trajectory (black curve) and estimated directivity (blue line) are shown. Each division is approximately 20 μm. For display purposes approximately 60 μm of charge movement is shown. The positions are clearly different (see text). (For interpretation of the references to color in this figure legend, the reader is referred to the web version of the article.)

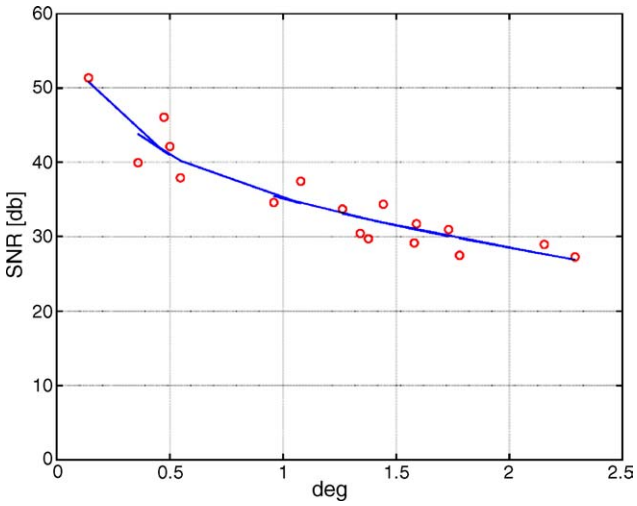

Fig. 5. The graph shows an estimation of dependence between signal to noise ratio and the error in computing deviation angle. Red circles are data obtained from several simulations with decreasing SNR while the blue curve represents the optimal nonlinear approximation. (For interpretation of the references to color in this figure legend, the reader is referred to the web version of the article.)

and yellow for the second, third and fourth channel of the tetrode respectively. Computed trajectories are curves in red, magenta and black. Each division on the axes is approximately 20 μm. One such trajectory is then used to further display computed directivity of the charge flow using the method presented above (Fig. 4). The computed charge directivity is shown by a blue bold line. Although the computed directivity does not map the actual charge directivity, it is clear that the proposed method provides a robust way to analyze variations of directivity in spike recordings between neuronal spikes. Importantly, one can observe that this computing approach can be performed without the full knowledge of actual tip positions.

Additionally, despite modern, high performance acquisition systems and filtering methods, all physiological recordings are susceptible to noise that occurs from various sources such as distant neurons, external electrical noise and animal behavioral artifacts.

In order to better understand the impact of this additional noise on the method for computing directivity, we added such noise to the data. In our simulations these sources of noise are modeled by Gaussian noise added to the "induced" signals in tetrode tips by the moving charges. Dependence of computed deviation in directivity and noise level is displayed in Fig. 5. For a signal noise ratio greater than 25 dB (SNR > 25 dB) the errors in computing deviations are usually less than 3° (Fig. 5). In case of higher noise levels, errors in computing deviation angle may increase. However, spikes that are very noisy should be eliminated from computing spike directivity. One way to perform this spike filtering is to analyze the computed trajectory from nonlinear equation system (Eq. (9)) and eliminate spikes that have trajectory points far away from tetrode tips coordinates. Thus our method can be used as an additional filtering mechanism to eliminate spikes that would randomly contaminate the data.

For real recorded spikes directivity is obtained in two main steps (Fig. 6). The trajectory is computed from recorded data in the first step with the Newton–Raphson algorithm. Then in the second step a linear approximation of the trajectory is performed by a singular value decomposition that gives the overall direction of AP propagation in "tetrode space".

We started our simulations with movements of simple charges that describe linear trajectories in 3D space to show how the method works. The reader may see that by applying this method, simple but curved trajectories are obtained from the computation. These curves (Figs. 3 and 4) that show trajectories of single charges in movement are far less complex than usual trajectories obtained from processing real spikes. The reader may have a false impression regarding the application of the presented method for real recorded data. The propagation of ionic fluxes within biological spikes implies simultaneous movement of several charges during the occurrence of an action potential. Therefore, we provide an example where several charges that are moving in space could generate similar trajectories to computed trajectories from real recorded spikes. We show an example where

Fig. 6. This shows a quick reference diagram for the method. The spatial trajectory $x(k)$, $y(k)$, $z(k)$ is firstly determined with Newton–Raphson algorithm. Spike directivity is then computed using trajectory coordinates and singular value decomposition.

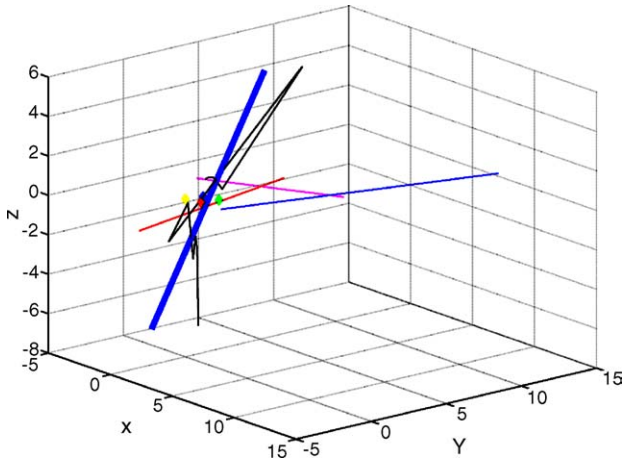

Fig. 7. Linear simultaneous movements of three charges (red, magenta, blue lines), computed trajectory (black curve) and computed directivity (bold blue line). Each division is approximately 20 μm. For display purposes approximately 60 μm of charge movement is shown. (For interpretation of the references to color in this figure legend, the reader is referred to the web version of the article.)

three identical charges with different angles of movement are represented in three different colors (Fig. 7). The simultaneous movement of charges (red, magenta and blue lines) is simulated in the presence of Gaussian noise (SNR = 25 dB). The overall computed trajectory (black curve) and computed directivity (bold blue line) are represented.

Finally, Fig. 8 shows the application of the method to a real recorded spike. Note the similarity of the computed trajectory from the recorded spike to the simulated multi-charge flow trajectory from Fig. 7. The black curve represents the trajectory while and computed directivity is the bold blue line.

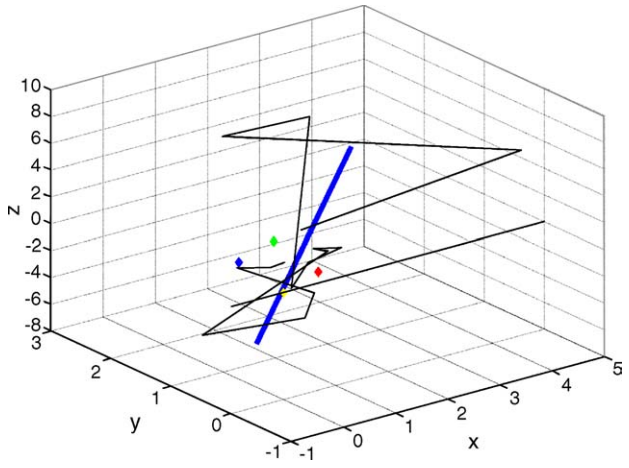

Fig. 8. An example of real spike trajectory (black curve) and computed directivity (bold blue line). Each division is approximately 20 μm. (For interpretation of the references to color in this figure legend, the reader is referred to the web version of the article.)

6. Conclusion

Neuronal spikes recorded in extracellular space by electrodes represent propagation of several electric charges. The alterations caused in the electric field within the extracellular space are recorded by the electrodes. Tetrodes have the ability to observe this phenomenon in four dimensions. However, a further analysis of the spike profile itself can be used to understand whether the process of action potential transmission along a conductor can itself be seen as a directed flow of charge that alters the extracellular milieu in a specific way.

This paper uses simulated charge movement in space and the induced voltages on a conductor as a model to understand whether it is possible to obtain information regarding directivity of such flow of charges. Simulated tetrodes perceive the charge movement as voltage that mimics the action potentials in spiking neurons. A process for computing the directivity of this charge flow is then proposed within the paper. This process of the induction of AP is then applied to the actual data obtained from tetrode recordings and a profile of spike directivity from these recordings is presented.

The weakness of the present method is that it relies on the quality of the electrical recordings. Factors common to all electrode recordings techniques which consist of noise level and number of days that a tetrode can be kept in the brain to record data contribute to this data recording quality. A discussion related to noise analysis was presented in the above simulations. Since new modern, high performance acquisition systems for in vivo recordings provide increased values of signal to noise ratio, the errors in computing deviations are usually small and the method works well in practice.

In addition, it is possible that the changes in directivity that could be seen occurring by the application of our method could result simply due to tetrode drift and movement. Firstly, the internal consistency of this method relies on the fact that the tetrodes are not actually physically moved during the analysis period. The hardware used to implant the drives has to be reliable enough to also avoid inadvertent movement. Additionally, we describe a method of demonstrating directivity changes that are expected to occur in the tens or hundreds of millisecond range. Natural tetrode movement around the brain would be at a much lower frequency.

There are various important applications of this work. First, action potentials can now be seen and analyzed as charge flow that may have directivity. This concept could have a direct impact on the understanding of the extracellular milieu within which electrical events such as the action potential are occurring. Second, the traditional methods of electrophysiology use only spike timing as a way of describing information coding by neurons. However, neurons may also code information in a true “spatial” way by dynamically altering the propagation of charge direction over time. It is possible that both the reception of information and the output of neurons could exhibit directivity. Such changes, over time may be behaviorally dependent. This may become a powerful method for selecting sources of input and output by

neuronal ensembles, thereby possibly determining the state of the space within which neural activity is occurring. Such a phenomenon of change of directivity can be thought of as a dynamical alteration of the spatial receptive field of neuronal ensembles. Such receptive field modulation has been observed often, without an adequate explanation of the mechanism (Mehta et al., 2004). The method proposed in our paper and the implications of behaviorally dependent spatial directivity changes are therefore important.

Third, in the larger sense, computations of directivity can be used a possible filtering technique where outlying spikes that have trajectory points that are unreasonably distant, could be eliminated from the data set.

The ability to compute trajectory and directivity of charge flow by tetrode recordings use the spike as a reflection of this flow and gives us a glimpse of the complexity of milieu within which neurons function. Our results show that besides improved spike sorting procedures, tetrodes can be used in computing the trajectory of equivalent electrical charges that model electrical events during AP. Based on obtained trajectory, estimation of changes in spike directivity over an arbitrary reference system in real recordings could be achieved. This is a new potentially powerful application of tetrode recording methodology.

References

Brenan KE, Campbell SL, Petzold LR. Numerical solution of initial-value problem in differential-algebraic equations. North-Holland, Amsterdam: Elsevier; 1989.

Chelaru MI, Jog MS. Spike source localization with tetrodes. J Neurosci Meth 2005;142(2):305–15.

Emondi AA, Rebrik SP, Kurgansky AV, Miller KD. Tracking neurons recorded from tetrodes across time. J Neurosci Meth 2004;135:95–105.

Gray C, Maldonado P, Wilson M, McNaughton B. Tetrodes markedly improve the reliability and yield of multiple single-unit isolation from multi-unit recordings in cat striate cortex. J Neurosci Meth 1995;63(1/2):43–54.

Griffiths DJ. Introduction to electrodynamics. Prentice-Hall; 1999.

Hebb DO. The organization of behavior. New York: John Wiley; 1949.

Jog MS, Kubota Y, Connolly CI, Hillegaart, Graybiel AM. Building neural representations of habits. Science 1999;286:1745–9.

Jog MS, Connolly CI, Kubota Y, Iyengar DR, Garrido L, Harlan R, Graybiel AM. Tetrode technology: advances in implantable hardware, neuroimaging, and data analysis techniques. J Neurosci Meth 2002;117:141–52.

Mehta MR, Lee AK, Wilson MA. Response to Melamed et al.: coding and learning of behavioral sequences—open questions and potential solutions. Trends Neurosci 2004;27(1):14–5.

Sahani M, Pezaris JS, Andersen RA. On the separation of signals from neighboring cells in tetrode recordings. In: Jordan I M, Kearns MJ, Solla SA, editors. Advances in neural information processing systems 10. Cambridge, MA: MIT Press; 1998.

Schwartz TL. The thermodynamic foundations of membrane physiology. In: Adelman Jr W, editor. Biophysics and physiology of excitable membranes. New York: Van Nostrand Reinhold Company; 1971. p. 47–95.

Stewart GW. The early history of the SVD. SIAM Rev 1993;35:558–61.

Takahashi S, Sakurai Y, Tsukada M, Anzai Y. A new approach to spike sorting for multi-neuronal activities recorded with a tetrode. Neurosci Res 2003;46:265–72.

Zhang K, Ginzburg I, McNaughton BL, Sejnowski TJ. Interpreting neuronal population activity by reconstruction: Unified framework with application to hippocampal place cells. J Neurophysiol 1998;79:1017–44.